

StablePCA: Distributionally Robust Learning of Shared Representations from Multi-Source Data

Zhenyu Wang¹, Molei Liu², Jing Lei³, Francis Bach^{4*}, and Zijian Guo^{5*}

¹Department of Statistics, Rutgers University

²Department of Biostatistics, Peking University Health Science Center;
Beijing International Center for Mathematical Research

³Department of Statistics, Carnegie Mellon University

⁴Inria, École Normale Supérieure, PSL Research University

⁵Center for Data Science, Zhejiang University.

March 10, 2026

Abstract

When synthesizing multi-source high-dimensional data, a key objective is to extract low-dimensional representations that effectively approximate the original features across different sources. Such representations facilitate the discovery of transferable structures and help mitigate systematic biases such as batch effects. We introduce *Stable Principal Component Analysis* (StablePCA), a distributionally robust framework for constructing stable latent representations by maximizing the worst-case explained variance over multiple sources. A primary challenge in extending classical PCA to the multi-source setting lies in the nonconvex rank constraint, which renders the StablePCA formulation a nonconvex optimization problem. To overcome this challenge, we conduct a convex relaxation of StablePCA and develop an efficient Mirror-Prox algorithm to solve the relaxed problem, with global convergence guarantees. Since the relaxed problem generally differs from the original formulation, we further introduce a data-dependent certificate to assess how well the algorithm solves the original nonconvex problem and establish the condition under which the relaxation is tight. Finally, we explore alternative distributionally robust formulations of multi-source PCA based on different loss functions.

Keywords: Matrix factorization, Principal component analysis, Multi-source analysis, Group distributionally robust learning, Minimax Optimization

*Correspondence to Francis Bach (francis.bach@inria.fr) and Zijian Guo (zijguo@zju.edu.cn).

1 Introduction

Extracting low-dimensional representations from high-dimensional data is a fundamental task in modern data science. Such representations are widely used for downstream tasks, including visualization, clustering, prediction, and knowledge discovery (Hastie et al. 2009, Jolliffe 2011). To extract these representations, classical approaches such as principal component analysis (PCA) and matrix factorization (MF) learn a low-rank structure that captures the dominant variation in the observed data by minimizing the reconstruction error. However, the structure learned in this way is optimized for the training distribution and may fail to generalize to data drawn from different distributions. This raises a fundamental question: how can one learn a low-rank transformation that remains informative for future unseen data under distributional shift?

Multi-source data provides a unique opportunity to learn generalizable low-rank transformation when the unseen target data has a distributional shift from training data. The multi-source data arises commonly, including single-cell RNA sequencing (scRNA-seq) studies measured across multiple batches (Hicks et al. 2018, Tran et al. 2020), electronic health records (EHRs) collected from different hospitals (Hong et al. 2021, Li et al. 2024), and medical images acquired under varying protocols (Hari et al. 2021). Although individual sources may have distinct source-specific variations, they tend to share similar underlying biological structures that generalize to future data. This observation motivates leveraging heterogeneous sources to identify a shared low-rank transformation while acknowledging the source-specific distributional shifts and mitigating source-specific biases.

To achieve a shared low-rank transformation, a naive strategy is to pool data from multiple sources and then apply PCA to the aggregated dataset. However, this strategy relies on the questionable assumption that source-specific biases cancel out when averaged across sources,

but such an assumption might not hold in practice, as these biases are frequently skewed or imbalanced (Hari et al. 2021). For instance, in scRNA-seq studies, batch effects arise from technical variations in sequencing platforms, reagents, and experimental protocols. Directly pooling data for PCA fails to remove these artifacts, which can artificially separate cells of the same biological type, leading to biased cell-type annotation and distorted differential gene expression analyzes (Tran et al. 2020). Moreover, when sources differ substantially in sample size or noise level, the learned low-rank structure may be dominated by a few large or high-variance sources, while underrepresented sources contribute little to the representation. As a result, naive pooling often leads to poor out-of-distribution generalization and raises fairness concerns when the learned representations are used downstream.

1.1 Our results and contributions

In this work, we propose *Stable Principal Component Analysis* (StablePCA), a distributionally robust framework to identify a stable low-rank structure based on multi-source data. As illustrated in Figure 1 of Section 2.3, StablePCA effectively captures the principal component common to heterogeneous multi-source data, motivating the name StablePCA.

To ensure that the learned structure generalizes to future data whose distribution may differ from the observed sources, we construct an uncertainty set for the unknown target distribution that consists of all possible mixtures of the source distributions. StablePCA then seeks a low-rank subspace that maximizes the worst-case explained variance over this uncertainty set. This formulation is designed to learn a low-rank transformation that generalizes beyond the observed sources and performs well on new target data.

The primary challenge in solving StablePCA arises from the nonconvexity associated with the fixed-rank constraint set for projection matrices. To address this issue, we employ a Fantope relaxation (Vu et al. 2013), enabling a convex reformulation of the original

nonconvex StablePCA problem. We then develop a Mirror-Prox algorithm to efficiently solve the relaxed problem. Unlike standard gradient descent–ascent methods, Mirror-Prox (Nemirovski 2004, Bubeck et al. 2015) incorporates an extra-gradient step and is specifically designed for constrained minimax problems with non-Euclidean geometry, as in our case. Building upon this, we derive explicit closed-form updates for each iteration of the Mirror-Prox algorithm, ensuring efficient implementation. From a theoretical perspective, we establish global convergence guarantees for the proposed algorithm, with convergence rates characterized in terms of both the sample size n and the number of iterations T .

Since the relaxed StablePCA problem generally differs from the original nonconvex formulation, we propose a data-dependent computable certificate to assess how well the proposed algorithm approximately solves the original StablePCA problem. Moreover, we also establish a sufficient condition under which the relaxation is indeed tight, that is, when the solution of the relaxed StablePCA problem is also the optimal solution for the original problem.

Finally, we explore alternative distributionally robust formulations of multi-source PCA beyond the proposed StablePCA, including variants based on squared loss and regret, where the regret loss recovers the FairPCA formulation in the literature (Samadi et al. 2018, Shen et al. 2025). An interesting observation is that different choices of loss functions lead to construction of different low-rank transformations in the multi-source setting. We design the proposed Mirror-Prox algorithm for these alternative formulations. In contrast to the semidefinite programming (SDP) method used in prior work (Samadi et al. 2018), which incurs a computational complexity of $\mathcal{O}(d^{6.5})$ for dimension d , our method yields a scalable gradient-based algorithm with a runtime of $\mathcal{O}(d^3T)$, where T denotes the number of iterations. As illustrated in Table 1 of Section 6, our approach achieves substantial computational gains when d is moderately large; for example, it is nearly 40 times faster than SDP when $d = 300$.

We summarize the key contributions of this work as follows:

1. We propose StablePCA, a distributionally robust framework for learning stable low-rank transformations that generalize beyond the observed sources. We further explore alternative robust formulations of multi-source PCAs using various loss functions.
2. For the relaxed (convex) StablePCA, we develop a computationally efficient algorithm and establish global convergence guarantees that jointly characterize optimization convergence and statistical estimation errors (Theorem 2).
3. For the original (nonconvex) StablePCA, we introduce a certificate to quantify how well the proposed algorithm solves it to global optimality (Theorem 3), and we establish a sufficient condition under which the convex relaxation is tight (Theorem 4).

1.2 Related literature

This section reviews relevant research and highlights how the proposed StablePCA relates to and differs from existing works.

Group DRO and Maximin effect. Group Distributionally Robust Optimization (DRO) (Sagawa et al. 2019, Hu et al. 2018) and the maximin effect framework (Guo 2023, Wang et al. 2025) have been extensively studied in supervised learning for constructing prediction models that generalize across heterogeneous source domains. Recent extensions include the study of optimal sample allocation for Group DRO in online learning settings (Zhang et al. 2024) and adaptations to semi-supervised learning (Awasthi et al. 2024). In contrast to these works focusing on supervised prediction tasks, StablePCA addresses the unsupervised learning setting, aiming to extract shared latent structures from multi-source data.

Multi-source PCA. Several formulations of PCA in multi-source settings have been proposed in the literature. For example, Samadi et al. (2018) and Shen et al. (2025)

introduced FairPCA, which enforces equal regret across sources, while [Olfat & Aswani \(2019\)](#) and [Kleindessner et al. \(2023\)](#) studied PCA variants that aim to remove source-specific information from learned representations. In contrast, StablePCA is formulated from a distributionally robust optimization perspective, explicitly maximizing the worst-case explained variance over all mixtures of source distributions. To address the nonconvexity of the fixed-rank constraint, we adopt the Fantope relaxation and develop the gradient-based Mirror-Prox algorithm to efficiently solve the resulting minimax problem. We note that our algorithm extends to solve FairPCA, avoiding the use of semidefinite programming in the original work ([Samadi et al. 2018](#)), which could be computationally prohibitive in high dimensions. Moreover, in contrast to prior works, we establish the global convergence guarantees of our proposal in terms of both the sample size n and the iteration number T .

Multi-source Learning. A broader body of work in multi-source learning aims to identify generalizable patterns from heterogeneous data sources. For transfer learning, [Li et al. \(2022\)](#) and [Tian & Feng \(2023\)](#) proposed to transfer knowledge from source domains to a target domain by leveraging structural similarity between source and target distributions. In meta-analysis, [Maity et al. \(2022\)](#) and [Guo et al. \(2025\)](#) identify and study models that the majority of source domains hold. For causal invariance learning, exist works ([Peters et al. 2016](#), [Fan et al. 2024](#), [Wang et al. 2024](#)) aim to learn causal models that remain invariant across sources. These works are typically designed for supervised settings with outcomes. In contrast, StablePCA addresses the problem in an unsupervised setting by identifying stable low-dimensional representations of data across heterogeneous sources.

1.3 Notations

We define $[m] = \{1, 2, \dots, m\}$ for the positive integer m . For a vector $v \in \mathbb{R}^d$, its ℓ_p -norm ($p \geq 1$) is given by $\|v\|_p = (\sum_{j=1}^d |v_j|^p)^{1/p}$. We denote by $\text{Diag}(v)$ the diagonal matrix

whose diagonal entries are given by the components of v . We use $\mathbf{1}_d$ to denote the d -dimensional vector of all ones. For two matrices A, B with compatible dimensions, we define the matrix inner product $\langle A, B \rangle = \text{Tr}(A^\top B)$ and the Frobenius norm $\|A\|_F = \sqrt{\langle A, A \rangle}$. If $A \in \mathbb{R}^{d \times d}$ is symmetric, we denote its eigenvalues in nonincreasing order by $\lambda_1(A) \geq \dots \geq \lambda_d(A)$. If A is positive definite with eigen-decomposition $A = U \text{Diag}(\lambda) U^\top$, we define $\log(A) = U \text{Diag}(\log \lambda) U^\top$. The d -dimensional identity matrix is denoted as \mathbf{I}_d . For sequences $a(n), b(n)$, we use $a(n) = \mathcal{O}(b(n))$ to represent that there exists some universal constant $C > 0$ such that $a(n) \leq C \cdot b(n)$ for all $n \geq 1$.

2 StablePCA: Definitions and Interpretations

This section introduces the definition of Stable PCA and provides interpretations of how it identifies a stable low-rank transformation across domains. We begin in Section 2.1 with reviewing the classical PCA (in the single-source setting), which lays the foundation for defining StablePCA using multi-source data in Section 2.2. Finally, Section 2.3 illustrates how StablePCA captures stable latent structures across heterogeneous sources.

2.1 Review of Classical PCA

The central goal of PCA is to identify a low-rank linear subspace that captures the dominant variation in the data. We now present two equivalent formulations of PCA: one based on minimizing reconstruction error and the other based on maximizing explained variance.

We start with the reconstruction-error formulation. For a random feature vector $X \in \mathbb{R}^d$, classical PCA seeks a k -dimensional linear subspace (with $k < d$) such that projecting X onto this subspace yields the best approximation of X itself. Formally, let $\mathcal{O}^{d \times k} = \{V \in \mathbb{R}^{d \times k} : V^\top V = \mathbf{I}_k\}$ denote the set of $d \times k$ matrices with orthonormal columns. For each $V \in \mathcal{O}^{d \times k}$, its column space $\text{col}(V)$ defines a k -dimensional linear subspace, and the

corresponding matrix $P = VV^\top$ is the orthogonal projection onto this subspace (with dimension k). PCA is then formulated as identifying the rank- k projection matrix P that minimizes the expected reconstruction error $X - PX$:

$$P^* \in \arg \min_{P \in \mathcal{P}^k} \mathbb{E} \|X - PX\|_2^2, \quad \text{with} \quad \mathcal{P}^k = \{P \in \mathbb{R}^{d \times d} : P = VV^\top, V \in \mathcal{O}^{d \times k}\}, \quad (1)$$

where PX represents the projection of X onto the associated subspace, and \mathcal{P}^k denotes the set of all rank- k projection matrices.

After learning P^* , we shall further leverage it to construct a low-dimensional representation of the original feature vector X . Specifically, decomposing $P^* = V^*V^{*\top}$ for some $V^* \in \mathcal{O}^{d \times k}$, we let $V^{*\top}X \in \mathbb{R}^k$ be a k -dimensional representation of $X \in \mathbb{R}^d$.

Next, we provide an alternative interpretation of PCA in terms of explained variance. We rewrite the optimization problem in (1) as follows:

$$P^* \in \arg \max_{P \in \mathcal{P}^k} \mathbb{E} \left(\|X\|_2^2 - \|X - PX\|_2^2 \right) = \arg \max_{P \in \mathcal{P}^k} \langle \Sigma, P \rangle, \quad (2)$$

where $\Sigma = \mathbb{E}[XX^\top]$ denotes the second-moment matrix of X , and $\mathbb{E} (\|X\|_2^2 - \|X - PX\|_2^2) = \langle \Sigma, P \rangle$ denotes the variance explained by the projection matrix P . Throughout this work, we slightly abuse terminology and refer to $\langle \Sigma, P \rangle$ as the variance explained by using P , even for the uncentered X . In practice, one can center the data by subtracting the sample mean prior to applying PCA. Therefore, P^* is the rank- k projection matrix that maximizes the explained variance of X .

Although the reconstruction-error and explained-variance formulations are equivalent in the single-source setting, they lead to different behaviors when generalized to multi-source data. In this work, we primarily focus on the explained-variance formulation (2) because the multi-source PCA formed with the explained variance tends to capture shared structure across heterogeneous sources, as illustrated in Section 2.3. We also consider the generalization of the reconstruction-error formulation to the multi-source setting in Section 6.

Despite the widespread use of classical PCA, the learned projection matrix P^* is optimal only for the observed single-source distribution and may fail to generalize to future target data that may have a distributional shift from the currently observed data. For example, naively applying P^* to new data \widetilde{X} drawn from a different distribution may yield poor explained variance $\mathbb{E} \left(\|\widetilde{X}\|_2^2 - \|\widetilde{X} - P^*\widetilde{X}\|_2^2 \right)$ due to distributional shifts. A fundamental challenge is whether we can construct a low-rank structure that generalizes beyond the observed data. In what follows, we address this challenge by leveraging data from multiple sources and constructing low-rank transformation from a view of distributional robustness.

2.2 Formulation of StablePCA

We now turn to the multi-source regime with data collected from multiple heterogeneous environments. Our goal is to identify a stable low-rank transformation that generalizes beyond the observed source distributions, in the presence of distributional shifts. We consider access to L source datasets, where for $1 \leq l \leq L$, we use $\mathbb{T}^{(l)}$ to denote the l -th source distribution and $X^{(l)} \in \mathbb{R}^d$ to denote the random feature vector drawn from $\mathbb{T}^{(l)}$.

We introduce an uncertainty class to account for the uncertainty about the unknown target distribution. Particularly, we introduce the following uncertainty class, comprising all mixtures of the source distributions:

$$\mathcal{C} = \left\{ \mathbb{Q} : \mathbb{Q} = \sum_{l=1}^L \omega_l \cdot \mathbb{T}^{(l)}, \omega \in \Delta^L \right\}, \quad (3)$$

where $\Delta^L = \{\omega \in \mathbb{R}_+^L : \sum_{l=1}^L \omega_l = 1\}$ denotes the $(L - 1)$ -dimensional simplex.

With such an uncertainty class, we generalize classical PCA in (2) by considering the worst-case explained variance and define StablePCA as:

$$P^* \in \arg \max_{P \in \mathcal{P}^k} \min_{\mathbb{Q} \in \mathcal{C}} \mathbb{E}_{X \sim \mathbb{Q}} \left(\|X\|_2^2 - \|X - PX\|_2^2 \right), \quad (4)$$

where the expectation is taken with respect to the random feature X drawn from the distribution \mathbb{Q} . With a slight abuse of notation, we denote the optimal solution by P^* ;

unless otherwise specified, P^* will henceforth refer to the solution to the StablePCA optimization problem defined in (4).

When there is no distributional shift, that is, $\mathbb{T}^{(1)} = \dots = \mathbb{T}^{(L)}$, the uncertainty class \mathcal{C} collapses to a single distribution, and StablePCA reduces to classical PCA in (2). However, when the distributional shift exists across domains, the inner minimization of (4) selects the most challenging mixture of source distributions for a given projection matrix P . As a result, StablePCA tends to yield a more generalizable low-rank transformation by evaluating the worst-case performance over a range of source-mixture distributions.

We now simplify the optimization problem in (4) to facilitate algorithm design and further analysis. We apply the definition of the uncertainty class \mathcal{C} and obtain

$$\begin{aligned} \min_{\mathbb{Q} \in \mathcal{C}} \mathbb{E}_{X \sim \mathbb{Q}} \left(\|X\|_2^2 - \|X - PX\|_2^2 \right) &= \min_{\omega \in \Delta^L} \sum_{l=1}^L \omega_l \cdot \mathbb{E}_{X \sim \mathbb{T}^{(l)}} \left(\|X\|_2^2 - \|X - PX\|_2^2 \right) \\ &= \min_{\omega \in \Delta^L} \sum_{l=1}^L \omega_l \cdot \langle \Sigma^{(l)}, P \rangle, \end{aligned}$$

where $\Sigma^{(l)} = \mathbb{E}[X^{(l)} X^{(l)\top}]$. Therefore, our proposed StablePCA in (4) simplifies as follows:

$$P^* \in \arg \max_{P \in \mathcal{P}^k} \min_{\omega \in \Delta^L} \sum_{l=1}^L \omega_l \cdot \langle \Sigma^{(l)}, P \rangle. \quad (5)$$

After learning P^* , we can $P^* = V^* V^{*\top}$ for some orthonormal matrix $V^* \in \mathcal{O}^{d \times k}$ and use $V^{*\top} X \in \mathbb{R}^k$ as a low-dimensional representation of X . In Appendix A.1, we further discuss incorporating prior information about the target distribution into defining StablePCA.

2.3 Geometric Interpretation: Stable Principal Direction

In the following, we illustrate the geometric interpretation of our proposed StablePCA method through simulation studies and show that StablePCA tends to capture the principal direction shared across multiple sources.

We consider the settings consisting of $L = 3$ sources. Across all settings, we vary two key

aspects of heterogeneity: (i) imbalance of sample sizes across sources and (ii) heterogeneity in source-specific relationships among features. The three settings are constructed as follows:

- **Setting 1.** The source sample sizes are unbalanced, with $n_1 = 300, n_2 = 300, n_3 = 1200$. For $l \in \{1, 2, 3\}$, the data are generated according to

$$X_1^{(l)} \sim \mathcal{N}(0, 3), \quad X_2^{(l)} = \beta^{(l)} \cdot X_1^{(l)} + \epsilon^{(l)}, \quad \epsilon^{(l)} \sim \mathcal{N}(0, 0.04), \quad (6)$$

with coefficients $(\beta^{(1)}, \beta^{(2)}, \beta^{(3)}) = (0.2, -0.4, -1)$.

- **Setting 2.** All sources have equal sample sizes with $n_l = 500$, and the data-generating process remains identical to (6) in Setting 1.
- **Setting 3.** All sources again have equal sample sizes $n_l = 500$. The data-generating process is identical to (6), but with different coefficients $(\beta^{(1)}, \beta^{(2)}, \beta^{(3)}) = (-0.5, 1, 0.6)$, introducing a different pattern of source-specific relationships among features.

Across all three settings, the data for each source $l \in \{1, 2, 3\}$ are driven by two underlying directions: (i) a shared latent direction X_1 that is common to all sources, and (ii) a source-specific direction X_2 , whose relationship to X_1 varies across sources through a heterogeneous data generating parameter $\beta^{(l)}$. The noise level in (6) is chosen to be small purely for visualization purposes to prevent excessive overlap of data points across sources in Figure 1.

Figure 1 compares our proposed StablePCA and PooledPCA, where PooledPCA applies classical PCA to data pooled from all sources. For PooledPCA, the estimated first principal component (PC) varies substantially across the three settings, indicating its sensitivity to both sample-size imbalance (Settings 1 vs. 2) and source-specific heterogeneity governed by $\beta^{(l)}$ (Settings 2 vs. 3). In contrast, StablePCA, implemented via the following Algorithm 1 with $k = 1$, consistently recovers the shared latent direction along X_1 across all settings. This result indicates that StablePCA not only mitigates the influence of imbalanced sample sizes but also remains stable under heterogeneous source-specific variations along X_2 .

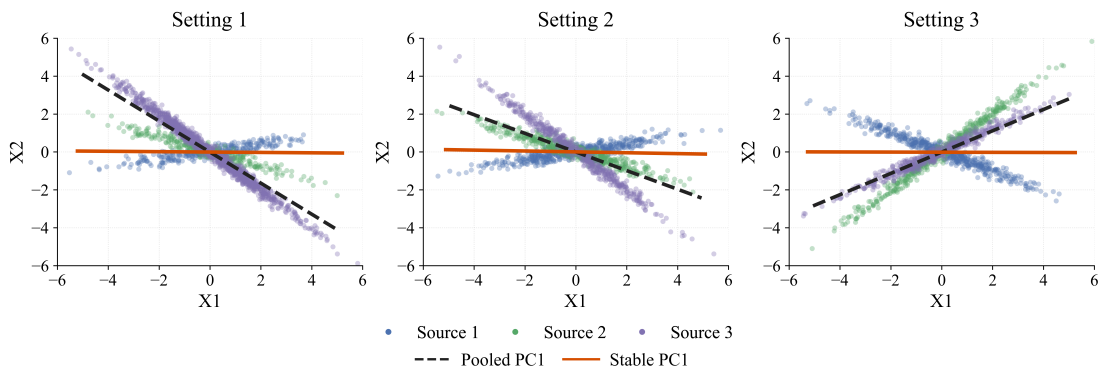


Figure 1: Comparison of the first principal component estimated by PooledPCA and StablePCA across settings. Settings 1 and 2 differ in sample-size imbalance across sources, whereas Settings 2 and 3 differ in the source-specific relationship between X_1 and X_2 .

3 Fantope Relaxation and Algorithm for Solving StablePCA

In this section, we focus on solving the StablePCA optimization problem in (5). The main computational challenge stems from the interaction between the nonconvex constraint imposed by the set of rank- k projection matrices \mathcal{P}^k , and the adversarial minimax structure of the problem. To address this issue, we introduce in Section 3.1 a convex Fantope relaxation of StablePCA, and in Section 3.2 we further develop an efficient gradient-based algorithm (Mirror-Prox) for computing the relaxed StablePCA.

3.1 Fantope Relaxation

We introduce the Fantope relaxation of the original StablePCA problem in (5). The k -dimensional Fantope (Dattorro 2010) is the convex hull of the nonconvex \mathcal{P}^k defined as:

$$\mathcal{F}^k = \left\{ M \in \mathbb{R}^{d \times d} : M = M^\top, 0 \preceq M \preceq \mathbf{I}_d, \text{Tr}(M) = k \right\}. \quad (7)$$

Substituting the nonconvex constraint $P \in \mathcal{P}^k$ in the original nonconvex StablePCA formulation (5) with the Fantope $M \in \mathcal{F}^k$ yields the following relaxed StablePCA problem:

$$M^* \in \arg \max_{M \in \mathcal{F}^k} \min_{\omega \in \Delta^L} \langle \Sigma(\omega), M \rangle, \quad \text{where} \quad \Sigma(\omega) := \sum_{l=1}^L \omega_l \cdot \Sigma^{(l)}. \quad (8)$$

The Fantope relaxation has also been employed in other contexts; for example, in sparse PCA, where the classical PCA objective is combined with an ℓ_1 -penalty; see [Vu et al. \(2013\)](#) for more details. The relaxation in (8) transforms the original nonconvex StablePCA into a convex optimization problem, for which we shall devise a computationally efficient algorithm that provably converges to the global optimum.

Even though we are able to solve the relaxed StablePCA problem efficiently, the solution to the relaxed problem may differ from the original StablePCA, since the optimal solution M^* in (8) is not guaranteed to be a rank- k projection matrix. In Section 5, we introduce a sufficient condition for when the Fantope relaxation is tight, meaning that the relaxed solution M^* is also the optimal solution of the original StablePCA. Throughout the remainder of the paper, unless otherwise specified, we refer to the original nonconvex problem in (5) as **original StablePCA**, and to its relaxed formulation (8) simply as **StablePCA**.

We now switch to the finite-sample setting, where we observe n_l i.i.d. samples $\{X_i^{(l)}\}_{i=1}^{n_l}$ drawn from the l -th source distribution $\mathbb{T}^{(l)}$ for $1 \leq l \leq L$. By substituting the population-level $\Sigma^{(l)}$ with its empirical counterpart $\widehat{\Sigma}^{(l)} = \frac{1}{n_l} \sum_{i=1}^{n_l} X_i^{(l)} [X_i^{(l)}]^\top$ in (5) and (8), respectively, we define the empirical version of the original StablePCA as:

$$\widehat{P} \in \arg \max_{P \in \mathcal{P}^k} \min_{\omega \in \Delta^L} \langle \widehat{\Sigma}(\omega), P \rangle, \quad \text{where} \quad \widehat{\Sigma}(\omega) := \sum_{l=1}^L \omega_l \cdot \widehat{\Sigma}^{(l)} \quad (9)$$

and the empirical StablePCA as:

$$\widehat{M} \in \arg \max_{M \in \mathcal{F}^k} \min_{\omega \in \Delta^L} \langle \widehat{\Sigma}(\omega), M \rangle. \quad (10)$$

In the next subsection, we present a computationally efficient algorithm for solving the empirical StablePCA problem (10) and further introduce a data-dependent certificate to assess how well the proposed algorithm solves the original StablePCA problem (9).

3.2 Mirror-Prox Algorithm with Certificate

We now turn to the design of algorithm solving the empirical StablePCA problem (10) by rewriting it in the following format:

$$\widehat{M} \in \arg \min_{M \in \mathcal{F}^k} \max_{\omega \in \Delta^L} f(M, \omega), \quad \text{with} \quad f(M, \omega) := -\langle \widehat{\Sigma}(\omega), M \rangle. \quad (11)$$

The objective function $f(M, \omega)$ is bilinear in (M, ω) and thus defines a convex-concave minimax problem. To solve the problem, we adopt the Mirror-Prox algorithm, which is designed for solving constrained minimax optimization problems (Nemirovski 2004); see Section 5.2 of Bubeck et al. (2015) for a detailed discussion.

Mirror-Prox is a gradient-based algorithm that iteratively updates the variables $(M, \omega) \in \mathcal{F}^k \times \Delta^L$. To build intuition, we briefly recall standard gradient descent for minimizing a non-constrained differentiable convex function $\min_{x \in \mathbb{R}^d} g(x)$, which takes the form:

$$x^{t+1} = x^t - \eta \nabla g(x^t) = \arg \min_{x \in \mathbb{R}^d} \left\{ g(x^t) + \eta \langle \nabla g(x^t), x - x^t \rangle + \frac{1}{2} \|x - x^t\|_2^2 \right\},$$

where $\eta > 0$ is a pre-specified step size. In the rightmost expression, the term $g(x^t) + \langle \nabla g(x^t), x - x^t \rangle$ represents the first-order approximation of the objective at the current point x^t , while the euclidean distance $\frac{1}{2} \|x - x^t\|_2^2$ penalizes deviation from x^t . Therefore, each update seeks a point that achieves the largest reduction in the first-order approximated objective while remaining close to the current iterate.

Mirror-Prox employs mirror updates that follow the same underlying principle as standard gradient descent. The key difference is that mirror updates replace the Euclidean distance $\frac{1}{2} \|x - x^t\|_2^2$ with Bregman divergences, which are better aligned with the geometry of constrained sets. For completeness, we provide formal definitions and a brief overview of Bregman divergences and mirror updates in Appendix A.4. In our setting, tailored to the

constraints $M \in \mathcal{F}^k$ and $\omega \in \Delta^L$, we adopt the following Bregman divergences:

$$D_{\psi_1}(M, M') = \text{Tr}(M(\log M - \log M')), \quad \text{and} \quad D_{\psi_2}(\omega, \omega') = \sum_{l=1}^L \omega_l \log \frac{\omega_l}{\omega'_l}, \quad (12)$$

for any $M, M' \in \mathcal{F}^k$ and $\omega, \omega' \in \Delta^L$. Here, $D_{\psi_1}(M, M')$ represents the distance between two projection matrices while $D_{\psi_2}(\omega, \omega')$ represents the distance between two probability measures. These choices are standard in the literature (Bubeck et al. 2015).

We now describe the Mirror-Prox algorithm for solving (11). We initialize the algorithm at a feasible point $(M^0, \omega^0) \in \mathcal{F}^k \times \Delta^L$, for example, $M^0 = \frac{k}{d} \mathbf{I}_d$ and $\omega^0 = \frac{1}{L} \mathbf{1}_L$. For each iteration $t = 0, 1, \dots, T - 1$, the Mirror-Prox algorithm proceeds in two steps. First, given the current iterate (M^t, ω^t) and the step sizes $\eta_M, \eta_\omega > 0$, we compute the midpoint iterate $(M^{t+\frac{1}{2}}, \omega^{t+\frac{1}{2}})$ by performing mirror updates over the constraints $M \in \mathcal{F}^k$ and $\omega \in \Delta^L$:

$$\begin{aligned} M^{t+\frac{1}{2}} &= \arg \min_{M \in \mathcal{F}^k} \left\{ \eta_M \cdot \langle \nabla_M f(M^t, \omega^t), M \rangle + D_{\psi_1}(M, M^t) \right\}, \\ \omega^{t+\frac{1}{2}} &= \arg \min_{\omega \in \Delta^L} \left\{ -\eta_\omega \cdot \langle \nabla_\omega f(M^t, \omega^t), \omega \rangle + D_{\psi_2}(\omega, \omega^t) \right\}. \end{aligned} \quad (13)$$

For the update on M , the linear term $\eta_M \langle \nabla_M f(M^t, \omega^t), M \rangle$ corresponds to the first-order approximation of the objective $f(M, \omega^t)$ at the current iterate M^t , and the Bregman divergence $D_{\psi_1}(M, M^t)$ prevents the update from deviating excessively from M^t . Similarly, the update on ω follows from a first-order approximation of $f(M^t, \omega)$ at ω^t .

After obtaining the midpoint $(M^{t+\frac{1}{2}}, \omega^{t+\frac{1}{2}})$, we compute the next iterate (M^{t+1}, ω^{t+1}) using a similar idea as in (13) but evaluating gradients at the midpoint $(M^{t+\frac{1}{2}}, \omega^{t+\frac{1}{2}})$

$$\begin{aligned} M^{t+1} &= \arg \min_{M \in \mathcal{F}^k} \left\{ \eta_M \cdot \langle \nabla_M f(M^{t+\frac{1}{2}}, \omega^{t+\frac{1}{2}}), M \rangle + D_{\psi_1}(M, M^t) \right\}, \\ \omega^{t+1} &= \arg \min_{\omega \in \Delta^L} \left\{ -\eta_\omega \cdot \langle \nabla_\omega f(M^{t+\frac{1}{2}}, \omega^{t+\frac{1}{2}}), \omega \rangle + D_{\psi_2}(\omega, \omega^t) \right\}. \end{aligned} \quad (14)$$

By evaluating the gradient at the midpoint iterate, the second step utilizes a more accurate approximation of the gradient at the subsequent iterate. Such an extra-gradient correction mitigates oscillations that commonly arise near saddle points in minimax optimization and

stabilizes the trajectory of the iterates. As a result, the Mirror-Prox algorithm achieves the improved convergence rate $\mathcal{O}(T^{-1})$ for smooth convex-concave problems, in contrast to the slower rate $\mathcal{O}(T^{-1/2})$ for methods without the extra-gradient step. We refer to works (Mokhtari et al. 2020, Bubeck et al. 2015) for a more detailed explanation.

For the mirror updates in (13) and (14), we derive in the following proposition the explicit closed-form expressions, which enable efficient updates.

Proposition 1. *The first step in (13) admits the following closed-form expression:*

$$M^{t+\frac{1}{2}} = \sum_{j=1}^d \min\{\exp(\lambda_j^t + \nu^t), 1\} U_j^t [U_j^t]^\top, \quad \omega_l^{t+\frac{1}{2}} = \frac{\omega_l^t \exp(-\eta_\omega \langle \widehat{\Sigma}^{(l)}, M^t \rangle)}{\sum_{r=1}^L \omega_r^t \exp(-\eta_\omega \langle \widehat{\Sigma}^{(r)}, M^t \rangle)}, \quad (15)$$

for $1 \leq l \leq L$, where $U^t \text{Diag}(\lambda^t) (U^t)^\top$ is the eigen decomposition of $\log M^t + \eta_M \sum_{l=1}^L \omega_l^t \widehat{\Sigma}^{(l)}$, and $\nu^t \in \mathbb{R}$ is the unique solution to $\sum_{j=1}^d \min\{\exp(\lambda_j^t + \nu), 1\} = k$. Similarly, the second step in (14) admits:

$$M^{t+1} = \sum_{j=1}^d \min\left\{\exp\left(\lambda_j^{t+\frac{1}{2}} + \nu^{t+\frac{1}{2}}\right), 1\right\} U_j^{t+\frac{1}{2}} [U_j^{t+\frac{1}{2}}]^\top, \quad \omega_l^{t+1} = \frac{\omega_l^t \exp(-\eta_\omega \langle \widehat{\Sigma}^{(l)}, M^{t+\frac{1}{2}} \rangle)}{\sum_{r=1}^L \omega_r^t \exp(-\eta_\omega \langle \widehat{\Sigma}^{(r)}, M^{t+\frac{1}{2}} \rangle)}, \quad (16)$$

for $1 \leq l \leq L$, where $U^{t+\frac{1}{2}} \text{Diag}(\lambda^{t+\frac{1}{2}}) (U^{t+\frac{1}{2}})^\top$ is the eigen decomposition of $\log M^t + \eta_M \sum_{l=1}^L \omega_l^{t+\frac{1}{2}} \widehat{\Sigma}^{(l)}$, and $\nu^{t+\frac{1}{2}}$ is the unique solution to $\sum_{j=1}^d \min\{\exp(\lambda_j^{t+\frac{1}{2}} + \nu), 1\} = k$.

After completing T iterations, we collect the midpoint iterates $\{(M^{t+\frac{1}{2}}, \omega^{t+\frac{1}{2}})\}_{t=0}^{T-1}$ and return their average:

$$\widehat{M}_T = \frac{1}{T} \sum_{t=0}^{T-1} M^{t+\frac{1}{2}}, \quad \text{and} \quad \widehat{\omega}_T = \frac{1}{T} \sum_{t=0}^{T-1} \omega^{t+\frac{1}{2}}. \quad (17)$$

We use \widehat{M}_T as an approximate solution to the empirical StablePCA optimization problem (10), and establish that the objective value attained by \widehat{M}_T converges to the global optimum with increasing T in later Section 4.1.

Since $\widehat{M}_T \in \mathcal{F}^k$ may not have rank exactly k , we enforce the rank constraint via a final

projection step, by computing the nearest rank- k projection matrix to \widehat{M}_T :

$$\widehat{P}_T = \arg \min_{P \in \mathcal{P}^k} \|P - \widehat{M}_T\|_F. \quad (18)$$

Thus $\widehat{P}_T = V_T V_T^\top$, where $V_T \in \mathcal{O}^{d \times k}$ comprises top- k eigenvectors of \widehat{M}_T . Although $\widehat{P}_T \in \mathcal{P}^k$ satisfies the rank constraint, it does not necessarily solve the original nonconvex StablePCA problem (9) to global optimality. To quantify how close \widehat{P}_T is to solving the original nonconvex StablePCA problem (9), we introduce a data-dependent certificate:

$$\tau := \min_{\omega \in \Delta^L} \langle \widehat{\Sigma}(\omega), \widehat{M}_T \rangle - \min_{\omega \in \Delta^L} \langle \widehat{\Sigma}(\omega), \widehat{P}_T \rangle = \min_{1 \leq l \leq L} \langle \widehat{\Sigma}^{(l)}, \widehat{M}_T \rangle - \min_{1 \leq l \leq L} \langle \widehat{\Sigma}^{(l)}, \widehat{P}_T \rangle, \quad (19)$$

where $\widehat{\Sigma}(\omega)$ is defined in (9). This certificate is directly computable and measures the difference between the worst-case explained variances incurred by replacing the relaxed solution $\widehat{M}_T \in \mathcal{F}^k$ with the exact rank- k $\widehat{P}_T \in \mathcal{P}^k$.

We now provide the rationale for why the certificate τ indicates whether \widehat{P}_T solves the original nonconvex StablePCA problem (9) to global optimality. Since $\mathcal{F}^k \supseteq \mathcal{P}^k$, the objective gap between the objective value $\min_{\omega \in \Delta^L} \langle \widehat{\Sigma}(\omega), \widehat{P}_T \rangle$ and the global optimal value is upper bounded as follows:

$$\begin{aligned} 0 &\leq \max_{P \in \mathcal{P}^k} \left[\min_{\omega \in \Delta^L} \langle \widehat{\Sigma}(\omega), P \rangle \right] - \min_{\omega \in \Delta^L} \langle \widehat{\Sigma}(\omega), \widehat{P}_T \rangle \\ &\leq \max_{M \in \mathcal{F}^k} \left[\min_{\omega \in \Delta^L} \langle \widehat{\Sigma}(\omega), M \rangle \right] - \min_{\omega \in \Delta^L} \langle \widehat{\Sigma}(\omega), \widehat{P}_T \rangle \\ &= \left\{ \max_{M \in \mathcal{F}^k} \left[\min_{\omega \in \Delta^L} \langle \widehat{\Sigma}(\omega), M \rangle \right] - \min_{\omega \in \Delta^L} \langle \widehat{\Sigma}(\omega), \widehat{M}_T \rangle \right\} + \tau. \end{aligned} \quad (20)$$

In Theorem 1, we will show that the first term $\max_{M \in \mathcal{F}^k} \left[\min_{\omega \in \Delta^L} \langle \widehat{\Sigma}(\omega), M \rangle \right] - \min_{\omega \in \Delta^L} \langle \widehat{\Sigma}(\omega), \widehat{M}_T \rangle$, which represents the objective gap of \widehat{M}_T for the relaxed StablePCA problem, converges to 0 as $T \rightarrow \infty$. Consequently, the data-dependent certificate τ controls how far \widehat{P}_T is from global optimality for the original StablePCA problem.

We summarize the entire procedure in Algorithm 1.

Algorithm 1: Mirror-Prox Algorithm for StablePCA

Data: Empirical matrices $\{\widehat{\Sigma}^{(l)}\}_{l=1}^L$; target dimension k ; step sizes η_M, η_ω ; iterations T

Initialize $M^0 = \frac{k}{d}\mathbf{I}_d \in \mathcal{F}^k$ and $\omega^0 = \frac{1}{L}\mathbf{1}_L \in \Delta^L$;

for $t = 1, \dots, T$ **do**

 First Step: compute $(M^{t+\frac{1}{2}}, \omega^{t+\frac{1}{2}})$ as in (15);

 Second Step: compute (M^{t+1}, ω^{t+1}) as in (16);

end

Compute $(\widehat{M}_T, \widehat{\omega}_T)$ by averaging midpoints as in (17);

Compute \widehat{P}_T as in (18) and the certificate τ as in (19).

return $\widehat{M}_T, \widehat{P}_T$, and certificate τ .

4 Theoretical Justification

In this section, we establish the convergence of Algorithm 1 and consider both the optimization error due to running the algorithm for a finite number of iterations and the statistical error arising from the finite samples. By leveraging the certificate τ in (19), we characterize how well the output \widehat{P}_T solves the original nonconvex StablePCA problem in (5).

We introduce additional notation used throughout the theoretical analysis, by defining the maximum operator norms over sources as:

$$\rho_{\max} := \max_{1 \leq l \leq L} \|\Sigma^{(l)}\|_{\text{op}}, \quad \text{and} \quad \widehat{\rho}_{\max} := \max_{1 \leq l \leq L} \|\widehat{\Sigma}^{(l)}\|_{\text{op}}.$$

4.1 Convergence to Relaxed StablePCA

This section presents the convergence analysis of \widehat{M}_T , the output of Algorithm 1, for solving the StablePCA problem. First, we study the *optimization convergence*, characterizing how well \widehat{M}_T solves the empirical StablePCA problem (10) after T iterations. Second, we study the *statistical convergence* by further accounting for the finite-sample errors.

We begin with the analysis of optimization error, depending on the number T of iterations.

Theorem 1. *With the step sizes*

$$\eta_M = \frac{\eta}{\log L}, \quad \eta_\omega = \frac{\eta}{k \log(d/k)}, \quad \text{where } \eta := \frac{1}{4\hat{\rho}_{\max}} \sqrt{\frac{\log L}{k \log(d/k)}},$$

the output \widehat{M}_T of Algorithm 1 satisfies

$$0 \leq \max_{M \in \mathcal{F}^k} \left[\min_{\omega \in \Delta^L} \langle \widehat{\Sigma}(\omega), M \rangle \right] - \min_{\omega \in \Delta^L} \langle \widehat{\Sigma}(\omega), \widehat{M}_T \rangle \leq \frac{8\hat{\rho}_{\max} \cdot k \sqrt{k \log(d/k) \log L}}{T}.$$

This theorem guarantees that \widehat{M}_T attains an objective value $\min_{\omega \in \Delta^L} \langle \widehat{\Sigma}(\omega), \widehat{M}_T \rangle$ that is within an $\mathcal{O}(T^{-1})$ error of the global optimal value of the empirical StablePCA. Equivalently, \widehat{M}_T approximately solves the empirical StablePCA problem, with an error of the order $\mathcal{O}(T^{-1})$. We note that the proof of this theorem follows standard convergence arguments for the Mirror-Prox algorithm and is adapted from Theorem 5.2 of [Bubeck et al. \(2015\)](#). Moreover, the $\mathcal{O}(T^{-1})$ dependence on the number of iterations T matches the lower bound for first-order methods applied to the bilinear minimax problem, when the dimensions of the problem are fixed ([Ouyang & Xu 2021](#)).

Building upon the optimization convergence result in Theorem 1, we further consider the finite sample errors and study how well \widehat{M}_T solves the population StablePCA problem (8). We impose the following standard sub-Gaussian assumption on the feature samples.

Condition 1 (Sub-Gaussian features). *For $1 \leq l \leq L$, $\{X_i^{(l)}\}_{i=1}^n$ are i.i.d. sub-Gaussian vectors with bounded sub-Gaussian norms $\sigma := \max_{1 \leq l \leq L} \sup_{\|u\|_2=1} \left\| \langle X_i^{(l)}, u \rangle \right\|_{\psi_2} / \|\Sigma^{(l)}\|_{\text{op}} < \infty$, where $\|\cdot\|_{\psi_2}$ denotes the sub-Gaussian norm for a random variable.*

The following theorem suggests that \widehat{M}_T approximately solves the population StablePCA problem (8) to the global optimality. We set $n = \min_l n_l$ for simplicity.

Theorem 2. *Suppose Condition 1 holds, the sample size satisfies $n \geq d$, and the step sizes η_M, η_ω are specified as in Theorem 1. Then for any value $t \in [0, n - d]$, with probability at*

least $1 - 2Le^{-t}$, the output \widehat{M}_T of Algorithm 1 satisfies

$$\max_{M \in \mathcal{F}^k} \left[\min_{\omega \in \Delta^L} \langle \Sigma(\omega), M \rangle \right] - \min_{\omega \in \Delta^L} \langle \Sigma(\omega), \widehat{M}_T \rangle \leq C \rho_{\max} \cdot k \left(\sqrt{\frac{d+t}{n}} + \frac{\sqrt{k \log(d/k) \log L}}{T} \right),$$

where $C > 0$ denotes a universal constant.

This theorem ensures that \widehat{M}_T approximately solves the population StablePCA problem. In the upper bound, the term $k\sqrt{(d+t)/n}$ arises from the finite-sample error, while the term $k\sqrt{k \log(d/k) \log L}/T$ reflects the optimization error, as established in Theorem 1, due to running a finite number of iterations. With n and T going to ∞ , the upper bound converges to 0, and thus \widehat{M}_T solves the population StablePCA problem to global optimality.

4.2 Convergence to Original Nonconvex StablePCA

We now turn to the original nonconvex StablePCA problem and analyze the projected output \widehat{P}_T of Algorithm 1. Inspired by (20), the following theorem leverages the data-dependent certificate τ in (19) to establish how well \widehat{P}_T solves the original StablePCA (8).

Theorem 3. *Under the same conditions of Theorem 2, for any value $t \in [0, n - d]$, with probability at least $1 - 2Le^{-t}$, the projected output \widehat{P}_T of Algorithm 1 satisfies*

$$\max_{P \in \mathcal{P}^k} \left[\min_{\omega \in \Delta^L} \langle \Sigma(\omega), P \rangle \right] - \min_{\omega \in \Delta^L} \langle \Sigma(\omega), \widehat{P}_T \rangle \leq C \rho_{\max} k \left(\sqrt{\frac{d+t}{n}} + \frac{\sqrt{k \log(d/k) \log L}}{T} \right) + \tau, \quad (21)$$

where $C > 0$ denotes a universal constant.

Similar to Theorem 2, the upper bound contains the finite-sample and the optimization error. Additionally, the upper bound involves the data-dependent τ , which measures the discrepancy between the relaxed and original StablePCA problems.

In practice, one aims to ensure that \widehat{P}_T is an ϵ -optimal solution that satisfies $\max_{P \in \mathcal{P}^k} [\min_{\omega \in \Delta^L} \langle \Sigma(\omega), P \rangle] - \min_{\omega \in \Delta^L} \langle \Sigma(\omega), \widehat{P}_T \rangle \leq \epsilon$, for a small tolerance $\epsilon > 0$. When the sample size n and the number of iterations T are sufficiently large such that

$n^{-1/2} + T^{-1} \lesssim \epsilon/2$, it suffices to compute the certificate τ defined in (19) and verify whether $\tau \leq \epsilon/2$. When this holds, \widehat{P}_T is guaranteed to be ϵ -optimal for the original StablePCA problem. Empirically, as shown in Appendix D.1.2, the certificate τ is negligible across all simulated settings that we have explored. Moreover, we show that under an additional eigengap condition specified in Section 5, τ can be further quantified theoretically.

5 Tightness of Fantope Relaxation

In this section, we study when the Fantope relaxation for the StablePCA is tight. If one can show that the relaxed solution M^* is a rank- k projection matrix, i.e., $M^* \in \mathcal{P}^k$, this implies that M^* is also an optimal solution to the original (nonconvex) StablePCA optimization problem. In what follows, we derive an equivalent expression for M^* and identify the condition under which $M^* \in \mathcal{P}^k$.

For relaxed StablePCA problem, the objective $\langle \Sigma(\omega), M \rangle$ is bilinear in (M, ω) , and both feasibility sets \mathcal{F}^k and ω^L are convex and compact. Hence, by Sion's minimax theorem (Sion 1958), we interchange the order of the max and min operators:

$$\max_{M \in \mathcal{F}^k} \min_{\omega \in \Delta^L} \langle \Sigma(\omega), M \rangle = \min_{\omega \in \Delta^L} \max_{M \in \mathcal{F}^k} \langle \Sigma(\omega), M \rangle.$$

The right-hand side of the above equation provides a dual formulation for computing an optimal solution M^* , involving a two-step procedure:

- **Step 1.** Solve the dual optimization problem obtained after swapping the order:

$$\omega^* \in \arg \min_{\omega \in \Delta^L} \phi(\omega), \quad \text{with} \quad \phi(\omega) = \max_{M \in \mathcal{F}^k} \langle \Sigma(\omega), M \rangle = \sum_{i=1}^k \lambda_i(\Sigma(\omega)), \quad (22)$$

where the last equality follows from Ky Fan's maximum principle (Fan 1949).

- **Step 2.** Given ω^* , compute $M^* \in \arg \max_{M \in \mathcal{F}^k} \langle \Sigma(\omega^*), M \rangle$.

We show that $\phi(\omega)$ is convex and provide implementation details of step 1 in Appendix A.2.

After computing the optimal ω^* , step 2 indicates that the relaxed solution M^* maximizes $\langle \Sigma(\omega^*), M \rangle$ over the Fantope \mathcal{F}^k .

Note that in Step 2, if $\Sigma(\omega^*)$ exhibits an eigengap between its k -th and $(k+1)$ -th largest eigenvalues, such that $\lambda_k(\Sigma(\omega^*)) > \lambda_{k+1}(\Sigma(\omega^*))$, then the maximizer M^* in Step 2 must be the projection matrix onto the top- k eigenspace of $\Sigma(\omega^*)$. In this case, M^* is itself a rank- k projection matrix such that $M^* \in \mathcal{P}^k$.

Based on the above observation, we establish when the Fantope relaxation is tight.

Theorem 4. *If there exists an ω^* defined in (22) satisfying $\lambda_k(\Sigma(\omega^*)) > \lambda_{k+1}(\Sigma(\omega^*))$, then M^* can be expressed as the projection matrix onto the top- k eigenspace of $\Sigma(\omega^*)$, and is the optimal solution to the original StablePCA problem (8).*

Theorem 4 provides a sufficient condition for when the relaxed solution M^* is also an optimal solution of the original StablePCA problem.

Recall that in Theorem 3, we utilize the data-dependent certificate τ in (19) to measure how well the output \hat{P}_T solves the original nonconvex StablePCA problem. Building upon the tightness of the Fantope relaxation, we next analyze the data-dependent certificate τ .

Theorem 5. *If there exists an ω^* defined in (22) satisfying $\lambda_k(\Sigma(\omega^*)) > \lambda_{k+1}(\Sigma(\omega^*))$, and the conditions of Theorem 3 are satisfied. Then for any value $t \in [0, n-d]$, with probability at least $1 - 2Le^{-t}$,*

$$|\tau|^2 \leq C\rho_{\max}^3 \cdot \frac{k^2}{\lambda_k(\Sigma(\omega^*)) - \lambda_{k+1}(\Sigma(\omega^*))} \left(\sqrt{\frac{d+t}{n}} + \frac{\sqrt{k \log(d/k) \log L}}{T} \right),$$

where $C > 0$ denotes a universal constant.

This theorem confirms that, under the additional eigengap condition, the certificate τ vanishes with increasing sample size n and number of iterations T . We note that the dependence on n, k might be suboptimal, and leave potential improvements for future work.

Combining Theorems 3 and 5, we obtain that

$$\max_{P \in \mathcal{P}^k} \left[\min_{\omega \in \Delta^L} \langle \Sigma(\omega), P \rangle \right] - \min_{\omega \in \Delta^L} \langle \Sigma(\omega), \hat{P}_T \rangle \lesssim \left(\frac{d+t}{n} \right)^{1/4} + \left(\frac{\sqrt{\log d}}{T} \right)^{1/2}, \quad (23)$$

where the above inequality holds by treating the target low dimension k , the number of sources L , and the eigengap as constants. Consequently, under the additional eigengap condition, the output \hat{P}_T of Algorithm 1 solves the original nonconvex StablePCA (5) to global optimality, as both the sample size n and the number of iterations T grow.

6 Exploration of Alternative Robust Multi-source PCA

While the proposed StablePCA is formulated based on the explained variance, as defined in (5), this section further explores alternative distributionally robust formulations of multi-source PCA based on other loss functions. Different choices of the loss function result in different learned low-rank representations. The impact of loss function selection has also been observed in multi-source regression problems (Wang et al. 2025).

Formulations of Alternative Robust Multi-source PCA. The first alternative approach is designed to minimize the worst-case squared reconstruction error over the uncertainty set \mathcal{C} defined in (3):

$$P^{\text{sq}} \in \arg \min_{P \in \mathcal{P}^k} \max_{\mathbb{Q} \in \mathcal{C}} \mathbb{E}_{\mathbb{Q}} \|X - PX\|_2^2 = \arg \min_{P \in \mathcal{P}^k} \max_{l \in [L]} \mathbb{E} \|X^{(l)} - PX^{(l)}\|_2^2, \quad (24)$$

where the equality follows because the inner maximization over \mathcal{C} is attained at one of the extreme points, corresponding to the worst-case source. Since it extends the squared reconstruction-error formulation of classical PCA in (1), we refer to it as SquaredPCA.

Note that $\mathbb{E} \|X^{(l)} - PX^{(l)}\|_2^2 = \langle \Sigma^{(l)}, \mathbf{I} - P \rangle$, which corresponds to the *unexplained variance* of $X^{(l)}$ by P , where $\Sigma^{(l)} = \mathbb{E}[X^{(l)} X^{(l)\top}]$. Therefore, SquaredPCA in (24) can be equivalently interpreted as minimizing the worst-case unexplained variance across sources, in contrast to the proposed StablePCA, which maximizes the worst-case explained variance. These two

formulations generally lead to different solutions under the multi-source regime, although they are equivalent in the single source setting, as shown in Section 2.1.

Moreover, one may instead consider a regret-based objective that measures the excess reconstruction error relative to the best subspace for each mixture of distributions. Given a distribution \mathbb{Q} and a projection matrix $P \in \mathcal{P}^k$, the corresponding regret is defined as:

$$\text{Regret}_{\mathbb{Q}}(P) := \mathbb{E}_{\mathbb{Q}}\|X - PX\|_2^2 - \min_{P' \in \mathcal{P}^k} \mathbb{E}_{\mathbb{Q}}\|X - P'X\|_2^2,$$

where $\min_{P' \in \mathcal{P}^k} \mathbb{E}_{\mathbb{Q}}\|X - P'X\|_2^2$ denotes the smallest reconstruction error for the distribution \mathbb{Q} . We then minimize the worst-case regret across the uncertainty set \mathcal{C} :

$$P^{\text{fair}} \in \arg \min_{P \in \mathcal{P}^k} \max_{\mathbb{Q} \in \mathcal{C}} \text{Regret}_{\mathbb{Q}}(P). \quad (25)$$

We refer to this approach as FairPCA, as it coincides with the worst-case regret formulation studied in Samadi et al. (2018). In their work, FairPCA was defined as $P^{\text{fair}} \in \arg \min_{P \in \mathcal{P}^k} \max_{l \in [L]} \text{Regret}_{\mathbb{T}^{(l)}}(P)$, which minimizes the maximum regret across individual source distributions. Our formulation instead takes the worst-case regret over the entire uncertainty class \mathcal{C} , consisting of all mixtures of the source distributions $\{\mathbb{T}^{(l)}\}_{l=1}^L$, thereby providing a distributionally robust interpretation of FairPCA. We show in Appendix A.3.1 that these two formulations are in fact equivalent.

Mirror-Prox Algorithm for SquaredPCA and FairPCA. We now generalize Algorithm 1 to solve SquaredPCA and FairPCA. We then compare this Mirror-Prox algorithm with the semidefinite programming approach adopted in prior work (Samadi et al. 2018) for solving FairPCA. We begin by presenting reformulations of SquaredPCA and FairPCA that parallel the StablePCA formulation in (5).

Proposition 2. *Let $\Sigma^{(l)} = \mathbb{E}[X^{(l)}X^{(l)\top}]$ have eigenvalues $\lambda_1^{(l)} \geq \dots \geq \lambda_d^{(l)}$ for each source $1 \leq l \leq L$. Then SquaredPCA defined in (24) and FairPCA defined in (25) admit the*

following equivalent reformulations:

$$P^{\text{sq}} \in \arg \max_{P \in \mathcal{P}^k} \min_{\omega \in \Delta^L} \sum_{l=1}^L \omega_l \cdot \left\langle \Sigma^{(l)} - \frac{1}{k} \sum_{i=1}^d \lambda_i^{(l)} \mathbf{I}_d, P \right\rangle,$$

$$P^{\text{fair}} \in \arg \max_{P \in \mathcal{P}^k} \min_{\omega \in \Delta^L} \sum_{l=1}^L \omega_l \cdot \left\langle \Sigma^{(l)} - \frac{1}{k} \sum_{i=1}^k \lambda_i^{(l)} \mathbf{I}_d, P \right\rangle.$$

Together with the StablePCA formulation in (5), this result shows that the three robust multi-source PCA methods differ only in the constant matrix subtracted from each $\Sigma^{(l)}$ within the objective. Specifically, SquaredPCA denoted as P^{sq} subtracts $\frac{1}{k} \sum_{i=1}^d \lambda_i^{(l)} \mathbf{I}_d$, and FairPCA denoted as P^{fair} subtracts $\frac{1}{k} \sum_{i=1}^k \lambda_i^{(l)} \mathbf{I}_d$, while the proposed StablePCA denoted as P^* subtracts no term at all. In Appendix A.3.3, we revisit the example in Section 2.3 to provide a geometric comparison of these formulations, where StablePCA is the only method that consistently recovers the shared latent direction along X_1 across all settings.

Based on this reformulation, SquaredPCA and FairPCA can be solved using the same algorithmic framework developed in Section 3.2. In particular, one may first apply the Fantope relaxation by replacing the nonconvex constraint $P \in \mathcal{P}^k$ with its convex hull $M \in \mathcal{F}^k$, and then solve the resulting minimax problem using the Mirror-Prox Algorithm 1. Due to space limitations, we provide the extended algorithm in Appendix A.3.2.

We remark on the computational complexity of the extended algorithm. The extended Mirror-Prox algorithm solves the SquaredPCA or FairPCA iteratively, where each iteration conducts an eigen-decomposition with a cost $\mathcal{O}(d^3)$, leading to a total runtime of $\mathcal{O}(d^3 T)$ over T iterations. In contrast, the original FairPCA work (Samadi et al. 2018) adopts semidefinite programming (SDP) with a runtime on the order of $\mathcal{O}(d^{6.5})$, which is computationally prohibitive in high-dimensional settings.

In addition, we compare the computational costs of different optimization methods using an experiment with varying dimensions $d \in \{10, 50, 100, 200, 300\}$. The exact experimental setup is provided in Appendix D.3. We solve FairPCA using the extended Mirror-Prox

algorithm with $T = 500$ iterations, and we also implement the SDP-based method following the procedure described in [Samadi et al. \(2018\)](#). All experiments are repeated 100 times, and we report the average runtime in seconds, together with standard deviations. For ease of comparison, we report the runtime ratio of the SDP method divided by Mirror-Prox.

Method	$d = 30$	$d = 50$	$d = 70$	$d = 100$	$d = 200$	$d = 300$
MP	0.263±0.023	0.324±0.035	0.511± 0.035	0.706±0.067	1.86±0.04	4.49±0.07
SDP	0.057±0.007	0.281±0.135	0.519±0.057	9.99±5.68	42.96±22.66	173.6±70.2
SDP/MP	0.22	0.89	1.02	14.25	23.07	38.79

Table 1: Comparison of the proposed Mirror-Prox(MP) algorithm and the SDP-based method ([Samadi et al. 2018](#)) for solving FairPCA. We report the average runtime (in seconds) and standard deviations for each method in 100 independent replications, across varying dimensions $d \in \{30, 50, 70, 100, 200, 300\}$. The ratio SDP/MP is defined as the averaged runtime of the SDP method divided by that of Mirror-Prox.

The results in Table 1 show that while the SDP-based approach is competitive in very low dimensions (e.g., $d = 30$), its runtime increases significantly as the dimension grows, making it impractical in high-dimensional settings. However, when d is large, the proposed Mirror-Prox algorithm performs much more efficiently. For example, when $d = 300$, our proposal is approximately 40 times faster than the SDP-based method.

7 Simulations

Throughout this section, we investigate the empirical performance of StablePCA through simulated experiments, by demonstrating that StablePCA effectively captures the shared latent structure in multi-source data and generalizes beyond the observed sources. Additional experiments, regarding the finite-sample convergence of Algorithm 1 and the magnitude of

the certificate τ , are provided in Appendix D.1.

We consider L independent data sources with the following data generation mechanism. First, we generate an orthonormal loading matrix $\Lambda_{\text{sh}} \in \mathcal{O}^{d \times 3}$ shared by all sources. Next, for each source $l \in [L]$, we randomly and independently generate an orthonormal loading matrix $\Lambda_{\text{sp}}^{(l)} \in \mathcal{O}^{d \times 5}$ orthogonal to the shared Λ_{sh} . The matrices $\{\Lambda_{\text{sp}}^{(l)}\}_{l=1}^L$ introduce the source-specific variations and may differ across sources. For each source $l \in [L]$ and each sample $i \in [n]$, the data are generated as:

$$X_i^{(l)} = \left(\Lambda_{\text{sh}}, \alpha^{(l)} \Lambda_{\text{sp}}^{(l)} \right) Z_i^{(l)} + \varepsilon_i^{(l)}, \quad \text{with } Z_i^{(l)} \sim \mathcal{N}(0_{\mathbf{8}}, \mathbf{I}_{\mathbf{8}}), \varepsilon_i^{(l)} \sim \mathcal{N}(0_d, \frac{1}{4} \mathbf{I}_d), \quad (26)$$

where $\alpha^{(l)} \stackrel{i.i.d.}{\sim} \text{Unif}(0.2, 3)$ controls the magnitude of source-specific variation in source l , $Z_i^{(l)}$ denotes the latent factors, and $\varepsilon_i^{(l)}$ is the random noise. Unless otherwise specified, we set $d = 40$, and generate $n = 2000$ samples for each source domain.

We evaluate the generalization performance of StablePCA, implemented via Algorithm 1, and compare it with alternative multi-source PCA methods as the number of sources varies over $L \in \{2, 4, 6, 8, 10\}$. Competing approaches include SquaredPCA, FairPCA, and PooledPCA, which pools all source data and applies classical PCA. All methods are fitted with the target low dimension $k = 3$, while the results for other choices of $k \in \{5, 10\}$ are provided in Appendix D.1.3. After training on the observed multi-source data, we denote the estimated projection matrix by \hat{P} . The results, averaged over 100 independent replications, are summarized in Figure 2.

On the left panel of Figure 2, we first assess whether the learned \hat{P} recovers the shared data structure, evaluated via the metric $\|\hat{P} - \Lambda_{\text{sh}} \Lambda_{\text{sh}}^T\|_F$, named as ‘‘Shared Subspace Recovery Error’’. Smaller values indicate closer alignment between the learned subspace of \hat{P} and the true shared subspace spanned by Λ_{sh} . We find that StablePCA achieves progressively smaller error as the number of sources L increases, indicating improved recovery of the shared subspace with more source domains. In contrast, other competing approaches

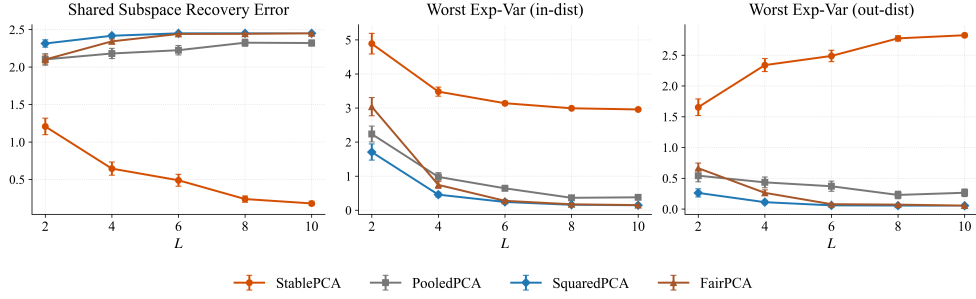


Figure 2: Performance comparison of StablePCA, PooledPCA, SquaredPCA, and FairPCA across different numbers of source domains $L \in \{2, 4, 6, 8, 10\}$. Leftmost: Subspace recovery error $\|\hat{P} - \Lambda_{\text{sh}}\Lambda_{\text{sh}}^T\|_F^2$. Middle: Worst-case explained variance among in-distribution sources. Rightmost: Worst-case explained variance among out-of-distribution domains. Results are averaged over 100 replications, with error bars representing one standard deviation.

have substantially larger $\|\hat{P} - \Lambda_{\text{sh}}\Lambda_{\text{sh}}^T\|_F$ than StablePCA. For example, when $L = 10$, the averaged recovery error of StablePCA is approximately 0.19, whereas the corresponding errors for the other methods exceed 2.0. The results align with the geometric insight illustrated in Figure 1. Under the multi-source data-generating mechanism in (26), each source contains additional source-specific components that can obscure the shared signal. By taking the minimum over the multi-source distributions, StablePCA effectively filters out source-specific variations, thereby preserving the shared structure.

We then compare the methods in terms of the worst-case explained variance, evaluated both in-distribution and out-of-distribution. Larger values indicate better generalization performance. Specifically, we consider the following two metrics:

- *In-distribution*: We report $\min_{l \in [L]} \langle \hat{\Sigma}^{(l)}, \hat{P} \rangle$, the worst-case explained variance over the L training sources.
- *Out-of-distribution*: We generate $L_{\text{out}} = 100$ new test distributions, each sharing the same Λ_{sh} but with independently sampled source-specific components $\Lambda_{\text{sp}}^{(l')}$ and scaling factors $\alpha^{(l')}$. The out-of-distribution performance is measured by $\min_{l' \in [L_{\text{out}}]} \langle \hat{\Sigma}^{(l')}, \hat{P} \rangle$.

As shown in the middle and right panels of Figure 2, StablePCA consistently achieves the largest worst-case explained variance under both in-distribution and out-of-distribution evaluations, outperforming the competing methods. This observation is consistent with the formulation of StablePCA, which explicitly maximizes worst-case explained variance.

8 Real Application

We evaluate the performance of StablePCA on a real single-cell RNA-sequencing (scRNA-seq) dataset. Our analysis uses the human bone marrow dataset from [Luecken et al. \(2021\)](#) containing gene expression (RNA) of cells from 12 experimental batches. Across 12 experimental batches, variations persist due to differences in sequencing depth, experimental protocols, and laboratory-specific effects. Our goal is to demonstrate that StablePCA can learn a stable low-rank transformation that generalizes across batches in terms of representing the original high-dimensional data while effectively suppressing batch variations.

We preprocess the RNA expression matrix using standard filtering procedures: genes expressed in fewer than three cells and cells with fewer than 200 detected genes are removed. Each cell is then normalized to a fixed total count (10^4), followed by log-transformation. Since the raw RNA dimensionality exceeds ten thousand genes and would cause excessive statistical noise and heavy computational burdens, we reduce the initial feature space by selecting the top 1000 highly variable genes using Scanpy ([Wolf et al. 2018](#)), a commonly used pipeline.

After preprocessing the data and reducing the original features to $d = 1000$ highly variable genes, we apply StablePCA with a target dimension of $k = 50$. This choice provides a moderate dimension suitable for downstream visualization methods such as t-SNE ([Maaten & Hinton 2008](#)) and UMAP ([Healy & McInnes 2024](#)). Results for additional choices of $k \in \{100, 150\}$ are reported in Appendix D.2, and exhibit similar patterns.

To assess generalization performance, we compare StablePCA against three alternative methods: SquaredPCA, FairPCA, and PooledPCA. We randomly select 8 of the 12 batches as training sources and fit all four methods to these batches. The learned projection matrix \hat{P} is then evaluated on the remaining four held-out batches. For each fitted projection matrix, we compute the worst-case explained variance over the hold-out samples from the training batches (“in-dist”) and over the test batches (“out-dist”):

$$\min_{l \in \text{Training Batches}} \langle \hat{\Sigma}^{(l)}, \hat{P} \rangle, \quad \text{and} \quad \min_{l' \in \text{Test Batches}} \langle \hat{\Sigma}^{(l')}, \hat{P} \rangle.$$

A higher worst-case explained variance indicates that the corresponding projection matrix has better generalization performance. We repeat this over 200 random train-test splits.

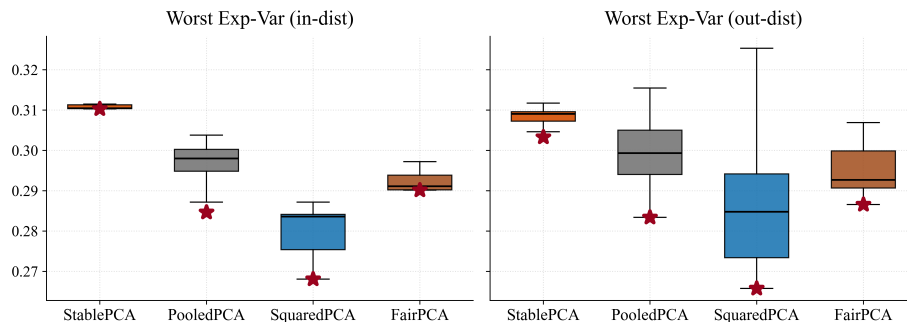


Figure 3: Worst-case explained variance of StablePCA, PooledPCA, SquaredPCA, and FairPCA on the single-cell RNA dataset. Left: worst-case explained variance among the training batches (in-dist). Right: worst-case explained variance among the held-out batches (out-dist). Each boxplot summarizes the results across 200 random train-test splits. The red stars indicate the lowest worst-case explained variance observed among the 200 splits.

Figure 3 summarizes the results across 200 random train-test splits, where we normalize the worst-case explained variance by dividing by the maximum scale $\max_{l \in [12]} \|\hat{\Sigma}^{(l)}\|_{\text{op}}$ among 12 experimental batches. Overall, StablePCA consistently achieves the highest worst-case explained variance on both training batches (left panel) and test batches (right panel), indicating that its extracted representations generalize not only to the training batches but

also remain stable to unseen batches.

We further examine the performance under the most challenging configurations among the 200 train-test splits. The red stars in Figure 3 represent the lowest worst-case explained variances across all 200 splits. In particular, on the held-out batches (right panel), StablePCA achieves approximately 7.0% higher worst-case explained variance than PooledPCA, 14.1% higher than SquaredPCA, and 5.8% higher than FairPCA. These results suggest that StablePCA maintains superior performance under the most challenging settings.

Next, we perform downstream visualizations based on the low-dimensional representations extracted by StablePCA. For multi-batch single-cell data, a desirable visualization on their pooled dataset should separate cells by biological cell types (not used for training) but not by the batch identities. In other words, the representations should preserve biological structure while reducing batch effects. We apply t-SNE (Maaten & Hinton 2008) and UMAP (Healy & McInnes 2024) to the representations learned by StablePCA with $k = 50$, while the results for other k 's are deferred to Appendix D.2. For clarity, we focus on four major immune cell types: B cells, NK cells, Monocytes, and T cells. Other annotated cell populations are excluded either because they contain very small numbers of cells or correspond to transitional, progenitor, or rare cell states (e.g., erythroid precursors, cycling progenitors, or dendritic subtypes).

Figure 4 shows the sample points visualized by t-SNE and UMAP colored by the batch identity and cell type. When colored by batch (top row), cells from 12 different experimental batches are well mixed, indicating that the representations learned by StablePCA effectively suppress batch effects. When colored by cell type (bottom row), the four major cell type samples form coherent clusters for both t-SNE and UMAP. We note the partial overlap between NK cells and T cells, which is expected, since NK cells and cytotoxic T cells share overlapping transcriptional programs and are difficult to be perfectly separated using

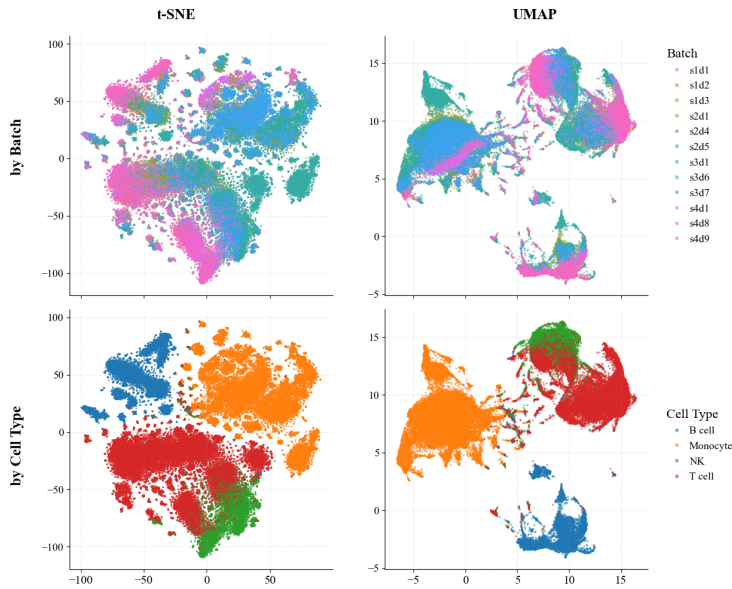


Figure 4: t-SNE and UMAP visualizations of the StablePCA embedding with target dimension $k = 50$ on the single-cell RNA dataset. Top row: cells colored by 12 experimental batches. Bottom row: cells colored by cell types (B cell, Monocyte, NK cell, and T cell).

RNA expression alone. Apart from the partial overlap between NK cells and T cells, the other major cell types are well separated. In conclusion, these results demonstrate that StablePCA effectively removes batch-specific variations, while preserving biologically meaningful structures to distinguish the major cell types.

9 Conclusions and Discussions

This work proposes StablePCA, a distributionally robust framework for extracting stable low-dimensional representations from multi-source feature data. To address the nonconvex rank constraint in the original formulation, we reformulate the problem via a convex Fantope relaxation. We then develop a computationally efficient Mirror-Prox algorithm to solve the relaxed problem, with provable convergence guarantees. Since the relaxed problem may differ from the original formulation, we provide a data-dependent certificate to assess how well the algorithm solves the original nonconvex problem.

As an extension, in the high-dimensional setting, one may consider a sparse StablePCA by introducing an ℓ_1 -type regularization, inspired by the sparse PCA formulation (Vu et al. 2013). Developing efficient algorithms and establishing corresponding theoretical guarantees for this sparse variant remain interesting directions for future research.

The proposed framework can be adapted to a stable Canonical Correlation Analysis (CCA) setting, building on the classical CCA formulation (Hotelling 1992) (see also recent work of sparse CCA (Gao et al. 2017)), where the goal is to seek low-dimensional representations of two feature sets whose correlations remain stable across multiple sources. As in StablePCA, the presence of rank constraints leads to a nonconvex minimax formulation. A natural extension of our approach is to design a computationally efficient Mirror-Prox algorithm for a convex relaxation of the stable CCA minimax problem. We leave the detailed development of this extension to future work.

10 Disclosure statement

The authors have the following conflicts of interest to declare.

SUPPLEMENTARY MATERIAL

Title: Supplements to “StablePCA”. The supplementary material contains additional theoretical results, methodologies, numerical results, and proofs.

References

- Awasthi, P., Kale, S. & Pensia, A. (2024), Semi-supervised group dro: Combating sparsity with unlabeled data, *in* ‘International Conference on Algorithmic Learning Theory’, PMLR, pp. 125–160.
- Bubeck, S. et al. (2015), ‘Convex optimization: Algorithms and complexity’, *Foundations and Trends® in Machine Learning* **8**(3-4), 231–357.
- Dattorro, J. (2010), *Convex Optimization & Euclidean Distance Geometry*, Lulu.com.
- Fan, J., Fang, C., Gu, Y. & Zhang, T. (2024), ‘Environment invariant linear least squares’, *The Annals of Statistics* **52**(5), 2268–2292.

- Fan, K. (1949), ‘On a theorem of Weyl concerning eigenvalues of linear transformations i’, *Proceedings of the National Academy of Sciences* **35**(11), 652–655.
- Gao, C., Ma, Z. & Zhou, H. H. (2017), ‘Sparse CCA: Adaptive estimation and computational barriers’.
- Guo, Z. (2023), ‘Statistical inference for maximin effects: Identifying stable associations across multiple studies’, *Journal of the American Statistical Association* pp. 1–17.
- Guo, Z., Li, X., Han, L. & Cai, T. (2025), ‘Robust inference for federated meta-learning’, *Journal of the American Statistical Association* pp. 1–16.
- Hari, S. N., Van Allen, E., Nyman, J., Mehta, N., Jiang, B., Elmarakeby, H., Dietlein, F., Rosenthal, J., Sengupta, E., Umeton, R. et al. (2021), Using distributionally robust optimization to improve robustness in cancer pathology, in ‘NeurIPS 2021 Workshop on Distribution Shifts: Connecting Methods and Applications’.
- Hastie, T., Tibshirani, R., Friedman, J. et al. (2009), ‘The elements of statistical learning’.
- Healy, J. & McInnes, L. (2024), ‘Uniform manifold approximation and projection’, *Nature Reviews Methods Primers* **4**(1), 82.
- Hicks, S. C., Townes, F. W., Teng, M. & Irizarry, R. A. (2018), ‘Missing data and technical variability in single-cell rna-sequencing experiments’, *Biostatistics* **19**(4), 562–578.
- Hong, C., Rush, E., Liu, M., Zhou, D., Sun, J., Sonabend, A., Castro, V. M., Schubert, P., Panickan, V. A., Cai, T. et al. (2021), ‘Clinical knowledge extraction via sparse embedding regression (keser) with multi-center large scale electronic health record data’, *NPJ digital medicine* **4**(1), 1–11.
- Hotelling, H. (1992), Relations between two sets of variates, in ‘Breakthroughs in statistics: methodology and distribution’, Springer, pp. 162–190.
- Hu, W., Niu, G., Sato, I. & Sugiyama, M. (2018), Does distributionally robust supervised learning give robust classifiers?, in ‘International Conference on Machine Learning’, PMLR, pp. 2029–2037.
- Jolliffe, I. (2011), Principal component analysis, in ‘International encyclopedia of statistical science’, Springer, pp. 1094–1096.
- Kleindessner, M., Donini, M., Russell, C. & Zafar, M. B. (2023), Efficient fair PCA for fair representation learning, in ‘International Conference on Artificial Intelligence and Statistics’, PMLR, pp. 5250–5270.
- Li, M., Li, X., Pan, K., Geva, A., Yang, D., Sweet, S. M., Bonzel, C.-L., Ayakulangara Panickan, V., Xiong, X., Mandl, K. et al. (2024), ‘Multisource representation learning for pediatric knowledge extraction from electronic health records’, *NPJ Digital Medicine* **7**(1), 319.
- Li, S., Cai, T. T. & Li, H. (2022), ‘Transfer learning for high-dimensional linear regression: Prediction, estimation and minimax optimality’, *Journal of the Royal Statistical Society Series B: Statistical Methodology* **84**(1), 149–173.
- Luecken, M. D., Burkhardt, D. B., Cannoodt, R., Lance, C., Agrawal, A., Aliee, H., Chen, A. T., Deconinck, L., Detweiler, A. M., Granados, A. A. et al. (2021), A sandbox for prediction and integration of dna, rna, and proteins in single cells, in ‘35th conference on neural information processing systems (NeurIPS 2021) track on datasets and benchmarks’.
- Maaten, L. v. d. & Hinton, G. (2008), ‘Visualizing data using t-sne’, *Journal of machine learning research* **9**(Nov), 2579–2605.

- Maity, S., Sun, Y. & Banerjee, M. (2022), ‘Meta-analysis of heterogeneous data: integrative sparse regression in high-dimensions’, *Journal of Machine Learning Research* **23**(198), 1–50.
- Mokhtari, A., Ozdaglar, A. & Pattathil, S. (2020), A unified analysis of extra-gradient and optimistic gradient methods for saddle point problems: Proximal point approach, *in* ‘International Conference on Artificial Intelligence and Statistics’, PMLR, pp. 1497–1507.
- Nemirovski, A. (2004), ‘Prox-method with rate of convergence $o(1/t)$ for variational inequalities with lipschitz continuous monotone operators and smooth convex-concave saddle point problems’, *SIAM Journal on Optimization* **15**(1), 229–251.
- Olfat, M. & Aswani, A. (2019), Convex formulations for fair principal component analysis, *in* ‘Proceedings of the AAAI Conference on Artificial Intelligence’, Vol. 33, pp. 663–670.
- Ouyang, Y. & Xu, Y. (2021), ‘Lower complexity bounds of first-order methods for convex-concave bilinear saddle-point problems’, *Mathematical Programming* **185**(1), 1–35.
- Peters, J., Bühlmann, P. & Meinshausen, N. (2016), ‘Causal inference by using invariant prediction: identification and confidence intervals’, *Journal of the Royal Statistical Society Series B: Statistical Methodology* **78**(5), 947–1012.
- Sagawa, S., Koh, P. W., Hashimoto, T. B. & Liang, P. (2019), ‘Distributionally robust neural networks for group shifts: On the importance of regularization for worst-case generalization’, *arXiv preprint arXiv:1911.08731* .
- Samadi, S., Tantipongpipat, U., Morgenstern, J. H., Singh, M. & Vempala, S. (2018), ‘The price of fair PCA: One extra dimension’, *Advances in Neural Information Processing Systems* **31**.
- Shen, J., Davis, A. J., Lu, D. & Bai, Z. (2025), ‘Hidden convexity of fair pca and fast solver via eigenvalue optimization’, *arXiv preprint arXiv:2503.00299* .
- Sion, M. (1958), ‘On general minimax theorems.’, *Pacific Journal of Mathematics* **8**(1), 171–176.
- Tian, Y. & Feng, Y. (2023), ‘Transfer learning under high-dimensional generalized linear models’, *Journal of the American Statistical Association* **118**(544), 2684–2697.
- Tran, H. T. N., Ang, K. S., Chevrier, M., Zhang, X., Lee, N. Y. S., Goh, M. & Chen, J. (2020), ‘A benchmark of batch-effect correction methods for single-cell RNA sequencing data’, *Genome Biology* **21**, 1–32.
- Vershynin, R. (2018), *High-dimensional Probability: An Introduction with Applications in Data Science*, Vol. 47, Cambridge University Press.
- Vu, V. Q., Cho, J., Lei, J. & Rohe, K. (2013), ‘Fantope projection and selection: A near-optimal convex relaxation of sparse PCA’, *Advances in Neural Information Processing Systems* **26**.
- Wang, Z., Bühlmann, P. & Guo, Z. (2025), ‘Distributionally robust learning for multi-source unsupervised domain adaptation’, *The Annals of Statistics* . to appear.
- Wang, Z., Hu, Y., Bühlmann, P. & Guo, Z. (2024), ‘Causal invariance learning via efficient optimization of a nonconvex objective’, *arXiv preprint arXiv:2412.11850* .
- Wolf, F. A., Angerer, P. & Theis, F. J. (2018), ‘Scanpy: large-scale single-cell gene expression data analysis’, *Genome biology* **19**(1), 15.
- Zhang, Z., Zhan, W., Chen, Y., Du, S. S. & Lee, J. D. (2024), Optimal multi-distribution learning, *in* ‘Conference on Learning Theory’, PMLR, pp. 5220–5223.

Supplements to “StablePCA”.

We provide a detailed Table of Contents for the Appendix below to facilitate navigation of the supplementary materials.

A	Additional Results	2
A.1	Incorporation of Target Information to StablePCA	2
A.2	Additional Discussions on Fantope Relaxation	3
A.3	Additional Discussions on Alternative Robust Multi-source PCA	6
A.4	Introduction of Mirror Updates	9
A.5	Mirror-Prox for General Convex-Concave Minimax Problems	12
B	Proof of Main Theoretical Results	15
B.1	Proof of Proposition 1	15
B.2	Proof of Theorem 1	20
B.3	Proof of Theorem 2	20
B.4	Proof of Theorem 3	22
B.5	Proof of Theorem 4	23
B.6	Proof of Theorem 5	24
B.7	Proof of Theorem 6	27
B.8	Proof of Theorem 7	28
C	Proof of Technical Lemmas	29

C.1	Proof of Lemma 1	29
C.2	Proof of Lemma 2	30
C.3	Proof of Lemma 3	31
C.4	Proof of Lemma 4	32
C.5	Proof of Lemma 6	39
C.6	Proof of Lemma 8	39
C.7	Proof of Lemma 10	42
C.8	Proof of Lemma 11	42
D	Additional Simulated Experiments and Real Applications	45
D.1	Additional Simulated Experiments	45
D.2	Additional Results for Real Applications	48
D.3	Omitted Experimental Setups	49

A Additional Results

A.1 Incorporation of Target Information to StablePCA

In Section 2.2, we use \mathcal{C} to account for the uncertainty about the unknown target distribution, which comprises all mixtures of the source distributions. In practice, one may not need robustness against all mixtures of source distributions but may wish to perform well on a specific target distribution. Such a preference can be incorporated into the StablePCA formulation. For example, suppose domain expertise suggests that the target distribution closely resembles a particular mixture of the sources with a prior weight vector $\omega^{\text{prior}} \in \Delta^L$. Alternatively, one may have access to a small amount of target data, which can be used to form a crude estimate of the mixture

weights. In either case, rather than optimizing over the entire simplex Δ^L , we may restrict the mixture weights to lie in a neighborhood of ω^{prior} , denoted as $\mathcal{H} = \{\omega \in \Delta^L \mid \|\omega - \omega^{\text{prior}}\|_2 \leq \rho\}$, where $\rho > 0$ encodes the level of confidence in the prior or in the estimated weights. We then refine the uncertainty set to $\mathcal{C}_{\mathcal{H}} := \{\mathbb{Q} : \mathbb{Q} = \sum_{l=1}^L \omega_l \cdot \mathbb{T}^{(l)} \text{ with } \omega \in \mathcal{H} \subseteq \Delta^L\}$. We may extend the definition in (4) by incorporating prior information as follows:

$$\arg \max_{P \in \mathcal{P}^k} \min_{\mathbb{Q} \in \mathcal{C}_{\mathcal{H}}} \mathbb{E}_{X \sim \mathbb{Q}} (\|X\|_2^2 - \|X - PX\|_2^2) = \arg \max_{P \in \mathcal{P}^k} \min_{\omega \in \mathcal{H}} \sum_{l=1}^L \omega_l \cdot \langle \Sigma^{(l)}, P \rangle.$$

A.2 Additional Discussions on Fantope Relaxation

We now provide additional discussions supplementing the results in Section 5. Specifically, Section A.2.1 studies the properties of the function $\phi(\omega)$ defined in (22). Section A.2.2 provides the detailed implementation to solve $\min_{\omega \in \Delta^L} \phi(\omega)$. Lastly, Section A.2.3 shows that the output \hat{P}_T of Algorithm 1 not only globally solves the original StablePCA problem in terms of the objective value, but also converges to the optimal solution of the original StablePCA problem.

A.2.1 Properties of the Function $\phi(\omega)$

The following lemma establishes that $\phi(\omega)$ is convex. The proof is provided in Appendix C.1.

Lemma 1. *The function $\phi(\omega)$ defined in (22) is continuous and convex over Δ^L , and it is differentiable at any ω for which $\lambda_k(\Sigma(\omega)) > \lambda_{k+1}(\Sigma(\omega))$, where $k > 0$ is the pre-specified targeted low dimension.*

We illustrate the convexity of $\phi(\omega)$ when $L = 2$ in Figure 5. The exact experimental setup is deferred to Appendix D.3.

By Lemma 1, the function $\phi(\omega)$ is convex but *not differentiable* everywhere. Nevertheless, it admits an explicit subgradient characterization, which enables efficient first-order algorithms to solve $\min_{\omega} \phi(\omega)$. The following lemma provides the expression for a subgradient of $\phi(\omega)$, whose proof is deferred to Appendix C.2.

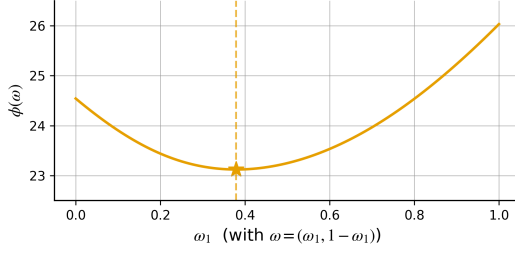


Figure 5: Illustration of $\phi(\omega)$ for $L = 2$. The minimizer ω^* is highlighted by a star marker. The exact experimental setup is deferred to Appendix D.3.

Lemma 2. For any $\omega \in \Delta^L$, let $V(\omega) \in \mathcal{O}^{d \times k}$ be the top- k eigenvectors of $\Sigma(\omega)$. Then the vector $g(\omega) = (g_1(\omega), \dots, g_L(\omega)) \in \mathbb{R}^L$ with coordinates

$$g_l(\omega) := \langle \Sigma^{(l)}, V(\omega)(V(\omega))^\top \rangle, \quad l = 1, \dots, L,$$

is a subgradient of ϕ at ω , i.e.,

$$\phi(\omega') \geq \phi(\omega) + \langle g(\omega), \omega' - \omega \rangle, \quad \forall \omega' \in \Delta^L.$$

A.2.2 Algorithm to minimize $\phi(\omega)$

This subsection details the algorithm to compute the optimal weight vector $\omega^* \in \arg \min_{\omega} \phi(\omega)$ in (22). For clarity, we describe the algorithm at the population level, while the same procedure can be applied to empirical second-moment matrices obtained from finite samples in practice.

We now present the algorithm for solving the convex problem $\min_{\omega \in \Delta^L} \phi(\omega)$. As in Algorithm 1, we employ mirror updates to respect the geometry of the simplex constraint $\omega \in \Delta^L$. However, since $\phi(\omega)$ is a non-differentiable convex function, as shown in Lemma 1, the updates here use the subgradients specified in Lemma 2, rather than the gradients.

We initialize $\omega^0 = \frac{1}{L} \mathbf{1}_L \in \Delta^L$. For each iteration $t = 0, 1, \dots, T - 1$, given the weight vector ω^t , we compute $V^t \in \mathcal{O}^{d \times k}$, the top- k eigenvectors of $\Sigma(\omega^t)$. By Lemma 2, this yields a subgradient g^t of $\phi(\omega^t)$ as follows:

$$g_l^t = \langle \Sigma^{(l)}, V^t(V^t)^\top \rangle, \quad l = 1, \dots, L. \quad (27)$$

Given the step size $\eta > 0$, we perform a mirror update over the constraint $\omega \in \Delta^L$:

$$\omega^{t+1} = \arg \min_{\omega \in \Delta^L} \left\{ \eta \langle g_l^t, \omega \rangle + D_{\psi_2}(\omega, \omega^t) \right\},$$

where $D_{\psi_2}(\omega, \omega^t) = \sum_{l=1}^L \omega_l \log \frac{\omega_l}{\omega_l^t}$ is the Bregman divergence associated with the simplex Δ^L , defined in (12). This update admits a closed-form solution:

$$\omega_l^{t+1} = \frac{\omega_l^t \exp\{-\eta g_l^t\}}{\sum_{r=1}^L \omega_r^t \exp\{-\eta g_r^t\}}, \quad l = 1, \dots, L. \quad (28)$$

The derivation of (28) follows from standard mirror descent updates on the simplex; see Chapter 4 of [Bubeck et al. \(2015\)](#) for details.

With slight abuse of notation, after T iterations, we form the averaged iterate

$$\hat{\omega}_T := \frac{1}{T} \sum_{t=0}^{T-1} \omega^t,$$

as the output to approximately solve the optimization problem in (22). We summarize the overall procedure in [Algorithm 2](#).

Algorithm 2: Algorithm to minimize $\phi(\omega)$ for $\omega \in \Delta^L$

Data: Second-moment Matrices $\{\Sigma^{(l)}\}_{l=1}^L$; target dimension k ; step size η ; iterations T

Initialize $\omega^0 = \frac{1}{L} \mathbf{1}_L \in \Delta^L$;

for $t = 0, \dots, T - 1$ **do**

Compute the top- k eigenvectors V^t of $\Sigma(\omega^t) = \sum_{l=1}^L \omega_l^t \Sigma^{(l)}$;

Compute the subgradient g^t as in (27);

Update ω^{t+1} by mirror update in (28);

end

Set $\hat{\omega}_T = \frac{1}{T} \sum_{t=0}^{T-1} \omega^t$.

return $\hat{\omega}_T$

A.2.3 Estimator Convergence under the Eigengap Condition

While the result (23) establishes that \hat{P}_T globally solves the original StablePCA problem in terms of the objective value, the following theorem further suggests that \hat{P}_T converges to the

optimal solution of the original StablePCA problem. Specifically, if there exists an ω^* defined in (22) satisfying $\lambda_k(\Sigma(\omega^*)) - \lambda_{k+1}(\Sigma(\omega^*)) > 0$, Theorem 4 implies that there exists an optimal solution P^* to the original StablePCA problem in the form of the projection matrix onto the top- k eigenspace of $\Sigma(\omega^*)$. The following theorem characterizes the distance between the output \hat{P}_T of Algorithm 1 and this particular P^* . The proof is provided in Appendix B.7.

Theorem 6. *If there exists an ω^* defined in (22) satisfying $\lambda_k(\Sigma(\omega^*)) - \lambda_{k+1}(\Sigma(\omega^*)) > 0$, and the conditions of Theorem 3 are satisfied. Then, for any value $t \in [0, n - d]$, with probability at least $1 - 2Le^{-t}$,*

$$\|\hat{P}_T - P^*\|_F^2 \leq C \rho_{\max} \frac{k}{\lambda_k(\Sigma(\omega^*)) - \lambda_{k+1}(\Sigma(\omega^*))} \left(\sqrt{\frac{d+t}{n}} + \frac{\sqrt{k \log(d/k) \log L}}{T} \right),$$

where $C > 0$ denotes a universal constant.

This theorem establishes that the output \hat{P}_T converges to the optimal solution P^* of the original StablePCA problem as both the sample size n and the number of iterations T increase, provided the additional eigengap condition. We note that the (n, d) dependence might be suboptimal and could potentially be improved in future work.

A.3 Additional Discussions on Alternative Robust Multi-source PCA

This subsection collects additional discussions about SquaredPCA and FairPCA omitted from the main text. We first clarify the equivalence of our FairPCA formulation in (25) and the existing FairPCA literature in Section A.3.1. We then extend Mirror-Prox Algorithm 1 to solve SquaredPCA and FairPCA in Section A.3.2. Lastly, we revisit the example in Section 2.3 and provide a geometric comparison among SquaredPCA, FairPCA and our proposed StablePCA.

A.3.1 Equivalence between FairPCA Formulations

The following lemma shows that the FairPCA objective, originally defined via a worst-case distribution over the uncertainty class \mathcal{C} , admits an equivalent formulation as a worst-case regret over the individual source distributions. The proof is provided in Appendix C.3.

Lemma 3. *Let \mathcal{C} be the uncertainty class defined in (3), and let P^{fair} be defined in (25). Then*

$$P^{\text{fair}} \in \arg \min_{P \in \mathcal{P}^k} \max_{\mathbb{Q} \in \mathcal{C}} \text{Regret}_{\mathbb{Q}}(P) = \arg \min_{P \in \mathcal{P}^k} \max_{l \in [L]} \text{Regret}_{\mathbb{T}^{(l)}}(P).$$

As an immediate corollary, when there are only two source distributions $\{\mathbb{T}^{(1)}, \mathbb{T}^{(2)}\}$ with $L = 2$, the FairPCA solution satisfies

$$P^{\text{fair}} \in \arg \min_{P \in \mathcal{P}^k} \max \{ \text{Regret}_{\mathbb{T}^{(1)}}(P), \text{Regret}_{\mathbb{T}^{(2)}}(P) \}.$$

This coincides exactly with the original FairPCA formulation studied in the prior works (Samadi et al. 2018, Shen et al. 2025).

A.3.2 Fantope-relaxation of SquaredPCA and FairPCA

Analogous to StablePCA, we conduct Fantope relaxation on SquaredPCA and FairPCA as well, by replacing $P \in \mathcal{P}^k$ to its convex hull $M \in \mathcal{F}^k$. For notation convenience, given the covariance matrices $\{\Sigma^{(l)}\}_{l=1}^L$, for any $\omega \in \Delta^L$, we define

$$\Sigma^{\text{sq}}(\omega) := \Sigma^{(l)} - \frac{1}{k} \sum_{i=1}^d \lambda_i^{(l)} \mathbf{I}_d, \quad \text{and} \quad \Sigma^{\text{fair}}(\omega) := \Sigma^{(l)} - \frac{1}{k} \sum_{i=1}^k \lambda_i^{(l)} \mathbf{I}_d, \quad (29)$$

where $\lambda_i^{(l)}$ denotes the i -th largest eigenvalue of $\Sigma^{(l)}$, for each $l \in [L]$.

It follows from Proposition 2 that, the Fantope-relaxed SquaredPCA and FairPCA are defined as follows:

$$M^{\text{sq}} \in \arg \max_{M \in \mathcal{F}^k} \min_{\omega \in \Delta^L} \langle \Sigma^{\text{sq}}(\omega), M \rangle, \quad (30)$$

and

$$M^{\text{fair}} \in \arg \max_{M \in \mathcal{F}^k} \min_{\omega \in \Delta^L} \langle \Sigma^{\text{fair}}(\omega), M \rangle. \quad (31)$$

As discussed in the main text, they differ from Fantope-relaxed StablePCA (8) only by the subtraction terms. Therefore, we can extend the proposed Algorithm 1 to solve M^{sq} and M^{fair} , analogous to StablePCA.

We summarize the procedure for solving SquaredPCA and FairPCA problems in Algorithm 3.

Algorithm 3: Mirror-Prox Algorithm for SquaredPCA and FairPCA

Data: Empirical matrices $\{\widehat{\Sigma}^{(l)}\}_{l=1}^L$; target dimension k ; step sizes η_M, η_ω ; iterations T

for $l = 1, \dots, L$ **do**

 | Compute the eigenvalues of $\widehat{\Sigma}^{(l)}$: $\widehat{\lambda}_1^{(l)} \geq \dots \geq \widehat{\lambda}_d^{(l)}$;

end

if SquaredPCA **then**

 | Run Algorithm 1 with the input $\widehat{\Sigma}^{(l)}$ replaced by $\widehat{\Sigma}^{(l)} - \frac{1}{k} \sum_{i=1}^d \widehat{\lambda}_i^{(l)} \mathbf{I}_d$;

end

else if FairPCA **then**

 | Run Algorithm 1 with the input $\widehat{\Sigma}^{(l)}$ replaced by $\widehat{\Sigma}^{(l)} - \frac{1}{k} \sum_{i=1}^k \widehat{\lambda}_i^{(l)} \mathbf{I}_d$.

end

A.3.3 Geometric Interpretation: Difference among Robust Multi-source PCAs

Having described how SquaredPCA, FairPCA and StablePCA can be solved within a unified Mirror-Prox algorithm, we now turn to a geometric comparison of these methods. We revisit the example in Section 2.3, where we compare their estimated principal component (PC) under two-types of changes: varying sample-size ratios across sources (Settings 1 vs. 2) and varying source-specific relationships between covariates (Settings 2 vs. 3). The only modification from the earlier setup is the noise level in the data-generating model (6), where $\epsilon^{(l)} \sim \mathcal{N}(0, [\sigma^{(l)}]^2)$ in (6) with $\sigma^{(1)} = 1$, $\sigma^{(2)} = 0.6$, and $\sigma^{(3)} = 0.3$. This modification introduces heterogeneous scales across source feature vectors.

As illustrated in Figure 6, StablePCA is the only method among the three that consistently recovers the shared principal component along X_1 across all settings. When comparing the leftmost and middle panels (Settings 1 vs. 2), we observe that all three methods remain unchanged, indicating that their distributionally robust designs make them insensitive to changes in sample-size ratios across sources. By contrast, the middle and right panels (Settings 2 vs. 3) reveal that SquaredPCA and FairPCA vary substantially when the source-specific relationships between covariates change.

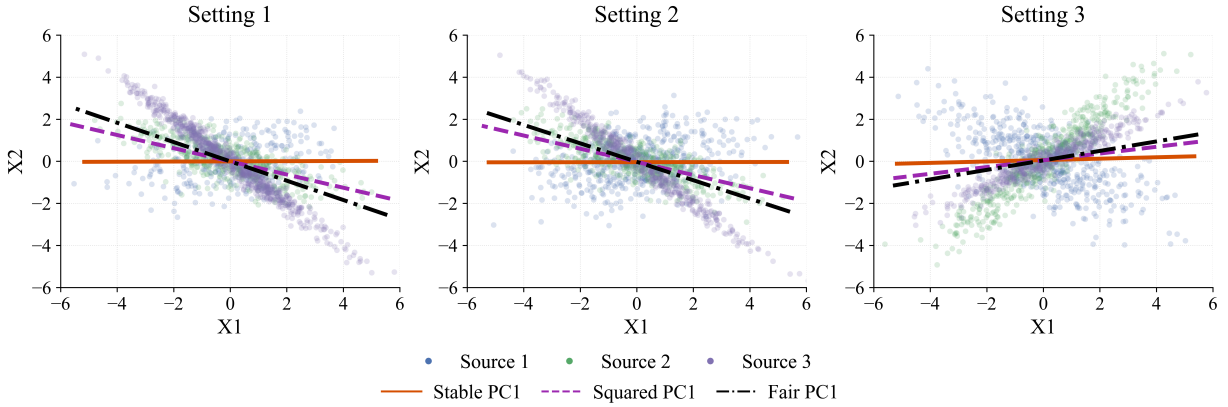


Figure 6: Comparison of the first principal component estimated by StablePCA, SquaredPCA and FairPCA across Settings 1, 2, and 3, described in Section 2.3. Settings 1 and 2 differ only in sample-size ratios among sources, under which all three methods do not change across two settings. In contrast, Settings 2 and 3 differ only in the source-specific relationship between X_1 and X_2 , where SquaredPCA and FairPCA change substantially, while StablePCA remains stable.

We emphasize that these differences in Figure 6 do not imply that one method is uniformly superior to the others. Rather, SquaredPCA, FairPCA, and StablePCA are formulated with distinct objectives, and this example highlights how the choice of loss function leads to geometric structure. And we show that under this specific example, StablePCA is able to capture the shared direction across sources, while the alternative formulations do not. Further empirical comparisons of these methods are provided in Sections 7 and 8.

A.4 Introduction of Mirror Updates

This subsection briefly reviews Bregman divergences and mirror-based updates, which form the algorithmic foundation of our optimization procedure in Section 3.2. A comprehensive introduction can be found in Chapter 4 of [Bubeck et al. \(2015\)](#).

We present the main insight of the mirror-based updates. It generalizes classical (projected) gradient descent by allowing *optimization in non-Euclidean geometries*. Rather than performing a

gradient step followed by a potentially expensive Euclidean projection, mirror updates linearize the objective in the primal space while measuring proximity between iterates in a dual space induced by a strictly convex mirror map. This dual space is chosen to match the structure of the constraint set so that feasibility is enforced implicitly through the mirror map rather than through explicit projection. As a result, mirror updates often admit simple closed-form solutions on structured domains such as simplices or spectrahedra.

Definition 1 (Mirror Map and Bregman Divergence). *Let $\mathcal{D} \subseteq \mathbb{R}^m$ be a convex set. A function $\psi : \mathcal{D} \rightarrow \mathbb{R}$ is called a **mirror map** if it is strictly convex and continuously differentiable on \mathcal{D} . The **Bregman divergence** induced by ψ is defined as*

$$D_\psi(x, y) := \psi(x) - \psi(y) - \langle \nabla \psi(y), x - y \rangle, \quad (32)$$

for any $x, y \in \mathcal{D}$.

Unlike the squared Euclidean distance $\|x - y\|_2^2$, the Bregman divergence is generally asymmetric and adapts to the geometry of the constraint set. In this work, we choose mirror maps $\psi_1(M) = \text{Tr}(M \log M)$ for Fantope $M \in \mathcal{F}^k$ and $\psi_2(\omega) = \sum_{l=1}^L \omega_l \log \omega_l$ for simplex $\omega \in \Delta^L$. We subsequently derive their associated Bregman divergences as specified in (12).

Derivation of $D_{\psi_1}(M, M')$.

For $M, M' \in \mathcal{F}^k$, recall

$$D_{\psi_1}(M, M') = \psi_1(M) - \psi_1(M') - \langle \nabla \psi_1(M'), M - M' \rangle, \quad \nabla \psi_1(M') = \log M' + I.$$

Using $\text{Tr}(M) = \text{Tr}(M') = k$, we have $\langle I, M - M' \rangle = \text{Tr}(M - M') = 0$, hence

$$D_{\psi_1}(M, M') = \text{Tr}(M \log M) - \text{Tr}(M \log M') - \text{Tr}(M') + \text{Tr}(M') = \text{Tr}(M \log M) - \text{Tr}(M \log M').$$

Derivation of $D_{\psi_2}(\omega, \omega')$.

For $\omega, \omega' \in \Delta^L$, it holds

$$\begin{aligned} D_{\psi_2}(\omega, \omega') &= \psi_2(\omega) - \psi_2(\omega') - \langle \nabla \psi_2(\omega'), \omega - \omega' \rangle \\ &= \sum_{l=1}^L \omega_l \log \omega_l - \sum_{l=1}^L \omega'_l \log \omega'_l - \sum_{l=1}^L (\log \omega'_l + 1)(\omega_l - \omega'_l) \\ &= \sum_{l=1}^L \omega_l \log \frac{\omega_l}{\omega'_l} =: \text{KL}(\omega \parallel \omega'). \end{aligned}$$

Throughout this subsection, we consider a convex function $f : \mathcal{D} \rightarrow \mathbb{R}$, with a subgradient $\partial f(\cdot)$, and we aim to minimize it with $\min_{x \in \mathcal{D}} f(x)$. We now introduce the mirror descent update to solve it.

Definition 2 (Mirror Descent Update). *Let $x^t \in \mathcal{D}$ be the current iterate. The mirror descent update is defined as*

$$x^{t+1} = \arg \min_{x \in \mathcal{D}} \left\{ \eta \langle \partial f(x^t), x \rangle + D_{\psi}(x, x^t) \right\}. \quad (33)$$

The update in (33) trades off descent in the linearized objective against proximity to the previous iterate, where proximity is measured in the geometry induced by the mirror map ψ . Different choices of ψ yield different algorithms that are tailored to the structure of \mathcal{D} .

We present a concrete case to better illustrate how mirror descent adapts to the constraints, in contrast to projected (sub)gradient descent.

Example 1 (Simplex Constraint). *Suppose the constraint set is the probability simplex $\mathcal{D} = \Delta^m$. If one applies projected subgradient descent with step size $\eta > 0$, the update takes the form*

$$x^{t+1} = \Pi_{\Delta^m}(x^t - \eta \partial f(x^t)),$$

where Π_{Δ^m} denotes the Euclidean projection onto the simplex. This update performs a subgradient step in the ambient Euclidean space \mathbb{R}^m , followed by an explicit projection to restore feasibility. Computing Π_{Δ^m} requires solving a constrained quadratic program, which typically involves sorting and thresholding operations.

In contrast, mirror descent incorporates the geometry of the simplex directly through the choice of the mirror map. Taking the entropy mirror map $\psi(x) = \sum_{j=1}^m x_j \log x_j$, the corresponding Bregman

divergence is the Kullback–Leibler divergence $D_\psi(x, y) = \sum_{j=1}^m x_j \log \frac{x_j}{y_j}$. The mirror descent update (33) becomes

$$x^{t+1} = \arg \min_{x \in \Delta^m} \left\{ \eta \langle \partial f(x^t), x \rangle + \sum_{j=1}^m x_j \log \frac{x_j}{x_j^t} \right\},$$

which admits the closed-form solution

$$x_j^{t+1} = \frac{x_j^t \exp(-\eta[\partial f(x^t)]_j)}{\sum_{s=1}^m x_s^t \exp(-\eta[\partial f(x^t)]_s)}, \quad j = 1, \dots, m. \quad (34)$$

This update naturally preserves feasibility and avoids explicit Euclidean projection onto the simplex.

Note that projected (sub)gradient descent arises as a special case of mirror descent when the mirror map is chosen as the squared Euclidean norm, $\psi(x) = \frac{1}{2}\|x\|_2^2$. In this case, the associated Bregman divergence reduces to

$$D_\psi(x, y) = \frac{1}{2}\|x - y\|_2^2,$$

and (33) becomes

$$\begin{aligned} x^{t+1} &= \arg \min_{x \in \mathcal{D}} \left\{ \eta \langle \partial f(x^t), x \rangle + \frac{1}{2}\|x - x^t\|_2^2 \right\} \\ &= \arg \min_{x \in \mathcal{D}} \left\{ \frac{1}{2}\|x - (x^t - \eta \partial f(x^t))\|_2^2 - \frac{1}{2}\eta^2 \|\partial f(x^t)\|_2^2 + \eta \langle \partial f(x^t), x^t \rangle \right\} \\ &= \arg \min_{x \in \mathcal{D}} \left\{ \frac{1}{2}\|x - (x^t - \eta \partial f(x^t))\|_2^2 \right\} \\ &= \Pi_{\mathcal{D}} \left(x^t - \eta \partial f(x^t) \right), \end{aligned}$$

where the third equality holds by removing constant terms regarding x . Therefore, the mirror descent with squared euclidean norm is precisely the projected (sub)gradient descent.

If, in addition, $\mathcal{D} = \mathbb{R}^m$ is applied without any constraint, then the update simplifies to

$$x^{t+1} = x^t - \eta \partial f(x^t),$$

recovering the classical (sub)gradient descent.

A.5 Mirror-Prox for General Convex-Concave Minimax Problems

This subsection reviews the Mirror-Prox algorithm for general smooth convex–concave minimax problems and states a standard $\mathcal{O}(1/T)$ convergence guarantee. Algorithm 1 is obtained by

specializing this result to the StablePCA objective in (11); consequently, Theorem 1 follows directly from the general result below. Our following discussions adapts follows Section 5.2.3 of [Bubeck et al. \(2015\)](#).

We start with the definition of a saddle point for a minimax problem.

Definition 3 (Saddle Point). *Let $f : \mathcal{X} \times \mathcal{Y} \rightarrow \mathbb{R}$ be a function. A point (x^*, y^*) is a saddle point of the minimax problem $\min_{x \in \mathcal{X}} \max_{y \in \mathcal{Y}} f(x, y)$, if*

$$f(x^*, y^*) = \max_{y \in \mathcal{Y}} f(x^*, y) = \min_{x \in \mathcal{X}} f(x, y^*).$$

Moreover, a point (\hat{x}, \hat{y}) is an ε -nearly saddle point of $f(\cdot, \cdot)$ if

$$0 \leq \max_{y \in \mathcal{Y}} f(\hat{x}, y) - \min_{x \in \mathcal{X}} f(x, \hat{y}) \leq \varepsilon.$$

Throughout this subsection, we aim to identify a (nearly) saddle point of the convex–concave minimax problem

$$\min_{x \in \mathcal{X}} \max_{y \in \mathcal{Y}} f(x, y),$$

where \mathcal{X} and \mathcal{Y} are compact convex sets, and

- for every fixed $y \in \mathcal{Y}$ the map $x \mapsto f(x, y)$ is convex on \mathcal{X} , and
- for every fixed $x \in \mathcal{X}$ the map $y \mapsto f(x, y)$ is concave on \mathcal{Y} .

Let \mathcal{X}, \mathcal{Y} be equipped with mirror maps: $\psi_{\mathcal{X}} : \mathcal{D}_{\mathcal{X}} \rightarrow \mathbb{R}$ and $\psi_{\mathcal{Y}} : \mathcal{D}_{\mathcal{Y}} \rightarrow \mathbb{R}$, respectively, with induced Bregman divergences $D_{\psi_{\mathcal{X}}}$ and $D_{\psi_{\mathcal{Y}}}$. Here, we use $\mathcal{D}_{\mathcal{X}}$ and $\mathcal{D}_{\mathcal{Y}}$ to denote the domain for mirror maps, which could be different from \mathcal{X}, \mathcal{Y} . We work on the product space $\mathcal{Z} := \mathcal{X} \times \mathcal{Y}$ with mirror map

$$\psi(z) := a \psi_{\mathcal{X}}(x) + b \psi_{\mathcal{Y}}(y), \quad z = (x, y) \in \mathcal{Z},$$

that is defined on $\mathcal{D}_{\mathcal{Z}} = \mathcal{D}_{\mathcal{X}} \times \mathcal{D}_{\mathcal{Y}}$, for fixed constants $a, b > 0$.

The associated Bregman divergence decomposes as

$$D_{\psi}(z, z') = a D_{\psi_{\mathcal{X}}}(x, x') + b D_{\psi_{\mathcal{Y}}}(y, y'), \quad z = (x, y), z' = (x', y').$$

Additionally, we define the monotone saddle-point operator

$$g(z) := (\nabla_x f(x, y), -\nabla_y f(x, y)), \quad z = (x, y) \in \mathcal{Z}. \quad (35)$$

We now describe the Mirror-Prox algorithm. We initialize at $z_0 \in \arg \min_{z \in \mathcal{Z} \cap \mathcal{D}_\psi} \psi(z)$. Given a step-size $\eta > 0$, for each iteration $t = 0, 1, \dots, T-1$, starting from the current iterate $z_t = (x_t, y_t)$, the first step computes the midpoint iterate $z_{t+\frac{1}{2}} = (x_{t+\frac{1}{2}}, y_{t+\frac{1}{2}})$ as follows:

$$z_{t+\frac{1}{2}} = \arg \min_{z \in \mathcal{Z} \cap \mathcal{D}_\psi} \eta \langle g(z_t), z \rangle + D_\psi(z, z_t). \quad (36)$$

The second step then updates the iterate using gradients evaluated at the midpoint $z_{t+\frac{1}{2}}$:

$$z_{t+1} = \arg \min_{z \in \mathcal{Z} \cap \mathcal{D}_\psi} \eta \langle g(z_{t+\frac{1}{2}}), z \rangle + D_\psi(z, z_t). \quad (37)$$

After completing T iterations, Mirror-Prox averages the midpoints $\{(x_{t+\frac{1}{2}}, y_{t+\frac{1}{2}})\}_{t=0}^{T-1}$ as the final output:

$$(\bar{x}_T, \bar{y}_T) := \left(\frac{1}{T} \sum_{t=0}^{T-1} x_{t+\frac{1}{2}}, \frac{1}{T} \sum_{t=0}^{T-1} y_{t+\frac{1}{2}} \right). \quad (38)$$

We next present the convergence analysis of the Mirror-Prox algorithm. We impose the following necessary conditions.

Condition 2. *Suppose that the mirror maps $\psi_{\mathcal{X}}(x), \psi_{\mathcal{Y}}(y)$ are strongly convex such that*

- $\psi_{\mathcal{X}}$ is $\mu_{\mathcal{X}}$ -strongly convex on $\mathcal{X} \cap \mathcal{D}_{\mathcal{X}}$ w.r.t. $\|\cdot\|_{\mathcal{X}}$. Define $R_{\mathcal{X}}^2 = \sup_{x \in \mathcal{X} \cap \mathcal{D}_{\mathcal{X}}} \psi_{\mathcal{X}}(x) - \inf_{x \in \mathcal{X} \cap \mathcal{D}_{\mathcal{X}}} \psi_{\mathcal{X}}(x)$.
- $\psi_{\mathcal{Y}}$ is $\mu_{\mathcal{Y}}$ -strongly convex on $\mathcal{Y} \cap \mathcal{D}_{\mathcal{Y}}$ w.r.t. $\|\cdot\|_{\mathcal{Y}}$. Define $R_{\mathcal{Y}}^2 = \sup_{y \in \mathcal{Y} \cap \mathcal{D}_{\mathcal{Y}}} \psi_{\mathcal{Y}}(y) - \inf_{y \in \mathcal{Y} \cap \mathcal{D}_{\mathcal{Y}}} \psi_{\mathcal{Y}}(y)$.

Moreover, the convex-concave function $f(x, y)$ is $(\beta_{11}, \beta_{12}, \beta_{21}, \beta_{22})$ -smooth, such that for any $x, x' \in \mathcal{X}$ and $y, y' \in \mathcal{Y}$,

$$\|\nabla_x f(x, y) - \nabla_x f(x', y)\|_{\mathcal{X},*} \leq \beta_{11} \|x - x'\|_{\mathcal{X}},$$

$$\|\nabla_x f(x, y) - \nabla_x f(x, y')\|_{\mathcal{X},*} \leq \beta_{12} \|y - y'\|_{\mathcal{Y}},$$

$$\|\nabla_y f(x, y) - \nabla_y f(x', y)\|_{\mathcal{Y},*} \leq \beta_{21} \|x - x'\|_{\mathcal{X}},$$

$$\|\nabla_y f(x, y) - \nabla_y f(x, y')\|_{\mathcal{Y},*} \leq \beta_{22} \|y - y'\|_{\mathcal{Y}}.$$

Here $\|\cdot\|_{\mathcal{X},*}$ and $\|\cdot\|_{\mathcal{Y},*}$ denote the dual norms of $\|\cdot\|_{\mathcal{X}}$ and $\|\cdot\|_{\mathcal{Y}}$, respectively, defined by

$$\|u\|_{\mathcal{X},*} := \sup_{\|x\|_{\mathcal{X}} \leq 1} \langle u, x \rangle, \quad \|v\|_{\mathcal{Y},*} := \sup_{\|y\|_{\mathcal{Y}} \leq 1} \langle v, y \rangle.$$

The following theorem establishes the convergence guarantee of the Mirror-Prox algorithm. The result is adapted from Theorem 5.2 of [Bubeck et al. \(2015\)](#). For completeness, we provide the proof in Section C.4, which is omitted in [Bubeck et al. \(2015\)](#).

Lemma 4. *Suppose Condition 2 holds. With the step size*

$$\eta = \frac{\mu_{\mathcal{X}} \wedge \mu_{\mathcal{Y}}}{2 \max \left\{ \frac{\beta_{11}}{a}, \frac{\beta_{22}}{b}, \frac{\beta_{12}}{\sqrt{ab}}, \frac{\beta_{21}}{\sqrt{ab}} \right\}},$$

the output (\bar{x}_T, \bar{y}_T) of Mirror-Prox algorithm satisfies:

$$\max_{y \in \mathcal{Y}} f(\bar{x}_T, y) - \min_{x \in \mathcal{X}} f(x, \bar{y}_T) \leq 2 \max \left\{ \frac{\beta_{11}}{a}, \frac{\beta_{22}}{b}, \frac{\beta_{12}}{\sqrt{ab}}, \frac{\beta_{21}}{\sqrt{ab}} \right\} \frac{aR_{\mathcal{X}}^2 + bR_{\mathcal{Y}}^2}{\mu_{\mathcal{X}} \wedge \mu_{\mathcal{Y}}} \cdot \frac{1}{T}.$$

Lemma 4 establishes an $\mathcal{O}(1/T)$ convergence rate for the Mirror-Prox algorithm in terms of the primal–dual gap, indicating that Mirror-Prox identifies an $\mathcal{O}(T^{-1})$ -nearly saddle point of the smooth convex-concave function $f(x, y)$, as defined in Definition 3.

We emphasize that the guarantee holds for the ergodic averages of the *midpoint iterates* $\{(x_{t+\frac{1}{2}}, y_{t+\frac{1}{2}})\}_{t=0}^{T-1}$. Such averaging is standard in convex–concave saddle-point problems and ensures stability in the presence of the rotational behavior of the minimax gradient field.

B Proof of Main Theoretical Results

B.1 Proof of Proposition 1

We mainly focus on the proof of the first-step update in (13), while similar arguments follow for the second-step update in (14).

Recall that in (11), we define

$$f(M, \omega) = - \sum_{l=1}^L \omega_l \cdot \langle \hat{\Sigma}^{(l)}, M \rangle.$$

Its gradients over M and ω are expressed as:

$$\nabla_M f(M, \omega) = -\sum_{l=1}^L \omega_l \widehat{\Sigma}^{(l)} \in \mathbb{R}^{d \times d}, \quad \text{and} \quad \nabla_\omega f(M, \omega) = \left(-\langle \widehat{\Sigma}^{(1)}, M \rangle, \dots, -\langle \widehat{\Sigma}^{(L)}, M \rangle \right)^\top \in \mathbb{R}^L.$$

We write the optimization problems in (13) as follows:

$$\begin{aligned} \omega^{t+\frac{1}{2}} &= \arg \min_{\omega \in \Delta^L} -\eta_\omega \langle \nabla_\omega f(M^t, \omega^t), \omega \rangle + D_{\psi_2}(\omega, \omega^t) \\ &= \arg \min_{\omega \in \Delta^L} \eta_\omega \cdot \sum_{l=1}^L \omega_l \langle \widehat{\Sigma}^{(l)}, M^t \rangle + \sum_{l=1}^L \omega_l \log \frac{\omega_l}{\omega_l^t}, \end{aligned} \quad (39)$$

and

$$\begin{aligned} M^{t+\frac{1}{2}} &= \arg \min_{M \in \mathcal{F}^k} \eta_M \langle \nabla_M \widehat{f}(M^t, \omega^t), M \rangle + D_{\psi_1}(M, M^t) \\ &= \arg \min_{M \in \mathcal{F}^k} -\eta_M \cdot \left\langle \sum_{l=1}^L \omega_l^t \widehat{\Sigma}^{(l)}, M \right\rangle + \text{Tr} \left(M (\log M - \log M^t) \right) \\ &= \arg \min_{M \in \mathcal{F}^k} \left\langle -\eta_M \sum_{l=1}^L \omega_l^t \widehat{\Sigma}^{(l)} - \log M^t, M \right\rangle + \text{Tr} (M \log M) \end{aligned} \quad (40)$$

In the following discussions, we present the closed-form expressions of ω -update and M -update in order.

Closed-form expressions of $\omega^{t+\frac{1}{2}}$ and ω^{t+1} . We derive the closed-form expression of $\omega^{t+\frac{1}{2}}$, while the update for ω^{t+1} follows by the same argument with M^t replaced by $M^{t+\frac{1}{2}}$.

For notation convenience, we define

$$h^{(l)} = \eta_\omega \langle \widehat{\Sigma}^{(l)}, M^t \rangle \quad \text{for } l = 1, \dots, L.$$

Then the optimization problem in (39) can be written as

$$\omega^{t+\frac{1}{2}} = \arg \min_{\omega \in \Delta^L} \sum_{l=1}^L \omega_l h^{(l)} + \sum_{l=1}^L \omega_l \log \frac{\omega_l}{\omega_l^t}. \quad (41)$$

This is a strictly convex problem over the probability simplex, hence it admits a unique minimizer.

Introducing a Lagrange multiplier $\mu \in \mathbb{R}$ for the simplex constraint $\sum_{l=1}^L \omega_l = 1$ and multipliers $\lambda_l \geq 0$ for the nonnegativity constraints $\omega_l \geq 0$, the Lagrangian is

$$\mathcal{L}(\omega, \mu, \lambda) = \sum_{l=1}^L \omega_l h^{(l)} + \sum_{l=1}^L \omega_l \log \frac{\omega_l}{\omega_l^t} + \mu \left(1 - \sum_{l=1}^L \omega_l \right) - \sum_{l=1}^L \lambda_l \omega_l.$$

The Karush–Kuhn–Tucker (KKT) conditions are given by

$$h^{(l)} + \log \frac{\omega_l^{t+\frac{1}{2}}}{\omega_l^t} + 1 - \mu - \lambda_l = 0, \quad l = 1, \dots, L, \quad (42)$$

$$\sum_{l=1}^L \omega_l^{t+\frac{1}{2}} = 1, \quad (43)$$

$$\omega_l^{t+\frac{1}{2}} \geq 0, \quad \lambda_l \geq 0, \quad \lambda_l \omega_l^{t+\frac{1}{2}} = 0, \quad l = 1, \dots, L. \quad (44)$$

Since $\omega^t \in \Delta^L$ has strictly positive entries, the objective in (41) acts as a logarithmic barrier and the minimizer satisfies $\omega_l^{t+\frac{1}{2}} > 0$ for all l . Therefore, $\lambda_l = 0$ for all l as implied by (44), and (42) reduces to

$$\log \frac{\omega_l^{t+\frac{1}{2}}}{\omega_l^t} = \mu - h^{(l)}, \quad l = 1, \dots, L.$$

Exponentiating both sides yields

$$\omega_l^{t+\frac{1}{2}} = \omega_l^t \exp(\mu - h^{(l)}), \quad l = 1, \dots, L.$$

Finally, enforcing the normalization condition (43) gives

$$1 = \sum_{l=1}^L \omega_l^{t+\frac{1}{2}} = \exp(\mu) \sum_{l=1}^L \omega_l^t \exp(-h^{(l)}),$$

which implies

$$\exp(\mu) = \left(\sum_{s=1}^L \omega_s^t \exp(-\eta_\omega \langle \widehat{\Sigma}^{(s)}, M^t \rangle) \right)^{-1}.$$

Substituting this expression back yields

$$\omega_l^{t+\frac{1}{2}} = \frac{\omega_l^t \exp(-\eta_\omega \langle \widehat{\Sigma}^{(l)}, M^t \rangle)}{\sum_{s=1}^L \omega_s^t \exp(-\eta_\omega \langle \widehat{\Sigma}^{(s)}, M^t \rangle)}, \quad l = 1, \dots, L,$$

which proves the first ω -update formula in (15). The expression for ω^{t+1} in (16) follows from an identical argument with M^t replaced by $M^{t+\frac{1}{2}}$.

Closed-form expressions of $M^{t+\frac{1}{2}}$ and M^{t+1} . We derive the closed-form expression of $M^{t+\frac{1}{2}}$, while the update for M^{t+1} follows by the same argument with ω^t replaced by $\omega^{t+\frac{1}{2}}$.

For notation convenience, we define

$$A^t := \log M^t + \eta_M \sum_{l=1}^L \omega_l^t \widehat{\Sigma}^{(l)}.$$

Then the optimization problem in (40) is equivalently written as

$$M^{t+\frac{1}{2}} = \arg \min_{M \in \mathcal{F}^k} \langle -A^t, M \rangle + \text{Tr}(M \log M). \quad (45)$$

The proof proceeds in two steps:

(Step-1) We show that $M^{t+\frac{1}{2}}$ shares the same eigenvectors as A^t . Therefore, the optimization problem

(45) reduces to identifying the eigenvalues of $M^{t+\frac{1}{2}}$;

(Step-2) We solve the eigenvalue optimization problem for $M^{t+\frac{1}{2}}$.

We first show that the minimizer $M^{t+\frac{1}{2}}$ of (45) must share the same eigenvectors as A^t . We recall the following classical trace inequality.

Lemma 5 (von Neumann trace inequality). *Let $A, B \in \mathbb{R}^{d \times d}$ be symmetric matrices with eigenvalues $\lambda_1(\cdot) \geq \dots \geq \lambda_d(\cdot)$. Then*

$$\sum_{j=1}^d \lambda_j(A) \lambda_{d+1-j}(B) \leq \text{Tr}(AB) \leq \sum_{j=1}^d \lambda_j(A) \lambda_j(B),$$

where equality holds if and only if A and B are simultaneously diagonalizable.

Applying this second inequality in the above Lemma with $A = -A^t$ and $B = M$, we obtain, for any $M \in \mathcal{F}^k$,

$$\langle -A^t, M \rangle \geq -\sum_{j=1}^d \lambda_j(A^t) \lambda_j(M),$$

with equality if and only if M and A^t share the same eigenvectors. Moreover, since

$$\text{Tr}(M \log M) = \sum_{j=1}^d \lambda_j(M) \log \lambda_j(M),$$

the entropy term depends only on the eigenvalues of M . Therefore, any minimizer of (45) must be co-diagonalizable with A^t .

Let the eigen decomposition of A^t be

$$A^t = U^t \text{Diag}(\lambda_1^t, \dots, \lambda_d^t) (U^t)^\top, \quad \lambda_1^t \geq \dots \geq \lambda_d^t.$$

Then $M^{t+\frac{1}{2}}$ must take the form

$$M^{t+\frac{1}{2}} = U^t \text{Diag}(\xi_1, \dots, \xi_d) (U^t)^\top, \quad \xi \in \mathcal{D}^k := \left\{ \xi \in \mathbb{R}^d : 0 \leq \xi_j \leq 1, \sum_{j=1}^d \xi_j = k \right\}, \quad (46)$$

where $\xi \in \mathcal{D}^k$ because $M^{t+\frac{1}{2}} \in \mathcal{F}^k$.

Substituting (46) into (45), the problem reduces to

$$\min_{\xi \in \mathcal{D}^k} - \sum_{j=1}^d \lambda_j^t \xi_j + \sum_{j=1}^d \xi_j \log \xi_j. \quad (47)$$

This is a strictly convex optimization problem and hence admits a unique minimizer.

We introduce a Lagrange multiplier $\alpha \in \mathbb{R}$ for the constraint $\sum_{j=1}^d \xi_j = k$, and multipliers $\tau_j \geq 0$ for the constraints $\xi_j \leq 1$. (The nonnegativity constraints $\xi_j \geq 0$ are inactive since the entropy term enforces $\xi_j > 0$ at the optimum.) The Lagrangian is

$$\mathcal{L}(\xi, \alpha, \tau) = - \sum_{j=1}^d \lambda_j^t \xi_j + \sum_{j=1}^d \xi_j \log \xi_j + \alpha \left(k - \sum_{j=1}^d \xi_j \right) + \sum_{j=1}^d \tau_j (\xi_j - 1).$$

The KKT stationarity condition yields

$$-\lambda_j^t + \log \xi_j + 1 - \alpha + \tau_j = 0, \quad j = 1, \dots, d,$$

which implies

$$\xi_j = \exp(\lambda_j^t + \alpha - 1 - \tau_j). \quad (48)$$

The complementary slackness condition $\tau_j(\xi_j - 1) = 0$ implies the following:

- if $\exp(\lambda_j^t + \alpha - 1) \leq 1$, then $\tau_j = 0$ and $\xi_j = \exp(\lambda_j^t + \alpha - 1)$;
- if $\exp(\lambda_j^t + \alpha - 1) > 1$, then $\tau_j > 0$ and $\xi_j = 1$.

Combining both cases, we obtain

$$\xi_j = \min \left\{ \exp(\lambda_j^t + \alpha - 1), 1 \right\}, \quad j = 1, \dots, d. \quad (49)$$

Finally, the scalar α is uniquely determined by the constraint in (46)

$$\sum_{j=1}^d \xi_j = \sum_{j=1}^d \min \left\{ \exp(\lambda_j^t + \alpha - 1), 1 \right\} = k.$$

Substituting (49) into (46) yields the closed-form expression of $M^{t+\frac{1}{2}}$ in (15). The formula for M^{t+1} in (16) follows analogously.

B.2 Proof of Theorem 1

To complete the proof, we introduce the following Theorem, which establishes the primal-dual gap of the output $(\widehat{M}_T, \widehat{\omega}_T)$ of Mirror-Prox algorithm 1. The proof is provided in Appendix B.8.

Theorem 7. *With the step sizes η_M, η_ω specified in Theorem 1, the primal-dual gap of the output $(\widehat{M}_T, \widehat{\omega}_T)$ of Algorithm 1 satisfies*

$$\max_{M \in \mathcal{F}^k} \langle \widehat{\Sigma}(\widehat{\omega}_T), M \rangle - \min_{\omega \in \Delta^L} \langle \widehat{\Sigma}(\omega), \widehat{M}_T \rangle \leq \max_{l \in [L]} \|\widehat{\Sigma}^{(l)}\|_{\text{op}} \cdot \frac{8k\sqrt{k \log(d/k) \log L}}{T}. \quad (50)$$

This result implies that the output $(\widehat{M}_T, \widehat{\omega}_T)$ of Algorithm 1 is an $\mathcal{O}(T^{-1})$ -nearly saddle point of the empirical Fantope-relaxed StablePCA objective (11); see Definition 3. Moreover, since $\widehat{\omega}_T \in \Delta^L$, it holds

$$\max_{M \in \mathcal{F}^k} \min_{\omega \in \Delta^L} \langle \widehat{\Sigma}(\omega), M \rangle \leq \max_{M \in \mathcal{F}^k} \langle \widehat{\Sigma}(\widehat{\omega}_T), M \rangle.$$

Combining the inequality above with (50) yields the following inequality:

$$\begin{aligned} \max_{M \in \mathcal{F}^k} \min_{\omega \in \Delta^L} \langle \widehat{\Sigma}(\omega), M \rangle - \min_{\omega \in \Delta^L} \langle \widehat{\Sigma}(\omega), \widehat{M}_T \rangle &\leq \max_{M \in \mathcal{F}^k} \langle \widehat{\Sigma}(\widehat{\omega}_T), M \rangle - \min_{\omega \in \Delta^L} \langle \widehat{\Sigma}(\omega), \widehat{M}_T \rangle \\ &\leq \max_{l \in [L]} \|\widehat{\Sigma}^{(l)}\|_{\text{op}} \cdot \frac{8k\sqrt{k \log(d/k) \log L}}{T}, \end{aligned}$$

which completes the proof.

B.3 Proof of Theorem 2

For any $M \in \mathcal{F}^k, \omega \in \Delta^L$, it holds that

$$\left| \langle \widehat{\Sigma}(\omega), M \rangle - \langle \Sigma(\omega), M \rangle \right| = \left| \sum_{l=1}^L \omega_l \cdot \langle \widehat{\Sigma}^{(l)} - \Sigma^{(l)}, M \rangle \right| \leq \sup_{l \in [L]} \left| \langle \widehat{\Sigma}^{(l)} - \Sigma^{(l)}, M \rangle \right|.$$

To control the right-hand side of the above inequality uniformly over $M \in \mathcal{F}^k$, we invoke the following lemma, which establishes a uniform concentration inequality that bounds the discrepancy between the empirical and population covariance matrices over \mathcal{F}^k . The proof is provided in Appendix C.5.

Lemma 6. *Suppose Condition 1 holds. Then for any $t \geq 0$, with probability at least $1 - 2Le^{-t}$:*

$$\begin{aligned} \max_{l \in [L]} \left| \|\widehat{\Sigma}^{(l)}\|_{\text{op}} - \|\Sigma^{(l)}\|_{\text{op}} \right| &\leq C\sigma^2 \max_{l \in [L]} \|\Sigma^{(l)}\|_{\text{op}} \cdot \left(\sqrt{\frac{d+t}{n}} + \frac{d+t}{n} \right), \\ \max_{l \in [L]} \sup_{M \in \mathcal{F}^k} \left| \langle \widehat{\Sigma}^{(l)} - \Sigma^{(l)}, M \rangle \right| &\leq C\sigma^2 \max_{l \in [L]} \|\Sigma^{(l)}\|_{\text{op}} \cdot k \left(\sqrt{\frac{d+t}{n}} + \frac{d+t}{n} \right), \end{aligned}$$

where $C > 0$ is a universal constant.

Then we apply Lemma 6 to conclude that with probability at least $1 - 2Le^{-t}$,

$$\forall M \in \mathcal{F}^k, \omega \in \Delta^L, \quad \left| \langle \widehat{\Sigma}(\omega), M \rangle - \langle \Sigma(\omega), M \rangle \right| \leq C \max_{l \in [L]} \|\Sigma^{(l)}\|_{\text{op}} \cdot k \left(\sqrt{\frac{d+t}{n}} + \frac{d+t}{n} \right).$$

Therefore, with high probability at least $1 - 2Le^{-t}$, it holds $\forall M \in \mathcal{F}^k$,

$$\begin{aligned} \left| \min_{\omega \in \Delta^L} \langle \widehat{\Sigma}(\omega), M \rangle - \min_{\omega \in \Delta^L} \langle \Sigma(\omega), M \rangle \right| &\leq \max_{\omega \in \Delta^L} \left| \langle \widehat{\Sigma}(\omega), M \rangle - \langle \Sigma(\omega), M \rangle \right| \\ &\leq C \max_{l \in [L]} \|\Sigma^{(l)}\|_{\text{op}} \cdot k \left(\sqrt{\frac{d+t}{n}} + \frac{d+t}{n} \right). \end{aligned} \quad (51)$$

We now turn to compare the output \widehat{M}_T of Algorithm 1 to the population optimum. Recall that M^* denotes a population StablePCA solution in (8), i.e.,

$$M^* \in \arg \max_{M \in \mathcal{F}^k} \min_{\omega \in \Delta^L} \langle \Sigma(\omega), M \rangle.$$

With probability at least $1 - 2Le^{-t}$, we proceed as follows:

$$\begin{aligned} \min_{\omega \in \Delta^L} \langle \Sigma(\omega), \widehat{M}_T \rangle &\geq \min_{\omega \in \Delta^L} \langle \widehat{\Sigma}(\omega), \widehat{M}_T \rangle - Ck \left(\sqrt{\frac{d+t}{n}} + \frac{d+t}{n} \right) \max_l \|\Sigma^{(l)}\|_{\text{op}} \quad (\text{by (51)}) \\ &\geq \max_{M \in \mathcal{F}^k} \min_{\omega \in \Delta^L} \langle \widehat{\Sigma}(\omega), M \rangle - \frac{8k\sqrt{k \log(d/k) \log L}}{T} \max_l \|\widehat{\Sigma}^{(l)}\|_{\text{op}} \\ &\quad - Ck \left(\sqrt{\frac{d+t}{n}} + \frac{d+t}{n} \right) \max_l \|\Sigma^{(l)}\|_{\text{op}} \quad (\text{Theorem 1}) \end{aligned}$$

Applying the first result in Lemma 6 which connects $\|\widehat{\Sigma}^{(l)}\|_{\text{op}}$ and $\|\Sigma^{(l)}\|_{\text{op}}$, and removing the cross-term, we establish that

$$\min_{\omega \in \Delta^L} \langle \Sigma(\omega), \widehat{M}_T \rangle \geq \max_{M \in \mathcal{F}^k} \min_{\omega \in \Delta^L} \langle \widehat{\Sigma}(\omega), M \rangle - Ck \left(\sqrt{\frac{d+t}{n}} + \frac{d+t}{n} + \frac{\sqrt{k \log(d/k) \log L}}{T} \right) \max_l \|\Sigma^{(l)}\|_{\text{op}}.$$

Moreover, since $M^* \in \mathcal{F}^k$, we continue to establish that

$$\begin{aligned}
\max_{M \in \mathcal{F}^k} \min_{\omega \in \Delta^L} \langle \widehat{\Sigma}(\omega), M \rangle &\geq \min_{\omega \in \Delta^L} \langle \widehat{\Sigma}(\omega), M^* \rangle \\
&\geq \min_{\omega \in \Delta^L} \langle \Sigma(\omega), M^* \rangle - Ck \left(\sqrt{\frac{d+t}{n}} + \frac{d+t}{n} \right) \max_l \|\Sigma^{(l)}\|_{\text{op}} \quad (\text{by (51)}) \\
&= \max_{M \in \mathcal{F}^k} \min_{\omega \in \Delta^L} \langle \Sigma(\omega), M \rangle - Ck \left(\sqrt{\frac{d+t}{n}} + \frac{d+t}{n} \right) \max_l \|\Sigma^{(l)}\|_{\text{op}} \quad (\text{Definition of } M^*)
\end{aligned}$$

Combining the above two results and rearranging terms yields the claimed convergence bound: for any value $t \geq 0$, with probability at least $1 - 2Le^{-t}$,

$$\max_{M \in \mathcal{F}^k} \min_{\omega \in \Delta^L} \langle \Sigma(\omega), M \rangle - \min_{\omega \in \Delta^L} \langle \Sigma(\omega), \widehat{M}_T \rangle \leq Ck \left(\sqrt{\frac{d+t}{n}} + \frac{d+t}{n} + \frac{\sqrt{k \log(d/k) \log L}}{T} \right) \max_{l \in [L]} \|\Sigma^{(l)}\|_{\text{op}}.$$

B.4 Proof of Theorem 3

By Theorem 1 and the definition of τ in (19),

$$\begin{aligned}
&\max_{M \in \mathcal{F}^k} \min_{\omega \in \Delta^L} \langle \widehat{\Sigma}(\omega), M \rangle - \min_{\omega \in \Delta^L} \langle \widehat{\Sigma}(\omega), \widehat{P}_T \rangle \\
&\leq \max_{M \in \mathcal{F}^k} \min_{\omega \in \Delta^L} \langle \widehat{\Sigma}(\omega), M \rangle - \min_{\omega \in \Delta^L} \langle \widehat{\Sigma}(\omega), \widehat{M}_T \rangle + \left\{ \min_{\omega \in \Delta^L} \langle \widehat{\Sigma}(\omega), \widehat{M}_T \rangle - \min_{\omega \in \Delta^L} \langle \widehat{\Sigma}(\omega), \widehat{P}_T \rangle \right\} \quad (52) \\
&\leq \frac{8k \sqrt{k \log(d/k) \log L} \cdot \max_{l \in [L]} \|\widehat{\Sigma}^{(l)}\|_{\text{op}}}{T} + \tau.
\end{aligned}$$

Since $\mathcal{F}^k \supseteq \mathcal{P}^k$, we have

$$\max_{M \in \mathcal{F}^k} \min_{\omega \in \Delta^L} \langle \widehat{\Sigma}(\omega), M \rangle \geq \max_{P \in \mathcal{P}^k} \min_{\omega \in \Delta^L} \langle \widehat{\Sigma}(\omega), P \rangle.$$

Combining the above two results yields the stated objective gap bound as follows:

$$\begin{aligned}
\max_{P \in \mathcal{P}^k} \min_{\omega \in \Delta^L} \langle \widehat{\Sigma}(\omega), P \rangle - \min_{\omega \in \Delta^L} \langle \widehat{\Sigma}(\omega), \widehat{P}_T \rangle &\leq \max_{M \in \mathcal{F}^k} \min_{\omega \in \Delta^L} \langle \widehat{\Sigma}(\omega), M \rangle - \min_{\omega \in \Delta^L} \langle \widehat{\Sigma}(\omega), \widehat{P}_T \rangle \\
&\leq \frac{8k \sqrt{k \log(d/k) \log L} \cdot \max_{l \in [L]} \|\widehat{\Sigma}^{(l)}\|_{\text{op}}}{T} + \tau.
\end{aligned}$$

Then we apply Lemma 6, which controls the finite-sample errors, to the above inequality and complete the proof.

B.5 Proof of Theorem 4

Since the objective of Fantope-relaxed StablePCA is bilinear, and both feasible sets \mathcal{F}^k and Δ^L are compact and convex, Sion's minimax theorem implies

$$\max_{M \in \mathcal{F}^k} \min_{\omega \in \Delta^L} \langle \Sigma(\omega), M \rangle = \min_{\omega \in \Delta^L} \max_{M \in \mathcal{F}^k} \langle \Sigma(\omega), M \rangle. \quad (53)$$

After exchanging the order of optimization, we observe that for any fixed $\omega \in \Delta^L$, the inner maximization for the right-hand-side term admits the closed-form expression

$$\max_{M \in \mathcal{F}^k} \langle \Sigma(\omega), M \rangle = \sum_{i=1}^k \lambda_i(\Sigma(\omega)), \quad (54)$$

where the equality follows from Ky Fan's eigenvalue maximization principle.

Substituting the expression (54) into to the right-hand side of (53), we have

$$\max_{M \in \mathcal{F}^k} \min_{\omega \in \Delta^L} \langle \Sigma(\omega), M \rangle = \min_{\omega \in \Delta^L} \sum_{i=1}^k \lambda_i(\Sigma(\omega)). \quad (55)$$

Recall that we define the optimal solutions of the above two optimization problems as M^* and ω^* , respectively:

$$M^* \in \arg \max_{M \in \mathcal{F}^k} \min_{\omega \in \Delta^L} \langle \Sigma(\omega), M \rangle, \quad \text{and} \quad \omega^* \in \arg \min_{\omega \in \Delta^L} \sum_{i=1}^k \lambda_i(\Sigma(\omega)). \quad (56)$$

Note that neither M^* nor ω^* is necessarily unique.

Plugging (M^*, ω^*) into (55), we establish that

$$\min_{\omega \in \Delta^L} \langle \Sigma(\omega), M^* \rangle = \sum_{i=1}^k \lambda_i(\Sigma(\omega^*)). \quad (57)$$

Since $M^* \in \mathcal{F}^k$ and $\omega^* \in \Delta^L$ as defined in (56), the following sandwich inequalities hold:

$$\min_{\omega \in \Delta^L} \langle \Sigma(\omega), M^* \rangle \leq \langle \Sigma(\omega^*), M^* \rangle \leq \max_{M \in \mathcal{F}^k} \langle \Sigma(\omega^*), M \rangle = \sum_{i=1}^k \lambda_i(\Sigma(\omega^*)),$$

where the last equality holds by (54). Combined with (57), all inequalities collapse into equalities, yielding

$$\langle \Sigma(\omega^*), M^* \rangle = \sum_{i=1}^k \lambda_i(\Sigma(\omega^*)).$$

By Ky Fan's theorem, the above equality implies that

$$M^* \in \arg \max_{M \in \mathcal{F}^k} \langle \Sigma(\omega^*), M \rangle.$$

Since for the selected optimizer ω^* , it holds $\lambda_k(\Sigma(\omega^*)) > \lambda_{k+1}(\Sigma(\omega^*))$, the maximizer of $\max_{M \in \mathcal{F}^k} \langle \Sigma(\omega^*), M \rangle$ is unique and equals the projection matrix onto the top- k eigenspace of $\Sigma(\omega^*)$. Therefore, the particular optimizer M^* identified above satisfies $M^* \in \mathcal{P}^k$ and is this projector.

Since $\mathcal{P}^k \subseteq \mathcal{F}^k$ and $M^* \in \mathcal{P}^k$, we have

$$\max_{P \in \mathcal{P}^k} \min_{\omega \in \Delta^L} \langle \Sigma(\omega), P \rangle = \max_{M \in \mathcal{F}^k} \min_{\omega \in \Delta^L} \langle \Sigma(\omega), M \rangle = \min_{\omega \in \Delta^L} \langle \Sigma(\omega), M^* \rangle = \langle \Sigma(\omega^*), M^* \rangle.$$

Therefore, the original and Fantope-relaxed problems attain the same optimal value, and M^* is the optimal solution of the original StablePCA problem:

$$M^* \in \arg \max_{P \in \mathcal{P}^k} \min_{\omega \in \Delta^L} \langle \Sigma(\omega), P \rangle.$$

This completes the proof.

B.6 Proof of Theorem 5

The proof proceeds in two steps. We first establish the convergence guarantee of $\|\widehat{M}_T - \widehat{P}_T\|_F$. Then, we continue showing the certificate τ vanishes with increasing T and n .

Bounding $\|\widehat{P}_T - \widehat{M}_T\|_F$.

By Theorem 7, the output $(\widehat{M}_T, \widehat{\omega}_T)$ of Algorithm 1 satisfies the following primal-dual gap:

$$\max_{M \in \mathcal{F}^k} \langle \widehat{\Sigma}(\widehat{\omega}_T), M \rangle - \min_{\omega \in \Delta^L} \langle \widehat{\Sigma}(\omega), \widehat{M}_T \rangle \leq \frac{8k\sqrt{k \log(d/k) \log L} \cdot \max_{l \in [L]} \|\widehat{\Sigma}^{(l)}\|_{\text{op}}}{T}.$$

Then we apply Lemma 6, to the above inequality, which controls the finite-sample errors of $\widehat{\Sigma}^{(l)}$ from the population $\Sigma^{(l)}$ for $l \in [L]$. Then for any $t \in [0, n - d]$, with a probability of at least $1 - 2Le^{-t}$:

$$\max_{M \in \mathcal{F}^k} \langle \Sigma(\widehat{\omega}_T), M \rangle - \min_{\omega \in \Delta^L} \langle \Sigma(\omega), \widehat{M}_T \rangle \leq Ck \left(\sqrt{\frac{d+t}{n}} + \frac{\sqrt{k \log(d/k) \log L}}{T} \right) \cdot \max_{l \in [L]} \|\Sigma^{(l)}\|_{\text{op}}. \quad (58)$$

By the definition of the optimal weight vector $\omega^* \in \Delta^L$,

$$\omega^* = \arg \min_{\omega \in \Delta^L} \phi(\omega) = \arg \min_{\omega \in \Delta^L} \max_{M \in \mathcal{F}^k} \langle \Sigma(\omega), M \rangle,$$

we have

$$\max_{M \in \mathcal{F}^k} \langle \Sigma(\widehat{\omega}_T), M \rangle \geq \max_{M \in \mathcal{F}^k} \langle \Sigma(\omega^*), M \rangle.$$

Therefore, it follows from (58) that for any $t \in [0, n - d]$, with a probability of at least $1 - 2Le^{-t}$:

$$\max_{M \in \mathcal{F}^k} \langle \Sigma(\omega^*), M \rangle - \min_{\omega \in \Delta^L} \langle \Sigma(\omega), \widehat{M}_T \rangle \leq Ck \left(\sqrt{\frac{d+t}{n}} + \frac{\sqrt{k \log(d/k) \log L}}{T} \right) \cdot \max_{l \in [L]} \|\Sigma^{(l)}\|_{\text{op}}.$$

Since the optimal weight vector $\omega^* \in \Delta^L$, it holds

$$\min_{\omega \in \Delta^L} \langle \Sigma(\omega), \widehat{M}_T \rangle \leq \langle \Sigma(\omega^*), \widehat{M}_T \rangle.$$

Combining the above two inequalities, we obtain the optimality gap for \widehat{M}_T :

$$\max_{M \in \mathcal{F}^k} \langle \Sigma(\omega^*), M \rangle - \langle \Sigma(\omega^*), \widehat{M}_T \rangle \leq Ck \left(\sqrt{\frac{d+t}{n}} + \frac{\sqrt{k \log(d/k) \log L}}{T} \right) \cdot \max_{l \in [L]} \|\Sigma^{(l)}\|_{\text{op}}. \quad (59)$$

Let $P^* \in \mathcal{P}^k$ be the projection matrix onto the top- k eigenspace of $\Sigma(\omega^*)$. Note that for the selected ω^* satisfying that $\lambda_k(\Sigma(\omega^*)) > \lambda_{k+1}(\Sigma(\omega^*))$, P^* is uniquely defined. By Ky Fan's maximum principle,

$$\max_{M \in \mathcal{F}^k} \langle \Sigma(\omega^*), M \rangle = \langle \Sigma(\omega^*), P^* \rangle.$$

Substituting this into the left-hand side of (59) yields

$$\langle \Sigma(\omega^*), P^* - \widehat{M}_T \rangle \leq Ck \left(\sqrt{\frac{d+t}{n}} + \frac{\sqrt{k \log(d/k) \log L}}{T} \right) \cdot \max_{l \in [L]} \|\Sigma^{(l)}\|_{\text{op}}. \quad (60)$$

We next introduce the following lemma, which converts the curvature inequality (60) into the distance between P^* and \widehat{M}_T . It was first introduced in the work [Vu et al. \(2013\)](#).

Lemma 7 (Lemma 3.1 of [Vu et al. \(2013\)](#)). *Let $A \in \mathbb{R}^{d \times d}$ be a symmetric matrix and E be the projection onto the subspace spanned by the eigenvectors of A corresponding to its k largest eigenvalues $\lambda_1 \geq \lambda_2 \geq \dots \geq \lambda_k$. If $\delta_A = \lambda_k - \lambda_{k+1} > 0$, then*

$$\frac{\delta_A}{2} \|E - F\|_F^2 \leq \langle A, E - F \rangle,$$

for all F satisfying that $0 \preceq F \preceq \mathbf{I}$ and $\text{Tr}(F) = k$.

Applying this lemma with $A = \Sigma(\omega^*)$, $E = P^*$, $F = \widehat{M}_T$, and $\delta_A = \delta^* := \lambda_k(\Sigma(\omega^*)) - \lambda_{k+1}(\Sigma(\omega^*)) > 0$ yields:

$$\frac{\delta^*}{2} \|P^* - \widehat{M}_T\|_F^2 \leq \langle \Sigma(\omega^*), P^* - \widehat{M}_T \rangle.$$

Together with the inequality (60), it holds for any $t \in [0, n - d]$, with a probability of at least $1 - 2Le^{-t}$:

$$\|\widehat{M}_T - P^*\|_F^2 \leq C \frac{k}{\delta^*} \left(\sqrt{\frac{d+t}{n}} + \frac{\sqrt{k \log(d/k) \log L}}{T} \right) \cdot \max_{l \in [L]} \|\Sigma^{(l)}\|_{\text{op}}.$$

Finally, recalling $\widehat{P}_T := \arg \min_{P \in \mathcal{P}^k} \|P - \widehat{M}_T\|_F$, we have

$$\|\widehat{P}_T - \widehat{M}_T\|_F^2 \leq \|P^* - \widehat{M}_T\|_F^2 \leq C \frac{k}{\delta^*} \left(\sqrt{\frac{d+t}{n}} + \frac{\sqrt{k \log(d/k) \log L}}{T} \right) \cdot \max_{l \in [L]} \|\Sigma^{(l)}\|_{\text{op}}. \quad (61)$$

Bounding the certificate $|\tau|$.

By definition,

$$|\tau| = \left| \min_{1 \leq l \leq L} \langle \widehat{\Sigma}^{(l)}, \widehat{M}_T - \widehat{P}_T \rangle \right|.$$

By Hölder's inequality,

$$|\tau| \leq \max_{l \in [L]} \|\widehat{\Sigma}^{(l)}\|_{\text{op}} \cdot \|\widehat{M}_T - \widehat{P}_T\|_*. \quad (62)$$

Next, we establish the upper bound of $\|\widehat{M}_T - \widehat{P}_T\|_*$. For notation convenience, we define

$$\Delta_T := \widehat{M}_T - \widehat{P}_T.$$

As $\widehat{M}_T \in \mathcal{F}^k$ and $\widehat{P}_T \in \mathcal{P}^k$, we have

$$\text{Tr}(\Delta_T) = \text{Tr}(\widehat{M}_T) - \text{Tr}(\widehat{P}_T) = k - k = 0.$$

Therefore, the total positive eigenvalues equal the total negative eigenvalues:

$$\sum_{i: \lambda_i(\Delta_T) > 0} \lambda_i(\Delta_T) = - \sum_{i: \lambda_i(\Delta_T) < 0} \lambda_i(\Delta_T).$$

Hence,

$$\|\Delta_T\|_* = \sum_{i=1}^d |\lambda_i(\Delta_T)| = 2 \sum_{i: \lambda_i(\Delta_T) < 0} (-\lambda_i(\Delta_T)). \quad (63)$$

More importantly, note that \widehat{P}_T is the Frobenius projection of \widehat{M}_T onto \mathcal{P}^k . Let

$$\widehat{M}_T = U \text{Diag}(\lambda_1, \lambda_2, \dots, \lambda_d) U^\top, \quad \text{with } \lambda_1 \geq \dots \geq \lambda_d, \quad 0 \leq \lambda_i \leq 1, \quad \sum_{i=1}^d \lambda_i = k.$$

Then \widehat{P}_T admits the form as:

$$\widehat{P}_T = U \text{Diag}(\underbrace{1, \dots, 1}_k, \underbrace{0, \dots, 0}_{d-k}) U^\top,$$

which implies that

$$\Delta_T = \widehat{M}_T - \widehat{P}_T = U \text{Diag}(\lambda_1 - 1, \dots, \lambda_k - 1, \lambda_{k+1}, \dots, \lambda_d) U^\top.$$

Consequently, Δ_T has at most k negative eigenvalues.

We then continue (63) to establish the upper bound of $\|\Delta_T\|_*$. By Cauchy-Schwartz,

$$\frac{1}{2} \|\Delta_T\|_* = \sum_{i: \lambda_i(\Delta_T) < 0} (-\lambda_i) \leq \sqrt{k} \left(\sum_{i: \lambda_i(\Delta_T) < 0} \lambda_i^2(\Delta_T) \right)^{1/2} \leq \sqrt{k} \|\Delta_T\|_F.$$

Therefore, it follows from (62) that

$$|\tau|^2 \leq 4k \max_{l \in [L]} \|\widehat{\Sigma}^{(l)}\|_{\text{op}}^2 \cdot \|\widehat{M}_T - \widehat{P}_T\|_F^2.$$

Together with (61), we complete the proof.

B.7 Proof of Theorem 6

It follows from the argument in (61) that for any $t \in [0, n - d]$, with a probability of at least

$1 - 2Le^{-t}$:

$$\|\widehat{P}_T - \widehat{M}_T\|_F^2 \leq \|P^* - \widehat{M}_T\|_F^2 \leq C \frac{k}{\delta^*} \left(\sqrt{\frac{d+t}{n}} + \frac{\sqrt{k \log(d/k) \log L}}{T} \right) \cdot \max_{l \in [L]} \|\Sigma^{(l)}\|_{\text{op}}.$$

Therefore, we shall further establish that

$$\begin{aligned} \|\widehat{P}_T - P^*\|_F^2 &\leq 2\|\widehat{P}_T - \widehat{M}_T\|_F^2 + 2\|P^* - \widehat{M}_T\|_F^2 \\ &\leq C \frac{k}{\delta^*} \left(\sqrt{\frac{d+t}{n}} + \frac{\sqrt{k \log(d/k) \log L}}{T} \right) \cdot \max_{l \in [L]} \|\Sigma^{(l)}\|_{\text{op}}. \end{aligned}$$

B.8 Proof of Theorem 7

Recall that Lemma 4 provides an $\mathcal{O}(T^{-1})$ convergence rate for general convex–concave minimax problems under Condition 2. Thus, to prove Theorem 7, it suffices to verify that Condition 2 holds for the empirical StablePCA objective

$$\min_{M \in \mathcal{F}^k} \max_{\omega \in \Delta^L} f(M, \omega), \quad f(M, \omega) := - \sum_{l=1}^L \omega_l \langle \widehat{\Sigma}^{(l)}, M \rangle.$$

We identify the primal and dual domains in Lemma 4 as $\mathcal{X} = \mathcal{F}^k, \mathcal{Y} = \Delta^L$, and choose the mirror maps

$$\psi_{\mathcal{F}^k}(M) = \psi_1(M) := \text{Tr}(M \log M), \quad \psi_{\Delta^L}(\omega) = \psi_2(\omega) := \sum_{l=1}^L \omega_l \log \omega_l.$$

Let D_{ψ_1} and D_{ψ_2} be the induced Bregman divergences, specified in (32).

The following lemma verifies Condition 2 for the empirical Fantope-relaxed StablePCA. The proof is provided in Appendix C.6.

Lemma 8. *The mirror maps $\psi_1(M)$ and $\psi_2(\omega)$ are strongly convex such that:*

- ψ_1 is $\frac{1}{2k}$ -strongly convex on \mathcal{F}^k with respect to the Schatten-1 (nuclear) norm $\|\cdot\|_*$. Moreover,

$$R_{\mathcal{F}^k}^2 := \sup_{M \in \mathcal{F}^k} \psi_1(M) - \inf_{M \in \mathcal{F}^k} \psi_1(M) = k \log \frac{d}{k}.$$

- ψ_2 is 1-strongly convex on Δ^L with respect to the ℓ_1 norm $\|\cdot\|_1$. Moreover,

$$R_{\Delta^L}^2 := \sup_{\omega \in \Delta^L} \psi_2(\omega) - \inf_{\omega \in \Delta^L} \psi_2(\omega) = \log L.$$

Furthermore, $f(M, \omega)$ is $(\beta_{11}, \beta_{12}, \beta_{21}, \beta_{22})$ -smooth in the sense of Condition 2 under the norm pair $\|M\|_*$ and $\|\omega\|_1$, with

$$(\beta_{11}, \beta_{12}, \beta_{21}, \beta_{22}) = (0, \beta, \beta, 0), \quad \beta := \max_{1 \leq l \leq L} \|\widehat{\Sigma}^{(l)}\|_{\text{op}}.$$

By Lemma 8, Condition 2 holds with

$$\mu_{\mathcal{X}} = \frac{1}{2k}, \quad \mu_{\mathcal{Y}} = 1, \quad (\beta_{11}, \beta_{12}, \beta_{21}, \beta_{22}) = (0, \beta, \beta, 0), \quad R_{\mathcal{X}}^2 = k \log \frac{d}{k}, \quad R_{\mathcal{Y}}^2 = \log L.$$

Substituting these quantities into Lemma 4 gives the desired $\mathcal{O}(T^{-1})$ duality-gap bound for the averaged midpoint iterates

$$\widehat{M}_T := \frac{1}{T} \sum_{t=0}^{T-1} M_{t+\frac{1}{2}}, \quad \widehat{\omega}_T := \frac{1}{T} \sum_{t=0}^{T-1} \omega_{t+\frac{1}{2}}.$$

Specifically, by setting

$$\eta = \frac{\mu_{\mathcal{X}} \wedge \mu_{\mathcal{Y}}}{2 \max \left\{ \frac{\beta_{11}}{a}, \frac{\beta_{22}}{b}, \frac{\beta_{12}}{\sqrt{ab}}, \frac{\beta_{21}}{\sqrt{ab}} \right\}} = \frac{\frac{1}{2k}}{2 \cdot \frac{\beta}{\sqrt{ab}}} = \frac{\sqrt{ab}}{4k\beta},$$

Theorem 4 gives

$$\begin{aligned} \max_{\omega \in \Delta^L} f(\widehat{M}_T, \omega) - \min_{M \in \mathcal{F}^k} f(M, \widehat{\omega}_T) &\leq 2 \max \left\{ \frac{\beta_{11}}{a}, \frac{\beta_{22}}{b}, \frac{\beta_{12}}{\sqrt{ab}}, \frac{\beta_{21}}{\sqrt{ab}} \right\} \frac{aR_{\mathcal{X}}^2 + bR_{\mathcal{Y}}^2}{\mu_{\mathcal{X}} \wedge \mu_{\mathcal{Y}}} \cdot \frac{1}{T} \\ &\leq \frac{4k\beta}{\sqrt{ab}} \left(ak \log \frac{d}{k} + b \log L \right) \frac{1}{T}. \end{aligned}$$

We take $a = \log L$ and $b = k \log(d/k)$, then the step size becomes

$$\eta = \frac{1}{4 \max_{l \in [L]} \|\widehat{\Sigma}^{(l)}\|_{\text{op}}} \sqrt{\frac{\log L}{k \log(d/k)}}.$$

By (36) and (37), it holds

$$\eta_M = \frac{\eta}{a} = \frac{1}{4 \max_{l \in [L]} \|\widehat{\Sigma}^{(l)}\|_{\text{op}}} \sqrt{\frac{1}{k \log(d/k) \log L}}, \quad \eta_{\omega} = \frac{\eta}{b} = \frac{1}{4 \max_{l \in [L]} \|\widehat{\Sigma}^{(l)}\|_{\text{op}}} \frac{\sqrt{\log L}}{(k \log(d/k))^{3/2}}$$

And the final primal-dual gap simplifies as

$$\max_{\omega \in \Delta^L} f(\widehat{M}_T, \omega) - \min_{M \in \mathcal{F}^k} f(M, \widehat{\omega}_T) \leq \frac{8k \sqrt{k \log(d/k) \log L}}{T} \max_{l \in [L]} \|\widehat{\Sigma}^{(l)}\|_{\text{op}}.$$

which completes the proof.

C Proof of Technical Lemmas

C.1 Proof of Lemma 1

Recall that $\phi(\omega)$ admits the form in (22):

$$\phi(\omega) = \max_{M \in \mathcal{F}^k} \sum_{l=1}^L \omega_l \langle \Sigma^{(l)}, M \rangle. \quad (64)$$

Continuity and Convexity.

For each fixed $M \in \mathcal{F}^k$, the map $\omega \mapsto \sum_{l=1}^L \omega_l \langle \Sigma^{(l)}, M \rangle$ is affine in ω . Since $\phi(\omega)$ is the pointwise maximum over $M \in \mathcal{F}^k$ of affine functions, it follows that ϕ is convex on Δ^L . Moreover, because \mathcal{F}^k is compact and the function $(\omega, M) \mapsto \sum_{l=1}^L \omega_l \langle \Sigma^{(l)}, M \rangle$ is continuous, the maximum in (64) depends continuously on ω . Hence, ϕ is continuous on Δ^L .

Differentiability under an eigengap.

Fix $\omega \in \Delta^L$ such that $\lambda_k(\Sigma(\omega)) > \lambda_{k+1}(\Sigma(\omega))$. Under this eigengap condition, the top- k eigenspace of $\Sigma(\omega)$ is unique, and therefore the maximizer of $\max_{M \in \mathcal{F}^k} \langle \Sigma(\omega), M \rangle$ is unique. Denote this maximizer by $P_k(\omega)$, the orthogonal projection matrix onto the top- k eigenspace of $\Sigma(\omega)$.

By Danskin's theorem, since the maximizer in (64) is unique at ω , the function ϕ is differentiable at ω , and its gradient is given by

$$\nabla \phi(\omega) = (\langle \Sigma^{(1)}, P_k(\omega) \rangle, \dots, \langle \Sigma^{(L)}, P_k(\omega) \rangle)^\top.$$

Nondifferentiability at eigenvalue collisions.

If $\lambda_k(\Sigma(\omega)) = \lambda_{k+1}(\Sigma(\omega))$, then the top- k eigenspace is not uniquely defined, and the maximizer of $\max_{M \in \mathcal{F}^k} \langle \Sigma(\omega), M \rangle$ is no longer unique. In this case, the subdifferential of ϕ at ω contains multiple elements, and ϕ fails to be differentiable at ω . Thus, nondifferentiability can occur only at points where eigenvalues collide.

Combining the above arguments completes the proof.

C.2 Proof of Lemma 2

For any symmetric matrix $A \in \mathbb{R}^{d \times d}$, Ky Fan's maximum principle states that

$$\sum_{i=1}^k \lambda_i(A) = \max_{P \in \mathcal{P}^k} \langle A, P \rangle, \quad (65)$$

Applying (65) to $\Sigma(\omega)$ gives

$$\phi(\omega) = \max_{P \in \mathcal{P}^k} \langle \Sigma(\omega), P \rangle. \quad (66)$$

Let $P(\omega) \in \arg \max_{P \in \mathcal{P}^k} \langle A(\omega), P \rangle$ be any maximizer. Equivalently, $P(\omega) = U(\omega)(U(\omega))^\top$ where the columns of $U(\omega)$ span a top- k eigenspace of $\Sigma(\omega)$. Then

$$\phi(\omega) = \langle \Sigma(\omega), P(\omega) \rangle. \quad (67)$$

For any $\omega' \in \Delta^L$, since $\phi(\omega')$ is the maximum over P , we can evaluate it at $P(\omega)$ to obtain

$$\phi(\omega') = \max_{P \in \mathcal{P}^k} \langle \Sigma(\omega'), P \rangle \geq \langle \Sigma(\omega'), P(\omega) \rangle. \quad (68)$$

Subtracting (67) from (68) yields

$$\phi(\omega') - \phi(\omega) \geq \langle \Sigma(\omega') - \Sigma(\omega), P(\omega) \rangle.$$

Using the linearity $\Sigma(\omega') - \Sigma(\omega) = \sum_{l=1}^L (\omega'_l - \omega_l) \Sigma^{(l)}$,

$$\langle \Sigma(\omega') - \Sigma(\omega), P(\omega) \rangle = \sum_{l=1}^L (\omega'_l - \omega_l) \langle \Sigma^{(l)}, P(\omega) \rangle = \langle g(\omega), \omega' - \omega \rangle,$$

where $g_l(\omega) = \langle \Sigma^{(l)}, P(\omega) \rangle$. Therefore,

$$\phi(\omega') \geq \phi(\omega) + \langle g(\omega), \omega' - \omega \rangle, \quad \forall \omega' \in \Delta^L,$$

which proves that $g(\omega) \in \partial\phi(\omega)$.

C.3 Proof of Lemma 3

Given a distribution \mathbb{Q} , the regret over a projection matrix $P \in \mathcal{P}^k$ is defined as:

$$\text{Regret}_{\mathbb{Q}}(P) = \mathbb{E}_{\mathbb{Q}} \|X - PX\|_2^2 - \min_{P' \in \mathcal{P}^k} \mathbb{E}_{\mathbb{Q}} \|X - P'X\|_2^2.$$

Recall that the uncertainty set \mathcal{C} consists of all mixtures of the source distributions. We take the worst-case regret over \mathcal{C} :

$$\max_{\mathbb{Q} \in \mathcal{C}} \text{Regret}_{\mathbb{Q}}(P) = \max_{\omega \in \Delta^L} \left\{ \mathbb{E}_{X \sim \sum_{l=1}^L \omega_l \mathbb{T}^{(l)}} \|X - PX\|_2^2 - \min_{P' \in \mathcal{P}^k} \mathbb{E}_{X \sim \sum_{l=1}^L \omega_l \mathbb{T}^{(l)}} \|X - P'X\|_2^2 \right\}.$$

We now simplify the right-hand side. First, by linearity of expectation,

$$\mathbb{E}_{X \sim \sum_{l=1}^L \omega_l \mathbb{T}^{(l)}} \|X - PX\|_2^2 = \sum_{l=1}^L \omega_l \cdot \mathbb{E}_{\mathbb{T}^{(l)}} \|X - PX\|_2^2.$$

Second, the optimal rank- k reconstruction error under ω -weighted mixture is

$$\min_{P' \in \mathcal{P}^k} \mathbb{E}_{X \sim \sum_{l=1}^L \omega_l \mathbb{T}^{(l)}} \|X - P'X\|_2^2 = \sum_{i=k+1}^d \lambda_i(\Sigma(\omega)),$$

which is a concave function of ω , since the sum of the bottom eigenvalues are concave for $\Sigma(\omega)$ and $\Sigma(\omega)$ itself is linear in ω . As a consequence, the function

$$\omega \mapsto \mathbb{E}_{X \sim \sum_{l=1}^L \omega_l \mathbb{T}^{(l)}} \|X - PX\|_2^2 - \min_{P' \in \mathcal{P}^k} \mathbb{E}_{X \sim \sum_{l=1}^L \omega_l \mathbb{T}^{(l)}} \|X - P'X\|_2^2,$$

is convex in ω , since the first term is linear in ω , while the second term is concave and appears with a minus sign.

Therefore, after taking maximization over $\omega \in \Delta^L$, the above convex function attains its maximum at an extreme point of Δ^L , i.e., at one of the vertices $\{e_1, \dots, e_L\}$. It follows that

$$\max_{\mathbb{Q} \in \mathcal{C}} \text{Regret}_{\mathbb{Q}}(P) = \max_{l \in [L]} \left\{ \mathbb{E}_{X \sim \mathbb{T}^{(l)}} \|X - PX\|_2^2 - \min_{P' \in \mathcal{P}^k} \mathbb{E}_{X \sim \mathbb{T}^{(l)}} \|X - P'X\|_2^2 \right\} = \max_{l \in [L]} \text{Regret}_{\mathbb{T}^{(l)}}(P).$$

Taking the minimization over $P \in \mathcal{P}^k$ on both sides completes the proof.

C.4 Proof of Lemma 4

The proof follows the standard extragradient analysis for smooth convex-concave minimax problems, which is outlined as follows:

1. We first collect several technical lemmas concerning Bregman geometry and the Mirror-Prox updates.
2. We then show that each iteration satisfies a one-step inequality controlling the primal-dual gap.
3. Finally, telescoping this inequality over iterations yields the desired $\mathcal{O}(1/T)$ convergence rate for the ergodic averages of the midpoint iterates.

Now, we present the preliminaries of the analysis.

Definition 4 (Bregman projection). *Let \mathcal{Z} be a closed convex set and let ψ be a mirror map defined on a convex domain $\text{dom}(\psi) \supseteq \mathcal{Z}$, with associated Bregman divergence D_ψ . For any $\nu \in \text{dom}(\psi)$, the Bregman projection of ν onto \mathcal{Z} is defined as*

$$\Pi_{\mathcal{Z}}^\psi(\nu) := \arg \min_{z \in \mathcal{Z}} D_\psi(z, \nu).$$

The following lemma collects two standard properties of Bregman divergences. The first identity is often referred to as the *three-point identity*, while the second expresses the optimality condition of Bregman projection. We omit the proof as it essentially follows the results in [Bubeck et al. \(2015\)](#).

Lemma 9 (Three-point identity and projection inequality). *For any $x, y, z \in \text{dom}(\psi)$,*

$$\langle \nabla\psi(x) - \nabla\psi(y), x - z \rangle = D_\psi(x, y) + D_\psi(z, x) - D_\psi(z, y). \quad (69)$$

Let \mathcal{Z} be a closed convex set with $\mathcal{Z} \subseteq \text{dom}(\psi)$. Then, for any $x \in \text{dom}(\psi)$, the following inequality holds for any $z \in \mathcal{Z}$,

$$\langle \nabla\psi(\Pi_{\mathcal{Z}}^\psi(x)) - \nabla\psi(x), z - \Pi_{\mathcal{Z}}^\psi(x) \rangle \geq 0.$$

The next lemma rewrites the Mirror-Prox steps as Bregman projections in the dual space. This formulation is crucial for linking the algorithmic updates with the three-point identity above. The proof is provided in [Appendix C.7](#).

Lemma 10 (Equivalent Mirror-Prox formulation). *The first step update (36) can be written as*

$$z_{t+\frac{1}{2}} = \Pi_{\mathcal{Z}}^\psi(\nu_{t+\frac{1}{2}}), \quad \text{with } \nu_{t+\frac{1}{2}} \text{ satisfies } \nabla\psi(\nu_{t+\frac{1}{2}}) = \nabla\psi(z_t) - \eta g(z_t).$$

Similarly, the second step update (37) admits the form

$$z_{t+1} = \Pi_{\mathcal{Z}}^\psi(\nu_{t+1}), \quad \text{with } \nu_{t+1} \text{ satisfies } \nabla\psi(\nu_{t+1}) = \nabla\psi(z_t) - \eta g(z_{t+\frac{1}{2}}).$$

The following lemma summarizes the geometric properties of the mirror map and the smoothness of the saddle-point operator on \mathcal{Z} . The proof is provided in [Appendix C.8](#).

Lemma 11. *Under Condition 2, the mirror map ψ is $(\mu_{\mathcal{X}} \wedge \mu_{\mathcal{Y}})$ -strongly convex with respect to $\|\cdot\|_{\mathcal{Z}}$, i.e.,*

$$D_{\psi}(z, z') \geq \frac{\mu_{\mathcal{X}} \wedge \mu_{\mathcal{Y}}}{2} \|z - z'\|_{\mathcal{Z}}^2.$$

Moreover, the operator $g(z)$ is β -Lipschitz with respect to $\|\cdot\|_{\mathcal{Z}}$, where

$$\beta = 2 \max \left\{ \frac{\beta_{11}}{a}, \frac{\beta_{22}}{b}, \frac{\beta_{12}}{\sqrt{ab}}, \frac{\beta_{21}}{\sqrt{ab}} \right\}.$$

Now we are prepared to present the proof of Lemma 4. We study the midpoint iterate $z_{t+\frac{1}{2}} = (x_{t+\frac{1}{2}}, y_{t+\frac{1}{2}})$.

Step-1: Upper bound the primal-dual gap.

Fix $y_{t+\frac{1}{2}}$. Since $x \mapsto f(x, y_{t+\frac{1}{2}})$ is convex on \mathcal{X} , by the first-order condition of convexity, for any $x \in \mathcal{X}$,

$$f(x_{t+\frac{1}{2}}, y_{t+\frac{1}{2}}) - f(x, y_{t+\frac{1}{2}}) \leq \left\langle \nabla_x f(x_{t+\frac{1}{2}}, y_{t+\frac{1}{2}}), x_{t+\frac{1}{2}} - x \right\rangle.$$

Similarly, fix $x_{t+\frac{1}{2}}$. Since $y \mapsto f(x_{t+\frac{1}{2}}, y)$ is concave on \mathcal{Y} , the first-order condition of concavity implies that for any $y \in \mathcal{Y}$,

$$f(x_{t+\frac{1}{2}}, y) - f(x_{t+\frac{1}{2}}, y_{t+\frac{1}{2}}) \leq - \left\langle \nabla_y f(x_{t+\frac{1}{2}}, y_{t+\frac{1}{2}}), y_{t+\frac{1}{2}} - y \right\rangle.$$

Adding the above two results yields, for any $(x, y) \in \mathcal{X} \times \mathcal{Y}$,

$$f(x_{t+\frac{1}{2}}, y) - f(x, y_{t+\frac{1}{2}}) \leq \left\langle \nabla_x f(x_{t+\frac{1}{2}}, y_{t+\frac{1}{2}}), x_{t+\frac{1}{2}} - x \right\rangle - \left\langle \nabla_y f(x_{t+\frac{1}{2}}, y_{t+\frac{1}{2}}), y_{t+\frac{1}{2}} - y \right\rangle.$$

Using the definition $g(z) = (\nabla_x f(x, y), -\nabla_y f(x, y))$ in (35), the right-hand side equals $\langle g(z_{t+\frac{1}{2}}), z_{t+\frac{1}{2}} - z \rangle$ and thus

$$f(x_{t+\frac{1}{2}}, y) - f(x, y_{t+\frac{1}{2}}) \leq \left\langle g(z_{t+\frac{1}{2}}), z_{t+\frac{1}{2}} - z \right\rangle. \quad (70)$$

We next decompose the RHS of (70). Note that

$$\left\langle g(z_{t+\frac{1}{2}}), z_{t+\frac{1}{2}} - z \right\rangle = \left\langle g(z_{t+\frac{1}{2}}), z_{t+1} - z \right\rangle + \left\langle g(z_{t+\frac{1}{2}}), z_{t+\frac{1}{2}} - z_{t+1} \right\rangle.$$

Next, add and subtract $g(z_t)$ inside the second inner product:

$$\left\langle g(z_{t+\frac{1}{2}}), z_{t+\frac{1}{2}} - z_{t+1} \right\rangle = \left\langle g(z_t), z_{t+\frac{1}{2}} - z_{t+1} \right\rangle + \left\langle g(z_{t+\frac{1}{2}}) - g(z_t), z_{t+\frac{1}{2}} - z_{t+1} \right\rangle.$$

Therefore,

$$\begin{aligned} \langle g(z_{t+\frac{1}{2}}), z_{t+\frac{1}{2}} - z \rangle &= \langle g(z_{t+\frac{1}{2}}), z_{t+1} - z \rangle + \langle g(z_t), z_{t+\frac{1}{2}} - z_{t+1} \rangle + \langle g(z_{t+\frac{1}{2}}) - g(z_t), z_{t+\frac{1}{2}} - z_{t+1} \rangle \\ &=: \text{Term-1} + \text{Term-2} + \text{Term-3}. \end{aligned} \tag{71}$$

Step-2: Upper bound Term-1.

By Lemma 10 (second-step),

$$\nabla\psi(\nu_{t+1}) = \nabla\psi(z_t) - \eta g(z_{t+\frac{1}{2}}),$$

hence

$$g(z_{t+\frac{1}{2}}) = \frac{1}{\eta} (\nabla\psi(z_t) - \nabla\psi(\nu_{t+1})).$$

Substituting into the inner product yields

$$\langle g(z_{t+\frac{1}{2}}), z_{t+1} - z \rangle = \frac{1}{\eta} \langle \nabla\psi(z_t) - \nabla\psi(\nu_{t+1}), z_{t+1} - z \rangle.$$

Since $z_{t+1} = \Pi_{\mathcal{Z}}^{\psi}(\nu_{t+1})$, as shown in Lemma 10 (second-step), the Bregman projection optimality condition in Lemma 9 implies that for any $z \in \mathcal{Z}$,

$$\langle \nabla\psi(z_{t+1}) - \nabla\psi(\nu_{t+1}), z - z_{t+1} \rangle \geq 0.$$

Therefore,

$$\begin{aligned} \langle \nabla\psi(z_t) - \nabla\psi(\nu_{t+1}), z_{t+1} - z \rangle &= \langle \nabla\psi(z_t) - \nabla\psi(z_{t+1}), z_{t+1} - z \rangle \\ &\quad + \langle \nabla\psi(z_{t+1}) - \nabla\psi(\nu_{t+1}), z_{t+1} - z \rangle \\ &\leq \langle \nabla\psi(z_t) - \nabla\psi(z_{t+1}), z_{t+1} - z \rangle. \end{aligned}$$

Dividing by η gives

$$\langle g(z_{t+\frac{1}{2}}), z_{t+1} - z \rangle \leq \frac{1}{\eta} \langle \nabla\psi(z_t) - \nabla\psi(z_{t+1}), z_{t+1} - z \rangle.$$

Now apply the three-point identity (69) with $(x, y, z) = (z_{t+1}, z_t, z)$:

$$\langle \nabla\psi(z_{t+1}) - \nabla\psi(z_t), z_{t+1} - z \rangle = D_{\psi}(z_{t+1}, z_t) + D_{\psi}(z, z_{t+1}) - D_{\psi}(z, z_t).$$

Substituting this identity into the previous bound gives

$$\langle g(z_{t+\frac{1}{2}}), z_{t+1} - z \rangle \leq \frac{1}{\eta} [D_\psi(z, z_t) - D_\psi(z, z_{t+1}) - D_\psi(z_{t+1}, z_t)]. \quad (72)$$

Step-3: Upper bound Term-2.

By Lemma 10 (first-step),

$$\nabla\psi(\nu_{t+\frac{1}{2}}) = \nabla\psi(z_t) - \eta g(z_t),$$

hence

$$g(z_t) = \frac{1}{\eta} (\nabla\psi(z_t) - \nabla\psi(\nu_{t+\frac{1}{2}})),$$

and therefore

$$\langle g(z_t), z_{t+\frac{1}{2}} - z_{t+1} \rangle = \frac{1}{\eta} \langle \nabla\psi(z_t) - \nabla\psi(\nu_{t+\frac{1}{2}}), z_{t+\frac{1}{2}} - z_{t+1} \rangle.$$

Since $z_{t+\frac{1}{2}} = \Pi_{\mathcal{Z}}^\psi(\nu_{t+\frac{1}{2}})$, as shown in Lemma 10 (first-step), Lemma 9 implies (taking $z = z_{t+1} \in \mathcal{Z}$) that

$$\langle \nabla\psi(z_{t+\frac{1}{2}}) - \nabla\psi(\nu_{t+\frac{1}{2}}), z_{t+1} - z_{t+\frac{1}{2}} \rangle \geq 0.$$

Hence, by adding and subtracting $\nabla\psi(z_{t+\frac{1}{2}})$,

$$\begin{aligned} \langle \nabla\psi(z_t) - \nabla\psi(\nu_{t+\frac{1}{2}}), z_{t+\frac{1}{2}} - z_{t+1} \rangle &= \langle \nabla\psi(z_t) - \nabla\psi(z_{t+\frac{1}{2}}), z_{t+\frac{1}{2}} - z_{t+1} \rangle \\ &\quad + \langle \nabla\psi(z_{t+\frac{1}{2}}) - \nabla\psi(\nu_{t+\frac{1}{2}}), z_{t+\frac{1}{2}} - z_{t+1} \rangle \\ &\leq \langle \nabla\psi(z_t) - \nabla\psi(z_{t+\frac{1}{2}}), z_{t+\frac{1}{2}} - z_{t+1} \rangle. \end{aligned}$$

Dividing by η yields

$$\langle g(z_t), z_{t+\frac{1}{2}} - z_{t+1} \rangle \leq \frac{1}{\eta} \langle \nabla\psi(z_t) - \nabla\psi(z_{t+\frac{1}{2}}), z_{t+\frac{1}{2}} - z_{t+1} \rangle.$$

Apply (69) with $(x, y, z) = (z_{t+\frac{1}{2}}, z_t, z_{t+1})$:

$$\langle \nabla\psi(z_t) - \nabla\psi(z_{t+\frac{1}{2}}), z_{t+\frac{1}{2}} - z_{t+1} \rangle = D_\psi(z_{t+1}, z_t) - D_\psi(z_{t+1}, z_{t+\frac{1}{2}}) - D_\psi(z_{t+\frac{1}{2}}, z_t).$$

Therefore,

$$\langle g(z_t), z_{t+\frac{1}{2}} - z_{t+1} \rangle \leq \frac{1}{\eta} [D_\psi(z_{t+1}, z_t) - D_\psi(z_{t+1}, z_{t+\frac{1}{2}}) - D_\psi(z_{t+\frac{1}{2}}, z_t)].$$

Finally, by strong convexity of ψ on \mathcal{Z} (Lemma 11),

$$D_\psi(z_{t+1}, z_{t+\frac{1}{2}}) \geq \frac{\mu}{2} \|z_{t+1} - z_{t+\frac{1}{2}}\|_{\mathcal{Z}}^2, \quad D_\psi(z_{t+\frac{1}{2}}, z_t) \geq \frac{\mu}{2} \|z_{t+\frac{1}{2}} - z_t\|_{\mathcal{Z}}^2,$$

where $\mu = \mu_{\mathcal{X}} \wedge \mu_{\mathcal{Y}}$. Substituting these lower bounds yields

$$\langle g(z_t), z_{t+\frac{1}{2}} - z_{t+1} \rangle \leq \frac{1}{\eta} \left[D_\psi(z_{t+1}, z_t) - \frac{\mu}{2} \|z_{t+1} - z_{t+\frac{1}{2}}\|_{\mathcal{Z}}^2 - \frac{\mu}{2} \|z_{t+\frac{1}{2}} - z_t\|_{\mathcal{Z}}^2 \right]. \quad (73)$$

Step-4: Upper bound Term-3.

By Cauchy–Schwarz,

$$\langle g(z_{t+\frac{1}{2}}) - g(z_t), z_{t+\frac{1}{2}} - z_{t+1} \rangle \leq \|g(z_{t+\frac{1}{2}}) - g(z_t)\|_{\mathcal{Z},*} \|z_{t+\frac{1}{2}} - z_{t+1}\|_{\mathcal{Z}}.$$

By the β -Lipschitz property of g (Lemma 11),

$$\|g(z_{t+\frac{1}{2}}) - g(z_t)\|_{\mathcal{Z},*} \leq \beta \|z_{t+\frac{1}{2}} - z_t\|_{\mathcal{Z}}.$$

Combining the previous two inequalities gives

$$\langle g(z_{t+\frac{1}{2}}) - g(z_t), z_{t+\frac{1}{2}} - z_{t+1} \rangle \leq \beta \|z_{t+\frac{1}{2}} - z_t\|_{\mathcal{Z}} \|z_{t+\frac{1}{2}} - z_{t+1}\|_{\mathcal{Z}}.$$

Applying Young's inequality $ab \leq \frac{1}{2}a^2 + \frac{1}{2}b^2$ yields

$$\langle g(z_{t+\frac{1}{2}}) - g(z_t), z_{t+\frac{1}{2}} - z_{t+1} \rangle \leq \frac{\beta}{2} \|z_{t+\frac{1}{2}} - z_{t+1}\|_{\mathcal{Z}}^2 + \frac{\beta}{2} \|z_{t+\frac{1}{2}} - z_t\|_{\mathcal{Z}}^2. \quad (74)$$

Step-5: Combine three terms and complete the proof.

Plugging (72), (73), and (74) into (71) yields

$$\begin{aligned} \langle g(z_{t+\frac{1}{2}}), z_{t+\frac{1}{2}} - z \rangle &\leq \frac{1}{\eta} [D_\psi(z, z_t) - D_\psi(z, z_{t+1})] \\ &\quad + \left(\frac{\beta}{2} - \frac{\mu}{2\eta} \right) \|z_{t+\frac{1}{2}} - z_{t+1}\|_{\mathcal{Z}}^2 + \left(\frac{\beta}{2} - \frac{\mu}{2\eta} \right) \|z_{t+\frac{1}{2}} - z_t\|_{\mathcal{Z}}^2. \end{aligned}$$

Choosing $\eta = \mu/\beta$ yields

$$\langle g(z_{t+\frac{1}{2}}), z_{t+\frac{1}{2}} - z \rangle \leq \frac{D_\psi(z, z_t) - D_\psi(z, z_{t+1})}{\eta}.$$

Combining with (70), we obtain

$$f(x_{t+\frac{1}{2}}, y) - f(x, y_{t+\frac{1}{2}}) \leq \frac{D_\psi(z, z_t) - D_\psi(z, z_{t+1})}{\eta}.$$

Summing over $t = 0, \dots, T-1$ gives

$$\sum_{t=0}^{T-1} [f(x_{t+\frac{1}{2}}, y) - f(x, y_{t+\frac{1}{2}})] \leq \frac{D_\psi(z, z_0) - D_\psi(z, z_T)}{\eta} \leq \frac{D_\psi(z, z_0)}{\eta}, \quad (75)$$

where we used the fact that $D_\psi(z, z_T) \geq 0$.

Now we bound $D_\psi(z, z_0)$. Since $z_0 \in \arg \min_{z \in \mathcal{Z} \cap \mathcal{D}_\mathcal{Z}} \psi(z)$ and ψ is convex, the first-order optimality condition implies that for all $z \in \mathcal{Z} \cap \mathcal{D}_\mathcal{Z}$,

$$\langle \nabla \psi(z_0), z - z_0 \rangle \geq 0.$$

Thus,

$$\begin{aligned} D_\psi(z, z_0) &= \psi(z) - \psi(z_0) - \langle \nabla \psi(z_0), z - z_0 \rangle \\ &\leq \psi(z) - \psi(z_0) \leq \sup_{u \in \mathcal{Z}} \psi(u) - \inf_{u \in \mathcal{Z}} \psi(u). \end{aligned}$$

Recalling $\psi(z) = a\psi_{\mathcal{X}}(x) + b\psi_{\mathcal{Y}}(y)$, we obtain

$$\sup_{u \in \mathcal{Z}} \psi(u) - \inf_{u \in \mathcal{Z}} \psi(u) \leq aR_{\mathcal{X}}^2 + bR_{\mathcal{Y}}^2,$$

where $R_{\mathcal{X}}^2$ and $R_{\mathcal{Y}}^2$ are defined in Condition 2. Hence,

$$D_\psi(z, z_0) \leq aR_{\mathcal{X}}^2 + bR_{\mathcal{Y}}^2.$$

Together with (75), dividing the telescoping inequality by T yields

$$\frac{1}{T} \sum_{t=0}^{T-1} [f(x_{t+\frac{1}{2}}, y) - f(x, y_{t+\frac{1}{2}})] \leq \frac{aR_{\mathcal{X}}^2 + bR_{\mathcal{Y}}^2}{\eta T}.$$

With $\eta = \mu/\beta = \frac{\mu_{\mathcal{X}} \wedge \mu_{\mathcal{Y}}}{\beta}$, this becomes

$$\frac{1}{T} \sum_{t=0}^{T-1} [f(x_{t+\frac{1}{2}}, y) - f(x, y_{t+\frac{1}{2}})] \leq \frac{\beta(aR_{\mathcal{X}}^2 + bR_{\mathcal{Y}}^2)}{(\mu_{\mathcal{X}} \wedge \mu_{\mathcal{Y}}) \cdot T}.$$

By convexity of $f(\cdot, y)$ and concavity of $f(x, \cdot)$, Jensen's inequality implies

$$f\left(\frac{1}{T} \sum_{t=0}^{T-1} x_{t+\frac{1}{2}}, y\right) - f\left(x, \frac{1}{T} \sum_{t=0}^{T-1} y_{t+\frac{1}{2}}\right) \leq \frac{\beta(aR_{\mathcal{X}}^2 + bR_{\mathcal{Y}}^2)}{(\mu_{\mathcal{X}} \wedge \mu_{\mathcal{Y}}) \cdot T}.$$

Since the inequality holds for all $(x, y) \in \mathcal{X} \times \mathcal{Y}$, we obtain

$$\max_{y \in \mathcal{Y}} f\left(\frac{1}{T} \sum_{t=0}^{T-1} x_{t+\frac{1}{2}}, y\right) - \min_{x \in \mathcal{X}} f\left(x, \frac{1}{T} \sum_{t=0}^{T-1} y_{t+\frac{1}{2}}\right) \leq \frac{\beta(aR_{\mathcal{X}}^2 + bR_{\mathcal{Y}}^2)}{(\mu_{\mathcal{X}} \wedge \mu_{\mathcal{Y}}) \cdot T}.$$

Substituting the expression of β in Lemma 11 completes the proof.

C.5 Proof of Lemma 6

Under Condition 1, it is a standard result (see Exercise 4.7.3 of Vershynin (2018)) that: for any $t \geq 0$, with probability at least $1 - 2e^{-t}$:

$$\|\widehat{\Sigma}^{(t)} - \Sigma^{(t)}\|_{\text{op}} \leq C\sigma^2 \|\Sigma^{(t)}\|_{\text{op}} \left(\sqrt{\frac{d+t}{n}} + \frac{d+t}{n} \right).$$

By Triangle inequality, it holds

$$\left| \|\widehat{\Sigma}^{(t)}\|_{\text{op}} - \|\Sigma^{(t)}\|_{\text{op}} \right| \leq C\sigma^2 \|\Sigma^{(t)}\|_{\text{op}} \left(\sqrt{\frac{d+t}{n}} + \frac{d+t}{n} \right).$$

Using Hölder's inequality, we obtain that

$$\sup_{M \in \mathcal{F}^k} \left| \langle \widehat{\Sigma}^{(t)} - \Sigma^{(t)}, M \rangle \right| \leq \sup_{M \in \mathcal{F}^k} \|M\|_* \|\widehat{\Sigma}^{(t)} - \Sigma^{(t)}\|_{\text{op}} = k \|\widehat{\Sigma}^{(t)} - \Sigma^{(t)}\|_{\text{op}},$$

where the last equality holds as $\|M\|_* = k$ for any $M \in \mathcal{F}^k$.

The combination of the above results yields that: with probability at least $1 - 2e^{-t}$:

$$\sup_{M \in \mathcal{F}^k} \left| \langle \widehat{\Sigma}^{(t)} - \Sigma^{(t)}, M \rangle \right| \leq C\sigma^2 \|\Sigma^{(t)}\|_{\text{op}} k \left(\sqrt{\frac{d+t}{n}} + \frac{d+t}{n} \right).$$

We next apply the union bound inequality to complete the proof.

C.6 Proof of Lemma 8

Strong Convexity of $\psi_1(M)$.

When $k = 1$, Section 4.3 of Bubeck et al. (2015) states that $\psi_1(X)$ is $\frac{1}{2}$ -strongly convex on $X \in \mathcal{F}^1$ with respect to the Schatten-1 (nuclear) norm $\|\cdot\|_*$. This means that

$$D_{\psi_1}(X, Y) \geq \frac{1}{4} \|X - Y\|_*^2, \quad \forall X, Y \in \mathcal{F}^1. \quad (76)$$

For general $k \geq 1$, fix $M, M' \in \mathcal{F}^k$, we define

$$X := \frac{1}{k}M, \quad Y := \frac{1}{k}M',$$

then $X, Y \in \mathcal{F}^1$ satisfies that

$$\|X - Y\|_* = \frac{1}{k}\|M - M'\|_*. \quad (77)$$

Moreover, recall the Bregman divergence associated with ψ_1 in (12):

$$D_{\psi_1}(M, M') = \text{Tr}(M(\log M - \log M')) = \text{Tr}(kX(\log(kX) - \log(kY))) = kD_{\psi_1}(X, Y).$$

Together with (76) and (77), we obtain

$$D_{\psi_1}(M, M') = kD_{\psi_1}(X, Y) \geq \frac{k}{4}\|X - Y\|_*^2 = \frac{1}{4k}\|M - M'\|_*^2.$$

This establishes that ψ_1 is $\frac{1}{2k}$ -strongly convex over $M \in \mathcal{F}^k$, with respect to the nuclear norm $\|M\|_*$.

Note that $\psi_1(M) = \sum_i \lambda_i \log \lambda_i \leq 0$ is always true since $\lambda_i \in [0, 1]$, where λ_i denotes the i -th eigenvalue of M . Therefore, the maximum is attained at any vertex when M is a rank- k projector, with $\sup_{M \in \mathcal{F}^k} \psi_1(M) = 0$.

Due to the convexity of $\psi_1(M)$, it is straightforward to see that the minimum of $\psi_1(M) = \sum_i \lambda_i \log \lambda_i$ is taken at when all $\lambda_i = \frac{k}{d}$, with $\inf_{M \in \mathcal{F}^k} \psi_1(M) = k \log(k/d)$. Therefore,

$$R_{\mathcal{F}^k}^2 = \sup_{M \in \mathcal{F}^k} \psi_1(M) - \inf_{M \in \mathcal{F}^k} \psi_1(M) = k \log \frac{d}{k}.$$

Strong Convexity of $\psi_2(\omega)$.

Recall in (12), we have

$$D_{\psi}(\omega, \omega') = \sum_{l=1}^L \omega_l \log \frac{\omega_l}{\omega'_l} =: \text{KL}(\omega \|\omega').$$

Pinsker's inequality states that for any probability distributions p, q on the simplex,

$$\text{KL}(p \|\| q) \geq \frac{1}{2}\|p - q\|_1^2.$$

Applying it to ω, ω' gives:

$$D_{\psi_2}(\omega, \omega') = \text{KL}(\omega \|\omega') \geq \frac{1}{2} \|\omega - \omega'\|_1^2,$$

which indicates that ψ_2 is 1-strongly convex over $\omega \in \Delta^L$.

Note that $\psi_2(\omega) \leq 0$ is always true, since $x \log x \leq 0$ for $x \in [0, 1]$, and the maximum is attained at any vertex. The minimum is attained at the uniform distribution $\frac{1}{L} \mathbf{1}_L$. Therefore,

$$R_{\Delta^L}^2 := \sup_{\omega \in \Delta^L} \psi_2(\omega) - \inf_{\omega \in \Delta^L} \psi_2(\omega) = \log L.$$

Smoothness of $f(M, \omega)$

We first compute the partial gradients:

$$\nabla_M f(M, \omega) = - \sum_{l=1}^L \omega_l \widehat{\Sigma}^{(l)}, \quad \nabla_\omega f(M, \omega) = \left(- \langle \widehat{\Sigma}^{(1)}, M \rangle, \dots, - \langle \widehat{\Sigma}^{(L)}, M \rangle \right)^\top.$$

The dual norms of nuclear norm $\|M\|_*$ and ℓ_1 norm $\|\omega\|_1$ are operator norm $\|M\|_{\text{op}}$ and ℓ_∞ -norm $\|\omega\|_\infty$, respectively. Since $\nabla_M f(M, \omega)$ does not depend on M and $\nabla_\omega f(M, \omega)$ does not depend on ω , we immediately have

$$\beta_{11} = 0, \quad \beta_{22} = 0.$$

Next, for β_{21} , for any $M_1, M_2 \in \mathcal{F}^k$ and any $l \in [L]$, Hölder's inequality for nuclear norms gives

$$|\langle \widehat{\Sigma}^{(l)}, M_1 - M_2 \rangle| \leq \|\widehat{\Sigma}^{(l)}\|_{\text{op}} \|M_1 - M_2\|_*.$$

Taking the maximum over l yields

$$\|\nabla_\omega \widehat{f}(M_1, \omega) - \nabla_\omega \widehat{f}(M_2, \omega)\|_\infty \leq \beta \|M_1 - M_2\|_*, \quad \text{with } \beta = \max_{l \in [L]} \|\widehat{\Sigma}^{(l)}\|_{\text{op}}.$$

so we may take $\beta_{21} = \beta$.

Finally, for β_{12} , for any $\omega_1, \omega_2 \in \Delta^L$,

$$\begin{aligned} \|\nabla_M f(M, \omega_1) - \nabla_M f(M, \omega_2)\|_{\text{op}} &= \left\| \sum_{l=1}^L (\omega_{1l} - \omega_{2l}) \widehat{\Sigma}^{(l)} \right\|_{\text{op}} \\ &\leq \sum_{l=1}^L |\omega_{1l} - \omega_{2l}| \|\widehat{\Sigma}^{(l)}\|_{\text{op}} \\ &\leq \beta \|\omega_1 - \omega_2\|_1, \end{aligned}$$

hence $\beta_{12} = \beta$.

C.7 Proof of Lemma 10

By the definition of the Bregman divergence, we have

$$\begin{aligned}
z_{t+\frac{1}{2}} &= \arg \min_{z \in \mathcal{Z} \cap \mathcal{D}_{\mathcal{Z}}} D_{\psi}(z, \nu_{t+\frac{1}{2}}) \\
&= \arg \min_{z \in \mathcal{Z} \cap \mathcal{D}_{\mathcal{Z}}} \psi(z) - \psi(\nu_{t+\frac{1}{2}}) - \langle \nabla \psi(\nu_{t+\frac{1}{2}}), z \rangle \\
&= \arg \min_{z \in \mathcal{Z} \cap \mathcal{D}_{\mathcal{Z}}} \psi(z) - \langle \nabla \psi(\nu_{t+\frac{1}{2}}), z \rangle && \text{as } \psi(\nu_{t+\frac{1}{2}}) \text{ is independent of } z \\
&= \arg \min_{z \in \mathcal{Z} \cap \mathcal{D}_{\mathcal{Z}}} \psi(z) - (\nabla \psi(z_t) - \eta \cdot \langle g(z_t), z \rangle) && \text{the expression of } \nabla \psi(\nu_{t+\frac{1}{2}}) \\
&= \arg \min_{z \in \mathcal{Z} \cap \mathcal{D}_{\mathcal{Z}}} D_{\psi}(z, z_t) + \eta \cdot \langle g(z_t), z \rangle.
\end{aligned}$$

Similarly, we shall show that

$$\begin{aligned}
z_{t+1} &= \arg \min_{z \in \mathcal{Z} \cap \mathcal{D}_{\mathcal{Z}}} D_{\psi}(z, \nu_{t+1}) \\
&= \arg \min_{z \in \mathcal{Z} \cap \mathcal{D}_{\mathcal{Z}}} \psi(z) - \langle \nabla \psi(\nu_{t+1}), z \rangle \\
&= \arg \min_{z \in \mathcal{Z} \cap \mathcal{D}_{\mathcal{Z}}} \psi(z) - \langle \nabla \psi(z_t) - \eta \cdot g(z_{t+\frac{1}{2}}), z \rangle \\
&= \arg \min_{z \in \mathcal{Z} \cap \mathcal{D}_{\mathcal{Z}}} D_{\psi}(z, z_t) + \eta \cdot \langle g(z_{t+\frac{1}{2}}), z \rangle.
\end{aligned}$$

C.8 Proof of Lemma 11

Strong convexity of ψ .

We first show the strong convexity of $\psi(z)$. By the $\mu_{\mathcal{X}}$ -strong convexity of $\psi_{\mathcal{X}}$ on \mathcal{X} with respect to $\|\cdot\|_{\mathcal{X}}$, for any $x, x' \in \mathcal{X}$,

$$\psi_{\mathcal{X}}(x') \geq \psi_{\mathcal{X}}(x) + \langle \nabla \psi_{\mathcal{X}}(x), x' - x \rangle + \frac{\mu_{\mathcal{X}}}{2} \|x' - x\|_{\mathcal{X}}^2.$$

Similarly, by the $\mu_{\mathcal{Y}}$ -strong convexity of $\psi_{\mathcal{Y}}$ on \mathcal{Y} with respect to $\|\cdot\|_{\mathcal{Y}}$, for any $y, y' \in \mathcal{Y}$,

$$\psi_{\mathcal{Y}}(y') \geq \psi_{\mathcal{Y}}(y) + \langle \nabla \psi_{\mathcal{Y}}(y), y' - y \rangle + \frac{\mu_{\mathcal{Y}}}{2} \|y' - y\|_{\mathcal{Y}}^2.$$

Let $z = (x, y)$ and $z' = (x', y')$, and define

$$\psi(z) := a \psi_{\mathcal{X}}(x) + b \psi_{\mathcal{Y}}(y).$$

Multiplying the two inequalities above by a and b respectively and summing, we obtain

$$\begin{aligned}
\psi(z') &= a\psi_{\mathcal{X}}(x') + b\psi_{\mathcal{Y}}(y') \\
&\geq a\psi_{\mathcal{X}}(x) + a\langle \nabla\psi_{\mathcal{X}}(x), x' - x \rangle + \frac{a\mu_{\mathcal{X}}}{2}\|x' - x\|_{\mathcal{X}}^2 \\
&\quad + b\psi_{\mathcal{Y}}(y) + b\langle \nabla\psi_{\mathcal{Y}}(y), y' - y \rangle + \frac{b\mu_{\mathcal{Y}}}{2}\|y' - y\|_{\mathcal{Y}}^2 \\
&= \psi(z) + \langle \nabla\psi(z), z' - z \rangle + \frac{a\mu_{\mathcal{X}}}{2}\|x' - x\|_{\mathcal{X}}^2 + \frac{b\mu_{\mathcal{Y}}}{2}\|y' - y\|_{\mathcal{Y}}^2.
\end{aligned}$$

Using the definition of $\|\cdot\|_{\mathcal{Z}}$,

$$\|z' - z\|_{\mathcal{Z}}^2 = a\|x' - x\|_{\mathcal{X}}^2 + b\|y' - y\|_{\mathcal{Y}}^2,$$

we further have

$$\frac{a\mu_{\mathcal{X}}}{2}\|x' - x\|_{\mathcal{X}}^2 + \frac{b\mu_{\mathcal{Y}}}{2}\|y' - y\|_{\mathcal{Y}}^2 \geq \frac{\mu_{\mathcal{X}} \wedge \mu_{\mathcal{Y}}}{2} (a\|x' - x\|_{\mathcal{X}}^2 + b\|y' - y\|_{\mathcal{Y}}^2) = \frac{\mu_{\mathcal{X}} \wedge \mu_{\mathcal{Y}}}{2}\|z' - z\|_{\mathcal{Z}}^2.$$

Therefore,

$$\psi(z') \geq \psi(z) + \langle \nabla\psi(z), z' - z \rangle + \frac{\mu_{\mathcal{X}} \wedge \mu_{\mathcal{Y}}}{2}\|z' - z\|_{\mathcal{Z}}^2,$$

which shows that ψ is $(\mu_{\mathcal{X}} \wedge \mu_{\mathcal{Y}})$ -strongly convex with respect to $\|\cdot\|_{\mathcal{Z}}$. As a consequence, the associated Bregman divergence satisfies

$$D_{\psi}(z, z') \geq \frac{\mu_{\mathcal{X}} \wedge \mu_{\mathcal{Y}}}{2}\|z - z'\|_{\mathcal{Z}}^2.$$

Lipschitz continuity of $g(z)$.

Next, we prove that g is β -Lipschitz. The dual norm associated with $\|\cdot\|_{\mathcal{Z}}$ is

$$\|u\|_{\mathcal{Z},*} = \sqrt{\frac{1}{a}\|u_x\|_{\mathcal{X},*}^2 + \frac{1}{b}\|u_y\|_{\mathcal{Y},*}^2}, \quad \text{for } u = (u_x, u_y) \in \mathcal{X}^* \times \mathcal{Y}^*.$$

Let $z = (x, y)$ and $z' = (x', y')$. Recall $g(z) = (\nabla_x f(x, y), -\nabla_y f(x, y))$, hence

$$g(z) - g(z') = (\nabla_x f(x, y) - \nabla_x f(x', y'), -(\nabla_y f(x, y) - \nabla_y f(x', y'))).$$

By definition of $\|\cdot\|_{\mathcal{Z},*}$,

$$\|g(z) - g(z')\|_{\mathcal{Z},*}^2 = \frac{1}{a}\|\nabla_x f(x, y) - \nabla_x f(x', y')\|_{\mathcal{X},*}^2 + \frac{1}{b}\|\nabla_y f(x, y) - \nabla_y f(x', y')\|_{\mathcal{Y},*}^2. \quad (78)$$

Using the triangle inequality,

$$\|\nabla_x f(x, y) - \nabla_x f(x', y')\|_{\mathcal{X},*} \leq \|\nabla_x f(x, y) - \nabla_x f(x', y)\|_{\mathcal{X},*} + \|\nabla_x f(x', y) - \nabla_x f(x', y')\|_{\mathcal{X},*}.$$

By Condition 2,

$$\|\nabla_x f(x, y) - \nabla_x f(x', y)\|_{\mathcal{X},*} \leq \beta_{11}\|x - x'\|_{\mathcal{X}}, \quad \|\nabla_x f(x', y) - \nabla_x f(x', y')\|_{\mathcal{X},*} \leq \beta_{12}\|y - y'\|_{\mathcal{Y}},$$

and therefore

$$\|\nabla_x f(x, y) - \nabla_x f(x', y')\|_{\mathcal{X},*} \leq \beta_{11}\|x - x'\|_{\mathcal{X}} + \beta_{12}\|y - y'\|_{\mathcal{Y}}.$$

Similarly,

$$\|\nabla_y f(x, y) - \nabla_y f(x', y')\|_{\mathcal{Y},*} \leq \beta_{21}\|x - x'\|_{\mathcal{X}} + \beta_{22}\|y - y'\|_{\mathcal{Y}}.$$

Substituting these bounds into (78) yields

$$\|g(z) - g(z')\|_{\mathcal{Z},*}^2 \leq \frac{(\beta_{11}\|x - x'\|_{\mathcal{X}} + \beta_{12}\|y - y'\|_{\mathcal{Y}})^2}{a} + \frac{(\beta_{21}\|x - x'\|_{\mathcal{X}} + \beta_{22}\|y - y'\|_{\mathcal{Y}})^2}{b}.$$

Using $(u + v)^2 \leq 2u^2 + 2v^2$, we obtain

$$\begin{aligned} \|g(z) - g(z')\|_{\mathcal{Z},*}^2 &\leq \frac{2\beta_{11}^2}{a}\|x - x'\|_{\mathcal{X}}^2 + \frac{2\beta_{12}^2}{a}\|y - y'\|_{\mathcal{Y}}^2 + \frac{2\beta_{21}^2}{b}\|x - x'\|_{\mathcal{X}}^2 + \frac{2\beta_{22}^2}{b}\|y - y'\|_{\mathcal{Y}}^2 \\ &= 2\left(\frac{\beta_{11}^2}{a} + \frac{\beta_{21}^2}{b}\right)\|x - x'\|_{\mathcal{X}}^2 + 2\left(\frac{\beta_{12}^2}{a} + \frac{\beta_{22}^2}{b}\right)\|y - y'\|_{\mathcal{Y}}^2. \end{aligned}$$

Now note that

$$\frac{\beta_{11}^2}{a} + \frac{\beta_{21}^2}{b} \leq 2 \max\left\{\frac{\beta_{11}^2}{a}, \frac{\beta_{21}^2}{b}\right\} = 2 \max\left\{\left(\frac{\beta_{11}}{a}\right)^2 a, \left(\frac{\beta_{21}}{\sqrt{ab}}\right)^2 a\right\},$$

and similarly

$$\frac{\beta_{12}^2}{a} + \frac{\beta_{22}^2}{b} \leq 2 \max\left\{\left(\frac{\beta_{12}}{\sqrt{ab}}\right)^2 b, \left(\frac{\beta_{22}}{b}\right)^2 b\right\}.$$

Consequently,

$$\|g(z) - g(z')\|_{\mathcal{Z},*}^2 \leq 4 \max\left\{\frac{\beta_{11}^2}{a^2}, \frac{\beta_{22}^2}{b^2}, \frac{\beta_{12}^2}{ab}, \frac{\beta_{21}^2}{ab}\right\} (a\|x - x'\|_{\mathcal{X}}^2 + b\|y - y'\|_{\mathcal{Y}}^2).$$

Recalling $\|z - z'\|_{\mathcal{Z}}^2 = a\|x - x'\|_{\mathcal{X}}^2 + b\|y - y'\|_{\mathcal{Y}}^2$ and taking square roots, we obtain

$$\|g(z) - g(z')\|_{\mathcal{Z},*} \leq 2 \max\left\{\frac{\beta_{11}}{a}, \frac{\beta_{22}}{b}, \frac{\beta_{12}}{\sqrt{ab}}, \frac{\beta_{21}}{\sqrt{ab}}\right\} \|z - z'\|_{\mathcal{Z}}.$$

This completes the proof.

D Additional Simulated Experiments and Real Applications

D.1 Additional Simulated Experiments

D.1.1 Finite-sample Convergence of Algorithm 1

We examine the finite-sample convergence of StablePCA, solved using the proposed Algorithm 1. We fix the number of sources at $L = 4$, while varying the dimension $d \in \{10, 30\}$, and the sample size n in the range of $[100, 40000]$. For each configuration (n, d) , we run Algorithm 1 with $T = 500$ iterations to obtain the empirical estimator \widehat{M} . We then compare \widehat{M} to the population solution M^* , which is computed by running the same algorithm but using the population second-moment matrices $\{\Sigma^{(l)}\}_{l=1}^L$. Figure 7 summarizes the following two metrics on the left and right panels, respectively:

- *Objective Gap.* We compute $\min_l \langle \Sigma^{(l)}, M^* \rangle - \min_l \langle \Sigma^{(l)}, \widehat{M} \rangle$, which quantifies how far \widehat{M} is from the population optimum in terms of objective value.
- *Estimation Error.* We compute $\|\widehat{M} - M^*\|_F$, which directly measures how close the empirical estimator \widehat{M} is to the population solution M^* .

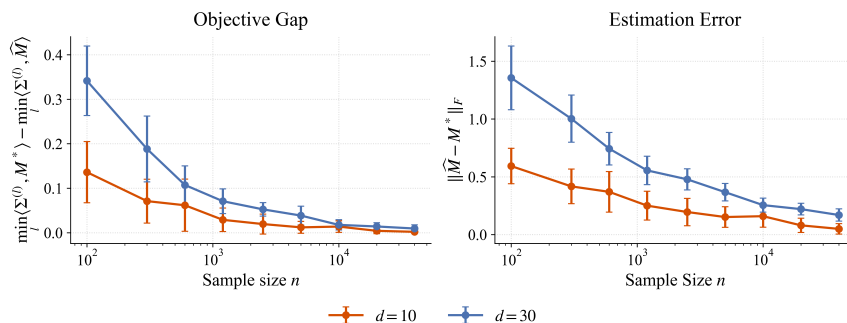


Figure 7: Finite-sample convergence behavior of Fantope-relaxed StablePCA across varying sample sizes n over $[300, 40000]$ and dimensions $d \in \{10, 30\}$. Left: Objective gap $\min_l \langle \Sigma^{(l)}, M^* \rangle - \min_l \langle \Sigma^{(l)}, \widehat{M}_T \rangle$. Right: Estimation error $\|\widehat{M} - M^*\|_F$. Results are averaged over 100 replications, with error bars representing one standard deviation.

As shown in Figure 7, both the objective gap and estimation error decrease steadily with increasing sample size, confirming the convergence of the empirical \widehat{M} to the population optimum of StablePCA.

D.1.2 Magnitude of Certificate.

We here examine the magnitude of the projection certificate τ defined in (19), which quantifies the loss incurred when projecting the relaxed solution $\widehat{M}_T \in \mathcal{F}^k$ onto a rank- k projection matrix $\widehat{P}_T \in \mathcal{P}^k$ in Algorithm 1. We fix the number of iterations at $T = 500$. Table 2 reports the certificate averaged over 100 replications.

Table 2 reports the certificate values averaged over 100 independent replications. Across all (n, d) configurations considered, the magnitude of the certificate is negligible (with $|\tau| < 0.003$). Together with Theorem 3, this result indicates that the proposed Mirror-Prox algorithm effectively solves the original nonconvex StablePCA problem in all the simulated setups we have explored.

$d \backslash n$	100	300	600	1200	2500	5000	10000	20000	40000
10	-0.0001	0.0018	0.0019	0.0024	0.0010	-0.0002	0.0027	0.0004	0.0002
20	-0.0015	-0.0008	-0.0006	-0.0005	-0.0004	-0.0003	-0.0002	-0.0003	-0.0003
30	0.0017	0.0002	0.0009	-0.0014	-0.0024	-0.0014	-0.0017	-0.0028	-0.0021

Table 2: Summary of the values of the certificate τ defined in (19) across samples sizes $n \in \{100, 300, \dots, 40000\}$ and dimensions $d \in \{10, 20, 30\}$. We set the number of iterations $T = 500$ in Algorithm 1. The table reports mean values averaged over 100 replications.

D.1.3 Generalization Performance

In addition to the results of $k = 3$ reported in Figure 2, we now present the results for $k = 5$ and $k = 10$ in Figure 8 and Figure 9, respectively.

Note that in Figure 2, we adopt the metric ‘‘Shared Subspace Recovery Error’’ $\|\widehat{P} - \Lambda_{\text{sh}}\Lambda_{\text{sh}}\|_F$ to

evaluate how well the estimated projection matrix \hat{P} recovers the shared subspace spanned by Λ_{sh} . However, this metric remains valid only when $\text{rank}(\hat{P}) = \text{rank}(\Lambda_{\text{sh}})$. When $k = 5$ and $k = 10$, we have $k = \text{rank}(\hat{P}) > \text{rank}(\Lambda_{\text{sh}}) = 3$, we adopt the following metric

$$1 - \frac{1}{\text{rank}(\Lambda_{\text{sh}})} \langle \Lambda_{\text{sh}} \Lambda_{\text{sh}}^\top, \hat{P} \rangle,$$

named as ‘‘Subspace Capture Error’’. Still, this metric measures the fraction of the true shared subspace (spanned by Λ_{sh}) that is *not* captured by the estimated projection \hat{P} . Importantly, this metric remains valid even when the rank of \hat{P} exceeds $\text{rank}(\Lambda_{\text{sh}})$. Smaller values indicate that the estimated subspace more fully contains the true shared subspace, with 0 indicating perfect recovery.

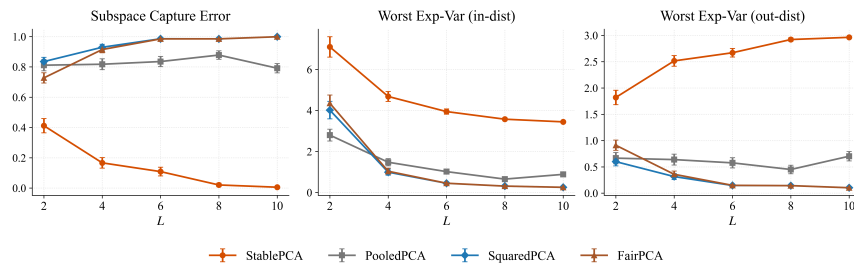


Figure 8: Performance comparison of StablePCA, PooledPCA, SquaredPCA, and FairPCA across different numbers of source domains $L \in \{2, 4, 6, 8, 10\}$, when the methods are fitted with $k = 5$.

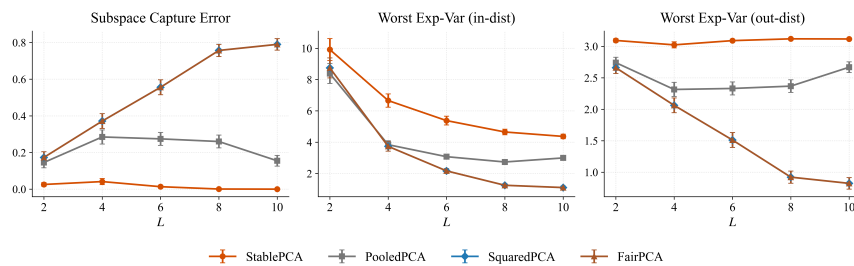


Figure 9: Performance comparison of StablePCA, PooledPCA, SquaredPCA, and FairPCA across different numbers of source domains $L \in \{2, 4, 6, 8, 10\}$, when the methods are fitted with $k = 10$.

As shown in Figure 8 and Figure 9, StablePCA achieves a substantially smaller capture error and

a higher worst-explained variance for both in distribution and out-of-distribution scenarios than other competing methods. This phenomenon aligns with what we have discussed in the main text for Figure 2.

D.2 Additional Results for Real Applications

In addition to Figure 3 for $k = 50$, we present the worst-case explained variance when we set $k = 100$ and $k = 150$ in Figure 10 and Figure 11, respectively. Analogous to $k = 50$, we find that in both $k = 100$ and $k = 150$, StablePCA consistently achieves the highest worst-case explained variance on both training batches (left panel) and test batches (right panel), indicating that the low-rank representations it extracts generalize not only to the training batches but also reliably to unseen batches.

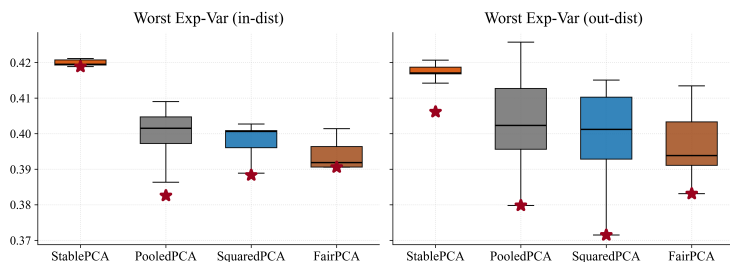


Figure 10: Worst-case explained variance ratio achieved by StablePCA, PooledPCA, SquaredPCA, and FairPCA on the single-cell RNA dataset with $k = 100$.

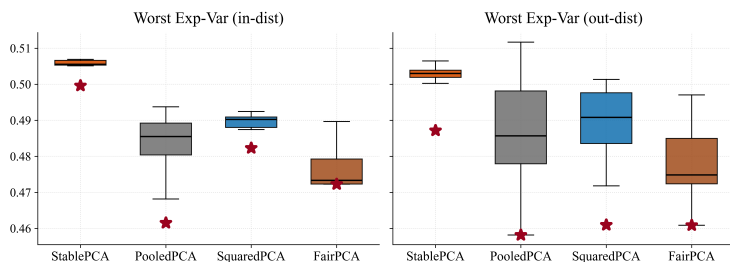


Figure 11: Worst-case explained variance ratio achieved by StablePCA, PooledPCA, SquaredPCA, and FairPCA on the single-cell RNA dataset with $k = 150$.

Analogous to Figure 4 for $k = 50$, we now present the visualizations of the StablePCA embedding

with $k = 25$ and $k = 75$ in Figure 12 and Figure 13, respectively. Analogous to Figure 4 for $k = 50$, when $k = 25$ and $k = 75$, cells from 12 different experimental batches are well mixed when colored by batch (top row), and the four major cell-type populations form coherent clusters when colored by cell type (bottom row). These results demonstrate that StablePCA effectively removes batch-specific variations, while preserving biologically meaningful structure to distinguish major cell types.

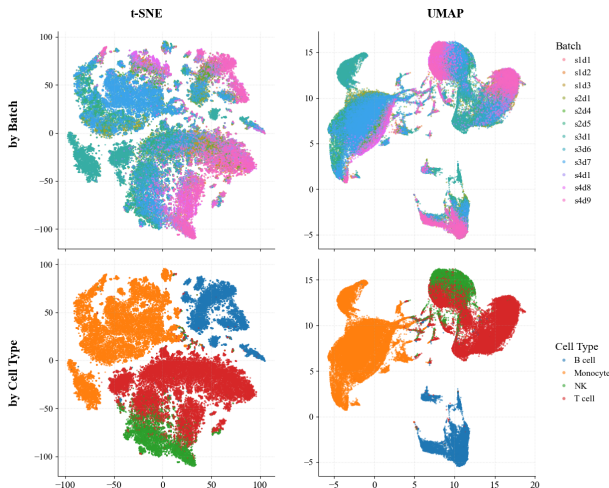


Figure 12: t-SNE and UMAP visualizations of the StablePCA embedding with target dimension $k = 25$ on the single-cell RNA dataset. Top row: cells colored by 12 experimental batches. Bottom row: cells colored by cell types (B cell, Monocyte, NK cell, and T cell).

D.3 Omitted Experimental Setups

Setup of Figure 5. We consider the two-source case $L = 2$. The matrices $\Sigma^{(1)}, \Sigma^{(2)}$ were independently generated as follows:

$$\Sigma^{(l)} = A^{(l)} A^{(l)\top} + \frac{1}{2} \mathbf{I}_d, \quad l = 1, 2,$$

where $A^{(l)} \in \mathbb{R}^{d \times d}$ has entries i.i.d. drawn from the standard normal distribution. The dimension is set to $d = 6$. For any $\omega = (\omega_1, \omega_2) \in \Delta^2$ with $\omega_1 + \omega_2 = 1$, the eigenvalue function is given by

$$\phi(\omega) = \sum_{i=1}^k \lambda_i(\omega_1 \Sigma^{(1)} + \omega_2 \Sigma^{(2)}),$$

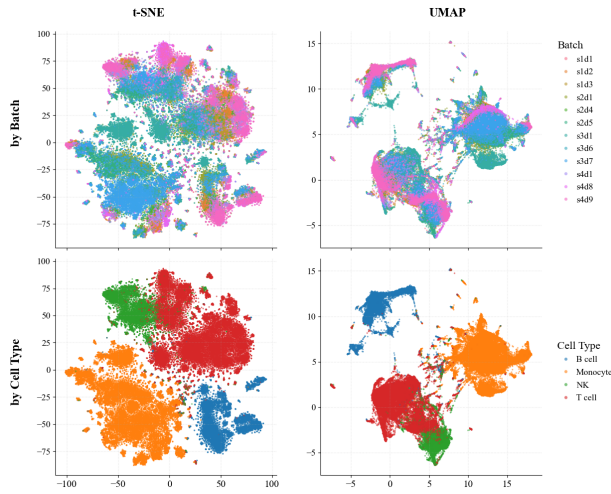


Figure 13: t-SNE and UMAP visualizations of the StablePCA embedding with target dimension $k = 75$ on the single-cell RNA dataset. Top row: cells colored by 12 experimental batches. Bottom row: cells colored by cell types (B cell, Monocyte, NK cell, and T cell).

where k is fixed at $k = 3$. We vary the value of ω_1 over $[0, 1]$ and compute the corresponding $\phi(\omega)$ values.

Setup of Table 1

We adopt the same simulation setup as in Section 7, fixing the number of sources L and the sample size at $n = 10,000$, while varying the ambient dimension over $d \in \{10, 50, 100, 200, 300\}$. For each dimension, we solve FairPCA using the proposed Mirror-Prox Algorithm 3 with $T = 500$ iterations. We also implement the SDP-based method following the procedure described in Samadi et al. (2018). All experiments are repeated 100 times, independently.